**POLITECNICO**

MILANO 1863

# Airframe design and optimisation of a H2-fuelled hybrid/electric 19-seat commuter

Tesi di Laurea Magistrale in
Aeronautical Engineering - Ingegneria Aeronautica

Author: **Luca Parisotto**

Student ID: 952925
Advisor: Prof. Lorenzo Trainelli (PoliMI) - Andrea Cini (UC3M)
Academic Year: 2021-22

# Abstract

The innovation in term of zero emission flight, lead to the necessity of develop non-standard aircraft designs, the objective of this thesis is the definition of a highly automated methodology to develop and size, in a mid-fidelity approach, the wing and fuselage airframe for one of this innovative commuter. A fully automated procedure for GFEM analysis is developed and used, first of all, for the definition of the *airframe architecture* in terms of structural elements dimensions, spacing and materials, secondly for the *load application* and then *analysis* for both static and buckling conditions are considered. The tool developed allow to test and model many different airframe solutions, very useful for non-standard commercial aircraft, for which previous experience in standard commuter may not be applicable, in a very short time. This work is completed with the testing of this methodology for the structural sizing of *Unifier19*, for which the preliminary airframe design have been conduced, in particular the airframe constraint for this innovative aircraft are highlighted and defined. A full understanding of these constraints is achieved by considering the interference with all the subsystem presents, in particular for the landing gears, for which a kinematic study on the retraction system is proposed. The outcome of this thesis is the definition of a proven automated procedure for the airframe model creation and analysis and a mass estimation for *Unifier19* which will be the base for proper optimization process in the following project steps.

**Keywords:** Unifier19, GFEM parametric deisgn, structrual sizing, preliminary design

# Abstract in lingua italiana

L'innovazione tecnologica in termini di voli a impatto zero sta portando alla necessità di sviluppare velivoli con una configurazione non ordinaria, l'obiettivo di questa tesi è lo sviluppo di una metodologia totalmente automatizzara per lo sviluppo e il dimensionamento, in un approccio a media fedeltà, la struttura alare e della fusoliera per un velivolo di trasporto a corto-medio raggio appartenente a questa categoria. Una procedura GFEM è stata sviluppata prima di tutto per la definizione generale dell'architettura, in particolare, caratterizzando ogni elemento strutturale in termini di dimensione, spaziatura e materiale; la successiva applicazione del carico permette l'esecuzione delle analisi statiche e di instabilità. Questo strumento permette di testare in maniera veloce diverse configurazioni strutturali, necessario per uno sviluppo ottimale di un velivolo innovativo per il quale l'esperienza in aerei convenzionali può non essere applicabile. Questo lavoro è completato con il test di questa metodologia per il progetto preliminare di *Unifier19*, nel quale si sono considerati con attenzione i vincoli generati da questa innovativa configurazione. La comprensione di requisiti è ottenuta considerando l'interazione tra gli elementi strutturali e i sottosistemi del velivolo, in particolare condierando il carrello, per il quale si propone un meccanismo cinematico per la retrazione. Il risultato di questo studio è, insieme alla verifica della metodologia utilizzata, la definzione del progetto strutturale preliminare per *Unifier19* che si prevede essere la base da utilizzare in processi di ottimizzazione da sviluppare nelle prossime fasi del progetto.

**Parole chiave:** Unifier19, modelleazione parametrica GFEM, dimensionamento struttruale, progettazione preliminare

# Contents

# Introduction



In the recent years the constant rise in climate temperature and the worsening of environmental conditions generate the necessity to go beyond a zero impact in terms of emission produced by human activities, the aerospace industry is going towards this challenge by the development of new technologies that have the objective of going towards a more sustainable flight. These technologies, even if in the recent years have made huge steps forward, are still not ready to be used in big intercontinental airliners embedded in CS-25 regulations, but may be applicable to smaller aircraft in line within CS-23. In this application many investment are made in particular by the European Union which with the project *CleanSky2* is pushing the development of near-zero emissions commuter.

*Unifier19* is part of this project which is in development by *Pipistrel Vertical Solutions*, *Politecnico di Milano*, *Universidad Carlos III de Madrid* and *Technische Universiteit Delft*. Intense analysis and concept development by the partners involved are producing an innovative configuration miniliner with near-zero emission capabilities. The non-standard configuration on Unifier19 is evident both from an aesthetic point of view, both from a technological and engineering side. The most clear innovation is visible in the engines: instead of a classical twin engine configuration, common in aircraft currently in service, the main engine is a pushing propeller located in the back of the plane. Innovation from an aerodynamic and propulsive point of view are the six smaller engines located in each wing, this *Distributed Electric Propellers* (DEP) consent the capability of high-performance maneuvering condition and short take-off and landing. These technologies

(a)



(b)



(c)



(d)

are used to accomplish Unifier19 requirements in terms of take-off and landing run length, consenting its operation in hundreds of airdrome across EU, even in unpaved runways.

The near-zero emission capability is achieved by the use of a new power source based on the use of batteries and fuel cells running using liquid hydrogen. Therefore the engineering challenge to include these system in aircraft is non-trivial being those big element located inside the fuselage.

This research, mainly conduced in *Universidad Carlos III de Madrid*, set itself the objective of define and propose a feasible airframe configuration to be implemented in Unifier19. In particular big effort will be put in understanding which are the constraints and condition that the innovative concept of this aircraft will impose in the structural development, both from a technical point of view and from a comfort and safety issue. This work have been conducted in strong collaboration and under review of *Pipistrel Vertical Solution* that set the milestone and the constraint that the project have to satisfy from top level requirement and from design and aesthetic appearance of the final product by ensuring the cooperation between the development of each subsystem.

# 1 | Literature Review

Being the objective of this project the size and development of Unifier19 airframe, the first aspect to analyze consists in study and understand all previous A/C structure configuration and technical solution in all possible aspects in order to have a detailed overview of the possible problems and solutions that are expected to encounter during the technical development, this research have been performed mostly with [8] and with technical drawings of existing aircraft. Much effort and detailed analysis should be done considering similar aircraft in terms of dimension, MTOW and concept, but the innovative and modern configuration of Unifier19 in terms of *Distributed Electric Propulsion* (DEP), pushing propeller and liquid hydrogen tank in the fuselage, prevents this necessity not being any plane in service today with any of these characteristics in place. Therefore the choice of analyze the airframe of mainly three aircraft whose mission and overall dimension are similar to Unifier19, these A/C are:

- Piaggio P180 Avanti (Figure 1.1a)

- Dornier Do 228 (Figure 1.1b)

- ATR 42 (Figure 1.1c)

The whole airframe technical solutions and configuration was object of this study considering in detail the wing structure, fuselage frame dimensions and position, wing-fuselage connection and lending gear design and retraction kinematics.



(a) Piaggio P180 Avanti          (b) Dornier Do 228          (c) ATR 42 Colibrì

Figure 1.1: Reference aircraft.

In Table 1.1 are reported the characteristics of each plane taken into consideration, in Appendix E are shown the cutaways used to perform this research showing the airframe of the planes considered.

|  | **P180** | **Do228** | **ATR42** |
|---|---|---|---|
| **Length** $[m]$ | 14.40 | 15.04 | 22.67 |
| **Wingspan** $[m]$ | 14.03 | 16.97 | 24.57 |
| **Height** $[m]$ | 3.98 | 4.86 | 7.59 |
| **Empty mass** $[kg]$ | 3400 | 2990 | 10285 |
| **MTOM** $[kg]$ | 5466 | 5980 | 16700 |
| **Passengers** | 9 | 19-25 | 42-50 |

Table 1.1: Reference aircraft characteristics.

## 1.1. Fuselage design

For the planes taken into consideration the fuselage present similar aspect and architectures. It is composed mostly by equidistant frames for the whole fuselage length, with the exception of regions where heavy subsystem are present or in correspondence of big cutout such as doors, emergency exits or cargo openings that inevitably weak the overall strength. In that area either the the spacing between each frame is reduced (Do228, P180), or the frame are reinforced though a bigger beam section (ATR42).

Moreover the frames are used as connection point between the fuselage and the wing, as described in section 1.2. The frames are used to withstand the loads from by all other subsystem as air conditioning, fuel tanks and landing gears, enforcing the presence of at least one frame where each one of these subsystem is located. Usually two types of frames are present in a given plane: one thicker and stronger to connect the fuselage with the aerodynamic surfaces and the second, lighter and not as big to provide structural thickness across the whole fuselage.

The overall frame spacing for each of these aircraft is about $0.5m$, with the exception above mentioned or where a frame is imposed by a structural discontinuity due to any kind of constraint the structural design have to satisfy.

## 1.2. Wing architecture and connection

The wing architecture of each one of the plane analyzed present common design choice. It is composed by two tapered spars respectively parallel to leading and trailing edge, connected each other with ribs equidistant frames across the whole wingspan. An extra strong rib is located in correspondence of the engines with the purpose of carry and transfer the thrust and gyroscopic loads generated by the propeller.

In particular the ribs developed for Do228 are not all equals but present different structures along the wing span: in correspondence of the connection with the fuselage and where the engine is mounted the ribs are stronger, made by a single element instead of the other ribs which are made as a truss system. The rib developed in P180 and ATR42 are composed by a single strong element.



Figure 1.2: ATR42 wing fuslage connection.

The spars and one rib per wing are used in Do228 and in ATR42 to connect the wing with the fuselage. The connection system, shown in Figure 1.2, is made using two lugs that connect the front and rear spas with two high-strength fuselage frames. The same concept is applied to Do228 but not in P180 considering that it is the only plane which does not present a high wing configuration.
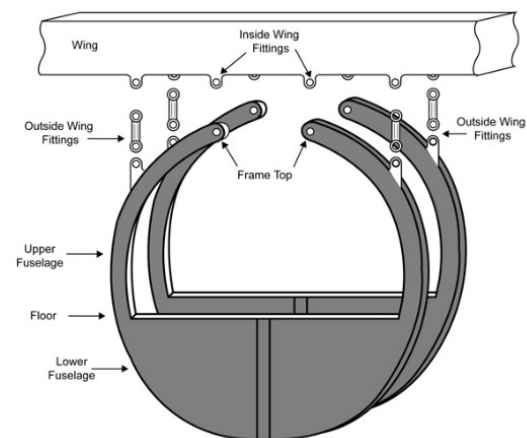
## 1.3. Landing gears

All these three aircraft analyzed present a similar tricycle landing gear configuration, but very different retraction mechanism for the main gear. ATR42 and Do228 present wider fuselage sections therefore the main gear is retracted toward the A/C symmetry plane, whereas P180 having a smaller fuselage cross section provide the main gear with a backward retraction mechanism that pivots the wheel around an axis which is not the longitudinal fuselage axis (Figure 1.3). In any case the nose landing gear present a forward retraction mechanism with the capability of turning the wheel of about 80°

For the smaller aircraft as P180 and Do228, whose dimensions are closer to Unifier19, nose gear present a double wheel configuration and a singe at the main.
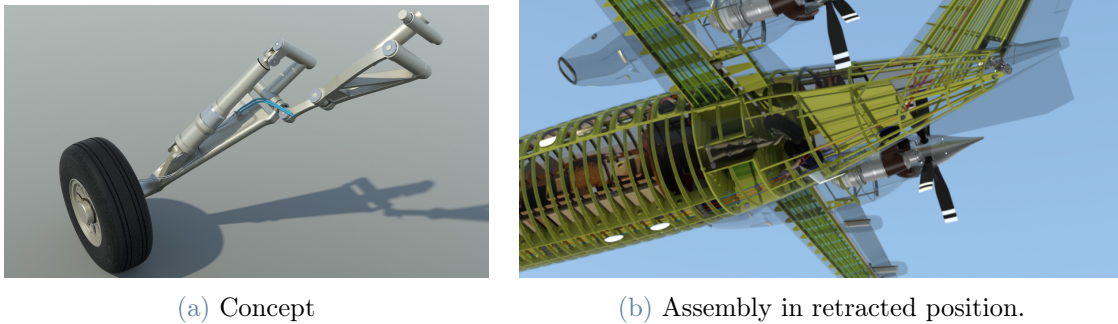
(a) Concept


(b) Assembly in retracted position.

Figure 1.3: P180 main landing gear design.

## 1.4.   Concluding remarks

The literature review performed had the objective of providing a good first hint on the airframe design that could be applied to Unifier19. However, given the radical new concept of C7HARW, is not necessary true that the solution developed in the previous years are valid for this application and if those are the best choice. Therefore the necessity to develop a tool and a methodology capable of quickly test different airframe solutions and configuration in a mid-fidelity approach.

The main scheme will be set as follow:

- Identification of critical cases

- Parametric GFEM model generation

- Analysis and results evaluation

- Sensitivity analysis on different parameters and optimization

# 2 | Research methodology

The non-conventional concept of the A/C under development leads to the necessity of design and analyze many different non standard structural configuration in order to find the optimal one, therefore is necessary to adopt a methodology that allows to make different changes to the model architecture in a quick and user-friendly way. The design process have been performed using the software CATIA for the geometrical design and Abaqus for FEM and analysis.

Being the objective of this research the preliminary structural configuration for Unifier, is necessary, before having any type of analysis, performing a input review, in which the concept of the aircraft is analyzed in detail and load assumptions are checked in terms of hypothesis and feasibility. The inputs are fully provided by PVS comprehensive of several data sheets on the load assumptions and the `OpenVSP` model developed in the previous months, Figure 2.1.
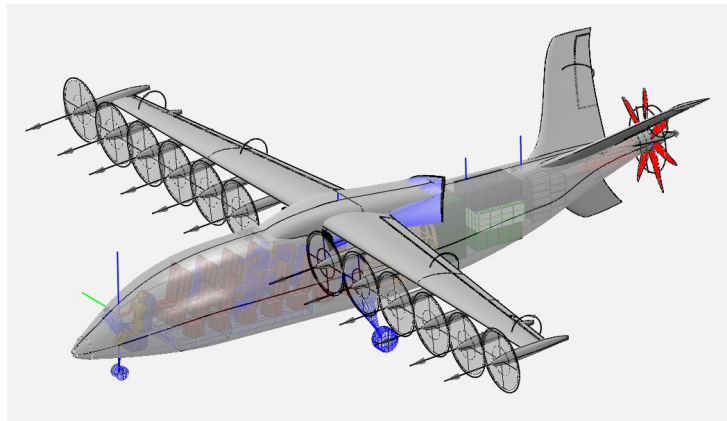


Figure 2.1: OpenVSP aerodynamic model.

The design process ave been performed in different fidelity approach, starting from an analytical approach to a detailed GFEM, using as inputs all the different load condition considered in Table A.2 for which the weight and balance configuration are reported in Table A.1. The analysis and sizing process considered the plane divided in three regions: main wing, fuselage and V-tail, sized individually and then joined together.

The steps of the procedure are:

1. Analytical beam model for main wing and fuselage with the objective to compute a first envelope of the internal forces in each load condition, and the reaction forces that the structure has to withstand.

2. Analytical connection design for the wing-fuselage and VT-fuselage assembly.

3. Parametric GFEM creation for Unifier19 airframe.

4. GFEM analysis

5. Fail-safeness prove of wing-fuselage connection lugs.

The details of each procedure step are reported in the next sections.

## 2.1.  Analytical beam model

Starting point for the airframe design process is a low fidelity analysis on the load cases and the flight condition that are expected in service. The load evaluation and computation are provided by PVS considering the flight envelope for the possible flight mission that are expected. The objective of this first analytical analysis is to have a good quantitative understanding of the forces and moments that the structure has to withstand and to define the envelope of internal forces.

To achieve this data is necessary to provide some hypothesis both on the load assumptions and in the beam model used, reported as follow, considering the coordinate reference system reported in Figure 2.2:

- **Load cases hypothesis:**
  - Neglect aerodynamic drag force effects
  - Lift is *always* parallel to $z$ axis, neglecting the effect of the angle of attack
  - Aerodynamic strip theory

- **Wing beam model hypothesis:**
  - Center of gravity of the section is located at the mean of the front and rear spars location.
  - Beam elastic axis is located in correspondence of the CG for the wing span
  - Cantilever beam, encastered in correspondence of the A/C symmetry plan.

    – Structural dynamic and aeroelastic effects are neglected

- **Fuselage beam model hypothesis:**

    – Free-free straight beam

    – Symmetrical structure

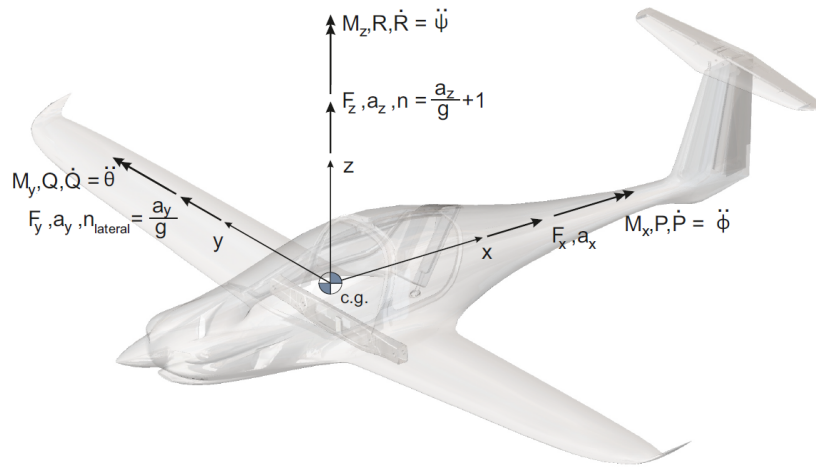    – Structural dynamic and aeroelastic effects are neglected



Figure 2.2: Global reference coordinate system.

By integration of the external forces using the equilibrium condition, the internal forces are computed along the length of both wing and fuselage for any load case. The result is the envelope of the internal forces from which is possible to find the most critical conditions. These load cases will be used to size the airframe in finite elements analysis.

## 2.2. Parametric GFEM creation

As explained in Section 1 to provide a good airframe design is necessary to develop a tool that enable the designer to test many different architectures in order to find the best one in terms of weight reduction using a mid fidelity global finite elements model.

This necessity is tackled by the development of a series of scripts that are able to generate, starting from the external aircraft loft and a few other inputs, the full finite elements model and the relative analysis producing directly the stress distribution on the airfare without any other operation needed to be done by the designer. To make the process

as straightforward as possible, the scripts are created in *Python* and executed directly in *Abaqus CAE*. The detailed steps implemented for the procedure follows:

1. **Input analysis:** As first step *external* loft is imported in Abaqus in `.CATPart` format and checked for any geometrical and numerical imprecision or invalid entities, if any issue is detected the part is repaired and converted to an analytical representation with the objective of start the process with the most precise component as possible.

   In this step the material library is imported and the inputs defined by the user are checked for any inconsistency, if none are detected the model creation procedure begins.

2. **Geometrical partitions:** The part imported at this point is just an uniform external shell without any division and other elements, so is necessary to partition the part in order to allow the possibility of defining different material proprieties to different section of the part. According to the inputs defined by the user, all the partitions are implemented creating both two dimensional elements, like wing ribs or fuselage bulkheads, and one dimensional element like stringers and fuselage frames. Moreover the model just created is saved. It is important to notice that the model at this point is just a geometrical part without any material propriety assigned.

   In Figures 2.3 the partitions done in this step for the fuselage are shown.



(a) Model imported                          (b) Model after step 2.
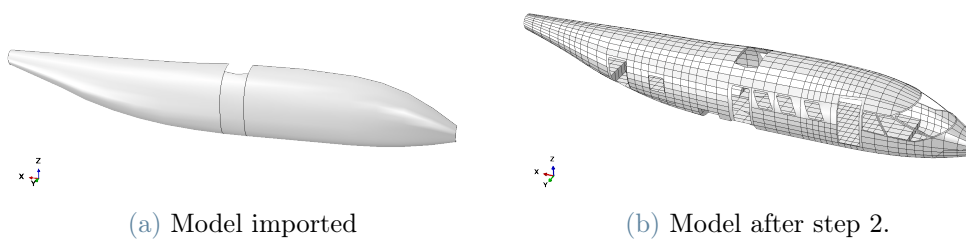
Figure 2.3: Geometrical model partitions for the fuselage.

3. **Faces and edges identifications:** In order to apply different material proprieties in a user-friendly way, is necessary to unequivocally identify each single shell face and stringer edge, naming those reporting in two `.csv` file: one for the bi-dimensional elements and one for the one dimensional ones. The user at this point edit the output `.csv` file by defining, for each single element the material and the relative thickness. In this way, if is necessary to change a given material or change the

thickness of some elements *without changing the airframe architecture*, the designer can simply load the model saved in the step before, change the proprieties interests and run the next sections of the script to have the stress distribution with different sectional proprieties.

4. **Section propriety assignment:** by reading the file mentioned above for both shell and beam elements, the sectional proprieties are assigned to the model. Consistent beam orientation and shell is applied to the one dimensional element considering the beam profile section offset with respect to the face it is in contact with, and shell elements normals are checked to avoid any errors or computational problems.

5. **Load(s) definitions:** The load condition that is wanted to be tested, defined by the user as input, is discretized and applied to the model. The loads considered for the analysis are aerodynamic lift, neglecting drag effects, and inertia forces applied as a load factor. Every payload element is modelled as a point mass.

6. **Boundary conditions definitions:** The boundary condition definition are parameters that are not possible to be modified by the user without direct action in the script.

7. **Mesh generation:** The mesh is generated considering limit in computational power available. Mesh controls are defined considering the application of a quadrilateral structured mesh where possible, the overall seeding part is defined by the user in the early project phases.

8. **Analysis:** Static and buckle analysis for limit and ultimate load are executed and the results are stored.

## 2.3.  Wing-fuselage connection

The definition of high-level subsystem is priority in the preliminary project because small changing in the connection system may have a big impact in the airframe design. The wing fuselage connection mechanism is based on a concept implement in ATR42 which is based in the development of two lugs and pin design. The design of the junction is performed in two consequent steps:

1. Analytical design

2. Fail-safeness modification and verification

### 2.3.1.   Analytical

A first analytical sizing process follows the sizing procedure reported in [8], for which a single non-fail safe lug is considered with a perfect axial force applied. The failure mode considered are:

- Net section tension

- Shear tearout

- bearing

where the last two can be condensed in a single shear-bearing failure. The allowable for each failure mode reads:

$$P_{bru} = K_{br} A F_{tu} \tag{2.1}$$

$$P_{tu} = K_t A_t F_{tu} \tag{2.2}$$

where $P_\bullet$ is the failure ultimate load, $A_\bullet$ is the resistant area, $F_\bullet$ is the ultimate strength of the material and $K_\bullet$ is a corrective factor accounting for the non uniform stress distribution across the resistant area for each failure modes. The subscript indicates the failure mode considered: $br$ for shear-bearing and $t$ for tensile. Following this analytical conditions, a `MATLAB` script is developed for sizing a single lug under axial force.

### 2.3.2.   FEM analysis and fail safeness

The junction sized analytically is then modelled using GFEM simulations in order to deeply understand the internal forces and, when proven, is possible to change the design in order to create a fail safe connection. A fail safe configuration for the wing-fuselage connection is mandatory in order to certify the plane, therefore is necessary to edit the design obtained from the analytical size and obtain a fail safe lug and prove its capability of withstand the load even in case of failure of a component. The fail-safe design is obtained by considering in the design a double configuration for each lug element. In this way the assembly is composed by two internals plate, each one capable of withstand the whole load, and two external ones. The connection is fixed in position using two concentric pins.

## 2.4.   Landing gear design

The definition of the landing gear is important in the first project phases because it can and will add constraint in the airframe model, therefore is necessary to develop a conceptual

design of that system. Starting from the landing gear track positions which have been defined in earlier project steps, the retraction system have been designed and analyzed. The landing gear development is considered only from a kinematic point of view, this analysis does not take into consideration any load applied to the system. The definition of the kinematic system have been performed first of all in an analytical approach, where the kinematic chain were modelled in MATLAB and then, when the concept is defined, the actual layout is designed in detail in CAD and assembled to checked for any clash or interference with other structural and non-structural elements. The CAD design is performed in CATIA V5 and the results in terms of the geometry are directly considered in the fuselage airframe architecture.

# 3 | Landing gears design

The design of the landing gear for a preliminary structural project is critical, in particular for a commuter type aircraft as Unifier19 is. The landing gear structure in terms of kinematic systems, positions and dimension provoke big impact in the conceptual airframe concept because many structural element have to be designed as function of the landing gear retraction systems. In particular the landing gear position, size and overall dimensions are driver to define the landing gears storing bay and openings which, being cutouts from a structural point of view, represent ares which are not available to place any structural element. Moreover being the gears big subsystem may interfere with other on boar equipment, these collisions must be highlighted and solved as soon as possible to not encounter bigger problems during the detail project phase, which became exponentially more difficult and require more cost for the project development. In conclusion the objective of the landing gear kinematics analysis and design is the definition of the PDR (Preliminary Design Review) which have the objective to define a feasible architecture configuration that may not be optimized but is a solution that satisfy all the requirements both in terms of strength and in terms of use and effectiveness of the solution.

To start the landing gear design procedure the first step is the definition of the global architecture producing as output the wheel ground position. This study based on an analysis of the center of mass of the whole plane have been provided by PVS. The outcome of the research is a standard forward tricycle with track length and wheel base equal to $4280mm$ and $6800mm$ respectively, with a consequent turnover angle of 50°. Due to the small dimensions of the A/C under development is has been chosen to use a single wheel configuration for the main gear, and a dual tween wheel for the nose gear. Starting from these input, the requirements and the kinematic development of the gears follow. It is important to notice that the development for both gears do not include considerations of the loads that are expected to be applied to the system, only a kinematic and a proof of concept for the retraction is provided.

The solutions proposed are based on use of hydraulic actuators, but in order to fit in *CleanSky2* policy into more electric aircraft, future development will consider and study

the implementation of system driven by electrical power based on skrewjack technologies.

## 3.1. Nose landing gear

To have a meaningful design of a given el-
ement, is necessary to define first of all,
the requirements and the constraints that
the element must obey. The nose landing
gear (N-LG) position, directly under the
cockpit, and below the avionic and instru-
ments area, must be as small as possible in
order to not interfere with the electric el-
ements inside the nose, the retraction sys-
tem has to include a single stage actuator,
to avoid reliability issues, and the landing
gear must be completed with a steering
system and a shock absorber. To accom-



Figure 3.1: Nose landing gear assembly.

plish these requirements, the landing gear
is composed by three sub elements, shown
in Figure 3.1:
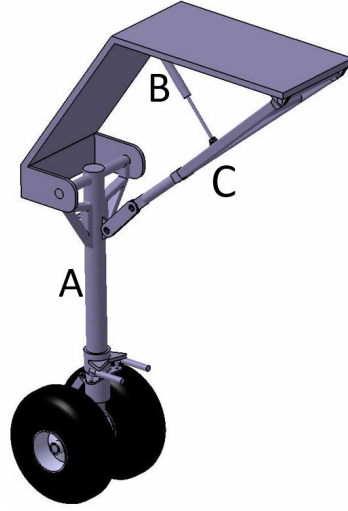
- *Main leg:* comprehensive of both the steering system and the damper (A).

- *Actuator:* the driver of the system (B).

- *Retraction kinematics chain:* the rod system that enable the leg to extend and
  retract (C).

### 3.1.1. Retraction system

The retraction system has to be as simple as possible to not increase the development and
production costs, to develop this concept a standard forward retraction system have been
considered. The system, shown in Figure 3.2 is composed by four rods hinged together
that, driven by an actuator pivots the whole wheel/leg assembly. The four rods positions
are defined as vectors, namely $\vec{a}$, $\vec{b}$, $\vec{c}$ and $\vec{d}$, whose movement can be analyzed by defining
a conventional Cartesian reference system with origin in the leg main hinge and $\hat{x}$ axis
toward the nose of the plane and $\hat{y}$ axis directed upwards. The kinematic chain is defined
by the equation:

$$a^{i\alpha} + b^{i\beta} = c^{i\gamma} + d^{i\delta} \tag{3.1}$$

which, considering Euler's formula $e^{ix} = cos(x) + i\sin(x)$ give a system of two non-linear equations:

$$\begin{cases} a\cos(\alpha) + b\cos(\beta) = c\cos(\gamma) + d\cos(\delta) \\ a\sin(\alpha) + b\sin(\beta) = c\sin(\gamma) + d\sin(\delta) \end{cases}$$

(3.2)

That, to be solved, require a maximum of two unknown terms. Moreover another requirement has to be defined: in extended position the rods $\vec{b}$ and $\vec{c}$ must present a relative orientation of about 180°, in order to fix the landing gear in position and avoiding any unintended folding. Considering this requirement, and hypothesizing the position $\vec{a} = \begin{bmatrix} x_A & y_A \end{bmatrix}$ and



Figure 3.2: Nose landing gear retraction system kinematic scheme.

$\vec{b} = \begin{bmatrix} x_B & y_B \end{bmatrix}$, is possible to define the sum length of rods $\vec{b}$ and $\vec{c}$, by hypothesizing the ratio between the two, the length of the four beams is properly defined. To solve the System 3.2 is necessary to define two angles, in particular, observing the system, is possible to notice that rod $\vec{b}$ is grounded i.e. does not move during the retraction movement, from which $\delta = const$ that, given the position, is easily computed. The rotation $\alpha$ instead is known, its initial position is obtained knowing $\begin{bmatrix} x_A & y_A \end{bmatrix}$ and, for the retraction, this is the degree of freedom of the movement, resulting the only unknown to be $\beta$ and $\gamma$. In Table 3.1 are reported the known and unknown terms for this analysis.

| | $\vec{a}$ | $\vec{b}$ | $\vec{c}$ | $\vec{d}$ |
|---|---|---|---|---|
| $\lVert \bullet \rVert$ | ✓ | ✓ | ✓ | ✓ |
| $\angle \bullet$ | DoF | ✗ | ✗ | ✓ |

Table 3.1: Nose landing gear retraction system kinematic degrees of freedom.

To fully retract the landing gear, the rotation angle of the leg must be 112°. Solving the system 3.2 for $\alpha = 0° \ldots 112°$, the envelope of the position of each rod is defined. A MATLAB script have been used to solve this systems and the envelope of the positions is obtained. Following an euristic approach for which the parameters were changed and

(a) Retraction positions envelope.



(b) Actuator excursion during retraction movement.

Figure 3.3: Nose landing gear kinematic system.

the envelope of the position have been analyzed, the final dimension of the mechanism have been defined. In Figure 3.3a the envelope of the position computed in MATLAB is shown for the final sizing.

Last item to be designed for complete the N-LG retraction system is the actuator position. To reliability issue is mandatory to use a single stage actuator for which the position must be defined. Knowing the envelope of the positions, is possible to define the actuator hing point on the ground $\vec{e} = \begin{bmatrix} x_E & y_E \end{bmatrix}$ and the connection point to the rod $\vec{c}$. Inreference as Figure 3.4, using an approach analogue to the closure kinematic chain equation done for the retraction system, the envelope of the position can be defined. In this case the closure equation reads:



Figure 3.4: Nose landing gear actuator system scheme.

$$e^{i\epsilon} + f^{i\psi} + g^{i\gamma} = 0 \qquad (3.3)$$

where $\gamma$ is the phase of vector $\vec{c}$. Therefore is possible to compute the phase and length of the actuator $\vec{e}$, considering $\vec{f}$ grounded, so fixed during the movement. The degrees of freedom in this analysis are reported in Table 3.2. The envelope of the positions have been analyzed and the final position of the actuator is obtaining by considering that the length when extracted must be not more that twice the length when the mechanism is

retracted. The length of the actuator, as function of the retraction angle $\alpha$ is shown in Figure 3.3b.

|  | $\vec{e}$ | $\vec{f}$ | $\vec{g}$ |
|---|---|---|---|
| $\| \bullet \|$ | ✗ | ✓ | ✓ |
| $\angle \bullet$ | ✗ | ✓ | DoF |

Table 3.2: Nose landing gear actuator system kinematic degrees of freedom.

As result of this process the dimensions and positions of the retraction system elements are found, using this data the CAD model of the landing gear is generated in CATIA V5.

### 3.1.2. Damper and turning system development

The retraction system just developed does not depend neither on the damping system of the gear neither on the steering system being those two elements rigid to the leg.

Being Unifier19 a commuter with the objective to have ta capability to operate in unprepared runways, is necessary to have a high performance steering system that allows the possibility of performing thigh turns, for this reason the steering system have the objective to turn the nose wheel up to 80°. This system must be compatible with the shock absorption movement of the lower part of the leg. In particular the leg is composed by a fixed cylinder



Figure 3.5: Nose landing gear steering system scheme.

in which an internal one can both move up and down (damping movement) and rotate (steering). Inner cylinder is connected to the other using two actuators that with their movement rotate the wheel. The designing process of the steering system focuses on find the actuators dimensions and hinge position both in A and B. To find these unknown a kinematic approach have been followed considering the symmetry of the problem. Considering the vector projection in the $\hat{x}$-$\hat{y}$ of Figure 3.5, the kinematic system to be solved is:

$$a^{i\alpha} + b^{i\beta} + c^{i\gamma} = 0 \tag{3.4}$$

In this case the parameter of the design are the initial position of the two hinges, and considering the degree of freedom the rotation of vector $\vec{c}$, being imposed, is possible to solve the kinematic system considering the unknowns in Table 3.3. Once the system is

solved for any turning angle, is possible to analyze the envelope of the positions and the actuator length during the movement. The elements checked are:

1. Collision and interference between the actuator and the leg cylinder

2. Length of the actuator that needs to be compatible with a single stage actuator

3. Arm of the actuator useful for the movement

|  | $\vec{a}$ | $\vec{b}$ | $\vec{c}$ |
|---|---|---|---|
| $\| \bullet \|$ | ✓ | ✗ | ✓ |
| $\angle \bullet$ | ✓ | ✗ | DoF |

Table 3.3: Nose landing gear steering system kinematic degrees of freedom.

Tuning properly the positions of the hinges is possible to satisfy properly conditions 1. and 2., but using only one actuator is noticed, as expected, that the efficiency of the actuator drops to zero for a wheel angle of $\pm 20°$, this leads to the necessity of use a second actuator, symmetrical to the first to avoid the dead position. As shown in Figure 3.6c the use of two actuators solve this issue being always one of the two, in the worst case condition, that is able to turn the wheel. Developing this subsystem in CAD eventual collision with the landing gear structure are searched and the proof of the concept is verified.
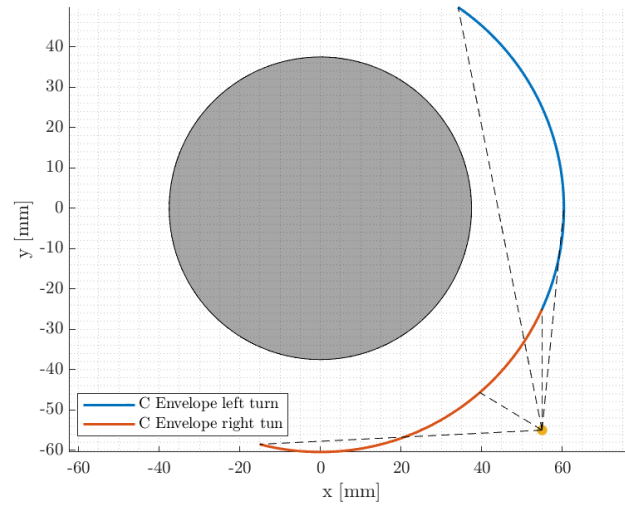
(a) Steering position envelope
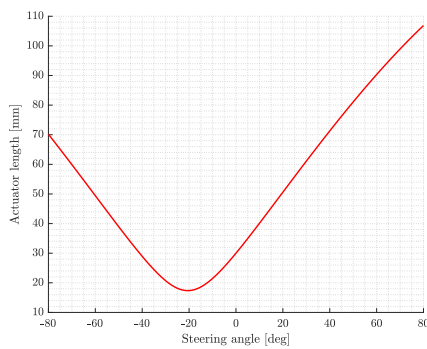


(b) Actuator length in steering motion.
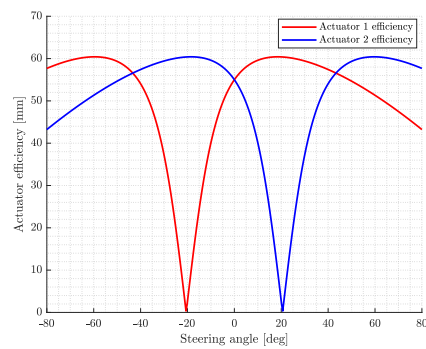


(c) Actuator efficiency in steering motion.

Figure 3.6: Landing gear steering system kinematics scheme.

The last element present in N-LG is the torsion mechanism, this one in particular does not impact directly the kinematics of both steering and retraction systems but is necessary to be designed in order to prove the capability of fitting a system like that. the steering system is necessary because it withstand the transversal loads that may be encountered during ground operations, avoiding the force to be transmitted directly to the steering actuators with failure possibility This system is compatible with the damping movement and it follow rigidly the when when turning. In Figures 3.7 the landing gear is shown in extended and retracted positions, and in Figures 3.8 a focus on the steering system is shown, where is possible to identify the dead position (when one of the two actuators is characterized by null efficiency).

(a) Front view, extended.

(b) Side view, extended.
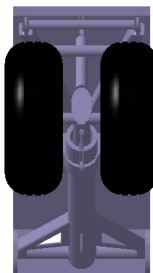
(c) Front view, retracted.
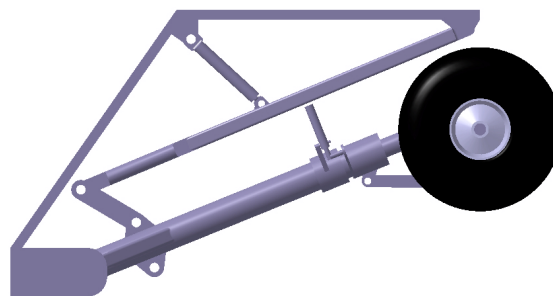
(d) Side view, retracted.

Figure 3.7: Nose landing gear assembly.

(a) Central position.  (b) Dead right position.  (c) Maximum right steering angle.
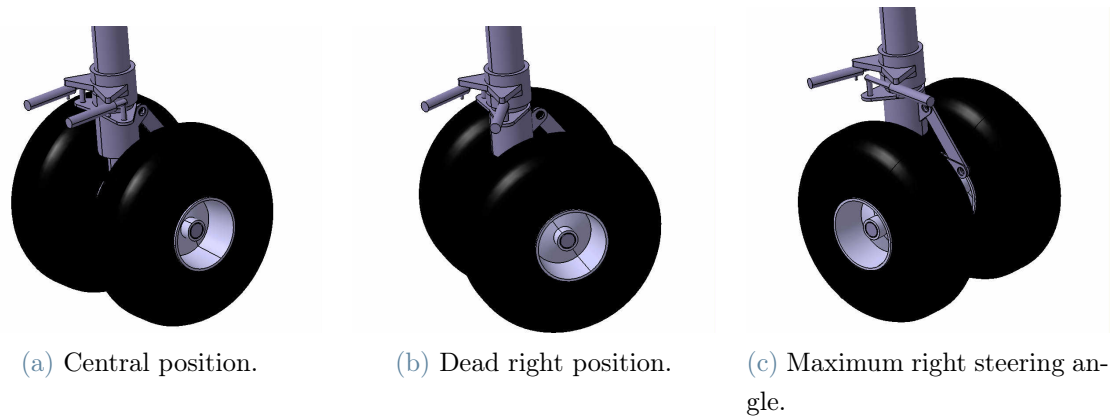
Figure 3.8: Nose landing gear steering assembly.

## 3.2.  Main landing gear

The definition of the main landing gear architecture and retraction system is very important for the whole development, in particular because of the few volume available for this subsystem in the fuselage, being it vastly occupied by batteries, electric system and liquid hydrogen tank. The first step for the retraction system definition is the choice of developing a forward or rear retraction system. This choice is based on volume consideration: as shown in the conceptual spacing diagram (Figure 3.9a) is not possible to have a forward retraction system because it would be necessary to move the batteries and the air conditioning system producing an enormous effect on the center of gravity position which is not feasible. Therefore a rear retraction system is necessary to be implemented. As reference for the kinematic design the landing gear of Piaggio P180 and Dornier Do228 are taken into consideration. The concept used in Do228 consists in a landing gear that pivots around the A/C longitudinal axis folding the main landing gear leg toward the central section of the fuselage. This concept is not applicable to Unifier19 because the fuselage section is too narrow for storing both wheels, therefore a concept like the one used in Piaggio P180 have been developed. In this approach the landing gear do not pivot around the plane longitudinal axis but around an axis which is rotate from the vertical one, in this way is possible to retract the wheel to the back, where there is more volume available. Designing a landing gear with the same concept of P180 however end up in interference problems between the wheel and the liquid hydrogen tank, as shown in Figure 3.9b. Modify the tank shape might not be a good solution because it add much complexity to the whole system and add the manufacturing costs, therefore the decision of creating a from scratch a kinematic chain capable of tilt the wheel during the retraction movement using only one degree of freedom in order to not create any reliability issue

(a)                                                                (b)
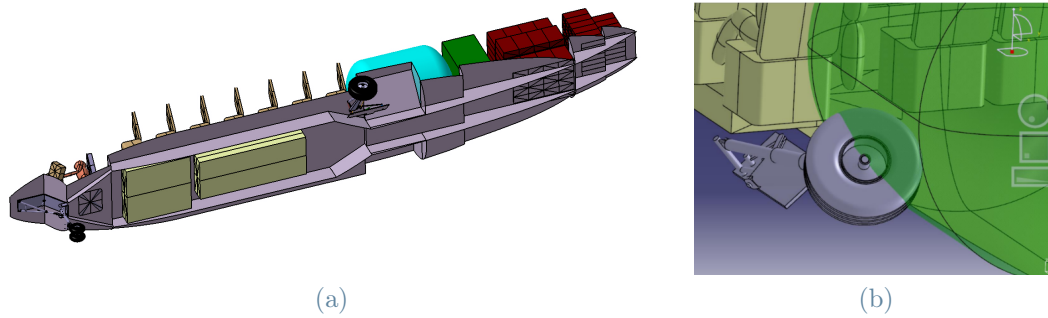
Figure 3.9: Main landing gear volume interfaces with other subsystem.

with the presence of more actuator than necessary. Meanwhile is not possible to retract the landing gear by a lower angle because it would be necessary to use an external fairing which vastly reduces the aerodynamic performance. This system must be compatible and allow vertical movements for the shock absorption mechanism.

The elements that compose the landing gear assembly are:

1. *Leg:* main landing gear structure

2. *Damper:* providing shock absorption capabilities

3. *Stopping system:* high-strength system that fixes the landing gear in extended position avoiding any damage to the actuator in case of big impact with debris on the runway.

4. *Leg-wheel motion coupling system:* kinematic system compatible with rotation due to shock absorption movements.

5. *Actuation system:* driver of the whole system.

The angle of rotation of both wheel and main leg, using a trial and error procedure these angle have been defined to be 93° for the leg rotation and 70° for the wheel.

First step for the design process is the definition of the main retraction system, the one that pivots the main landing gear and allow for the shock absorption movement. In Figure 3.10 the assembly is shown, together with the main axis of rotation (1) and the axis around which the shock absorption movement is allowed (2). In particular axis 1 is rotated with respect to the vertical $\hat{z}$ axis of 55° and, axis 2, in extended position, is parallel to the longitudinal plane axis. The damper is hinged to both the leg and the main axis of rotation.

The wheel pivoting mechanism is composed by two beams hinged together as shown in
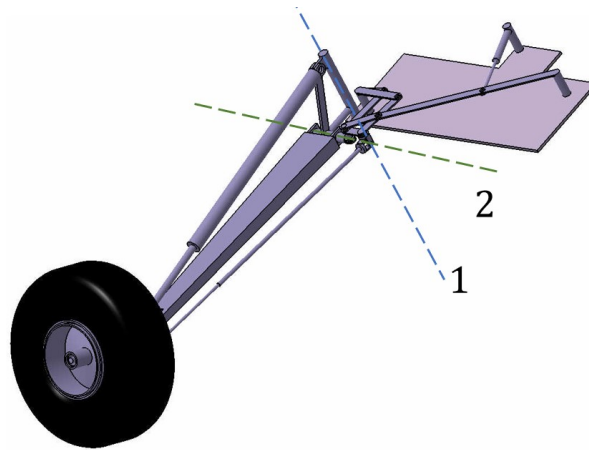
Figure 3.10: Man landing gear assembly axis of rotation.

Figure 3.11a, this movement must be coupled with the leg retraction movement in order to define a system with only one degree of freedom and avoid the use of a second actuator.



(a) Detail wheel view.



(b) Coupling mechanism.



(c)
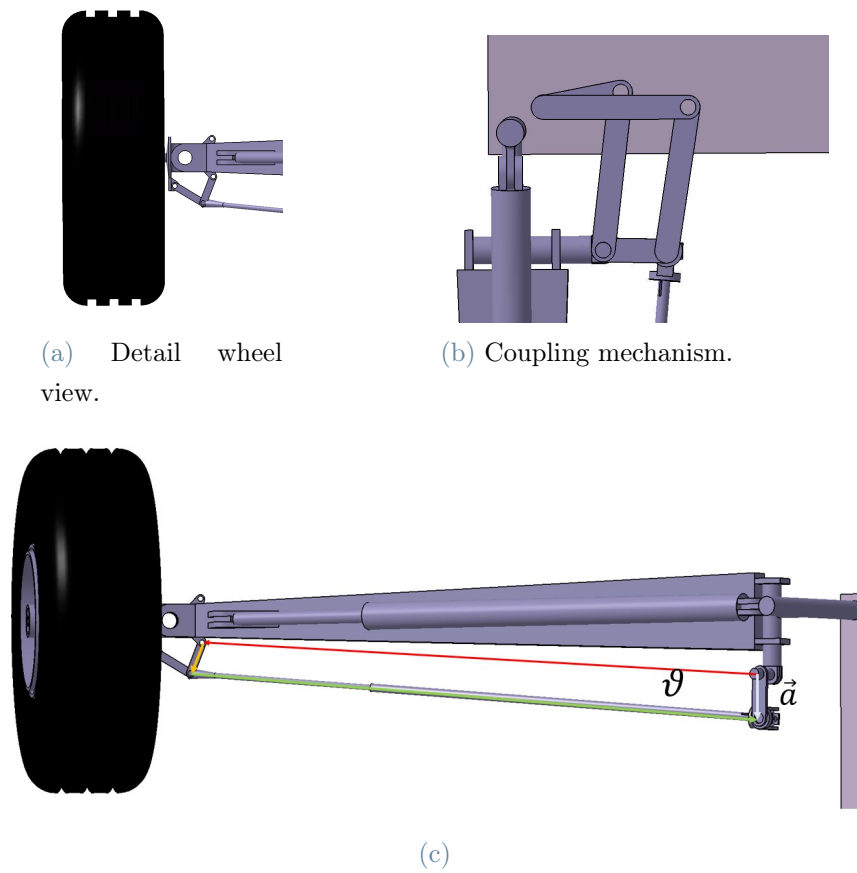
Figure 3.11: Wheel pivoting mechanism.

To couple the movement between the the wheel and the main retraction system is neces-
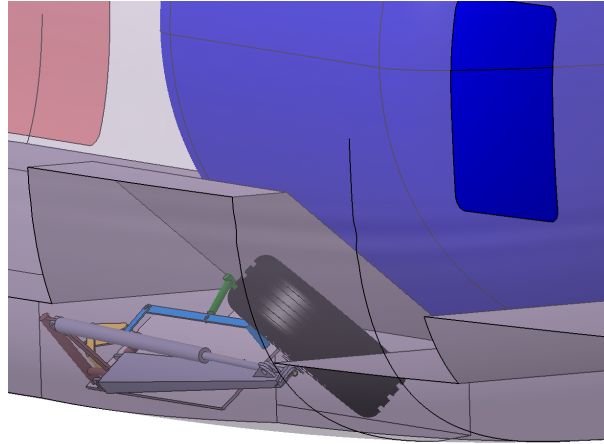
Figure 3.12: Main landing gear retracted position with respect to other plane subsystems.

sary to design a kinematic chain composed by four rods, sh shown in Figure 3.11c with the arm length are tuned properly to have a wheel rotation of 70°. However the global system as it is have 2 degrees of freedom: main leg rotation ($\vartheta$) and rod $\vec{a}$ rotation, considering the length of systems fixed. In order to have a one degree of freedom system is necessary to couple those movements. The coupling mechanism concept is shown in Figure 3.11b. It is composed by five rods, two are grounded and the other are hinged together. This concept presents 15 degrees of freedom and 14 constraints: $2n$ given by the grounded hinges and $2(n-1)$ for the internal ones, where $n$ is the number of beams that a single hinge connect. Using this system the wheel pivots during the retraction movement, storing in a position which does not have any interference with neither the fuselage or the liquid hydrogen tank, Figure 3.12.

A further constraint on the system is that it must allow the shock absorption movement when the landing gear is extend. This results is a imposition on the initial position of point A, that must lie on the axis (2). In order to allow the rotation in each direction, the rod connecting the base of the system with the wheel must have a spherical joint at the lower end, and a cardanic joint in the other end.

The length definition of each element is performed by solving the kinematic equations in MATLAB from which eventual interference and small modification have been performed developing the CAD model.

The last two elements to be designed are the stopping system and the actuator. The stopping system is designed to withstand and transmit all the horizontal loads generated in the take off and landing and fixing the gear in position to not be folded by error. The stopping system and the actuators are shown in Figure 3.13 and, using the same concept developed for the nose landing gear, the actuator of the whole system is located in the

upper frame in a position in which allow the possibility to use a single stage actuator. The positions of the main pivoting point, of the actuator and of the stopping system ground position, are located to be close to one fuselage frame allowing the possibility of connect those points to strong structural element.

In Appendix B the drawing for the main landing gear are presented.
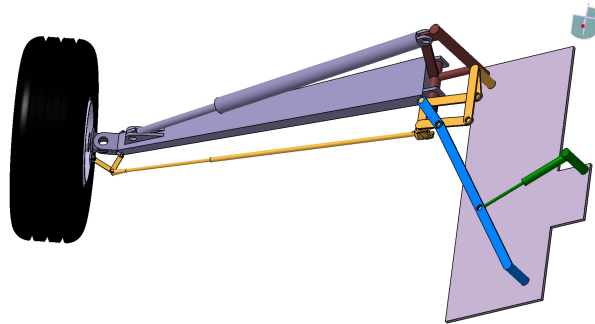


Figure 3.13: Main landing gear assembly.

# 4 | Main wing design

As descried in section 2, the wing design is performed following two steps that follows.

## 4.1.  Wing beam model

For the airframe sizing is necessary first of all to identify which are the most demanding load conditions that are expected in service, to achieve this data is necessary to have a first level internal forces envelope for the most relevant points in $V - n$ diagram. Therefore is necessary to develop a toll capable of quickly processing all the 32 load cases provided by PVS. Therefore an analytical beam model have been developed in MATLAB in which the wing is considered as a beam encastered in the A/C symmetry plane, it is important to notice that being the encasterd the *only* constraint, the structure is isotatic, allowing the computation of the internal forces without making any hypothesis on the material used in the wing. For the beam analysis is necessary to define the wing elastic axis position and direction so the position of rear and forward spar have been hypothesized to be at a constant chord position, and the EA is considered to be in the mean points of the two spars, obtaining a geometrical locus not perfectly perpendicular to the aircraft symmetry plane.

The hypothesis for this model follows

- Aerodynamic lift is located in the vertical direction, neglecting the deviation caused by the angle o attack.

- Aerodynamic drag is negligible.

- Aeroelastic effects and structural dynamics is neglected.

The external forces applied to the structure therefore are:

1. Lift, provided by the load assumption department in PVS expressed in force per unit of length spanwise.

2. Engines inertial loads for both engine body and propeller.

3. Structure inertial load.

Not having any data on the wing structure mass, a uniform mass per unit of area distribution have been hypothesized to be

$$m_{ws} = 25 \ \frac{kg}{m^2} \tag{4.1}$$

By integration of the external forces imposing the equilibrium of each section, the internal forces have been computed. The integration have been performed numerically dividing the wing span in 20 elements. Being the lift given per unit of length, is necessary to discretize the distribution applying the trapezoidal integration technique. Wing mass internal load is computed by calculating the mass of the *i-th* section as:

$$m_i = m_{ws}c(y_i)\Delta y_i \tag{4.2}$$

where $c(i)$ is the chord length and $\Delta y_i$ is the element length. In Figures 4.1 the wing planform scheme for load cases LC1, LC2, LC3 and LC4 is shown, elastic axis, center of gravity and location of engines and propeller are shown. In particular is possible to notice the center of pressure spanwise envelope for each load case. The reference system for this analysis is defined as follow:

- Origin in the wing elastic axis.
- $x$-axis positive backwards (as free stream velocity)
- $y$-axis coincident with the elastic axis.
- $z$-axis orientated in such a way to generate a right-handed reference system.

Therefore the forces and moments sign convection reads:

- Shear force $T_z$ positive for positive lift.
- Bending moment $M_x$ positive as wing is bent upwards.
- Torsional moment $M_y$ positive as LE moving up.

(a) LC1

(b) LC2

(c) LC3

(d) LC4
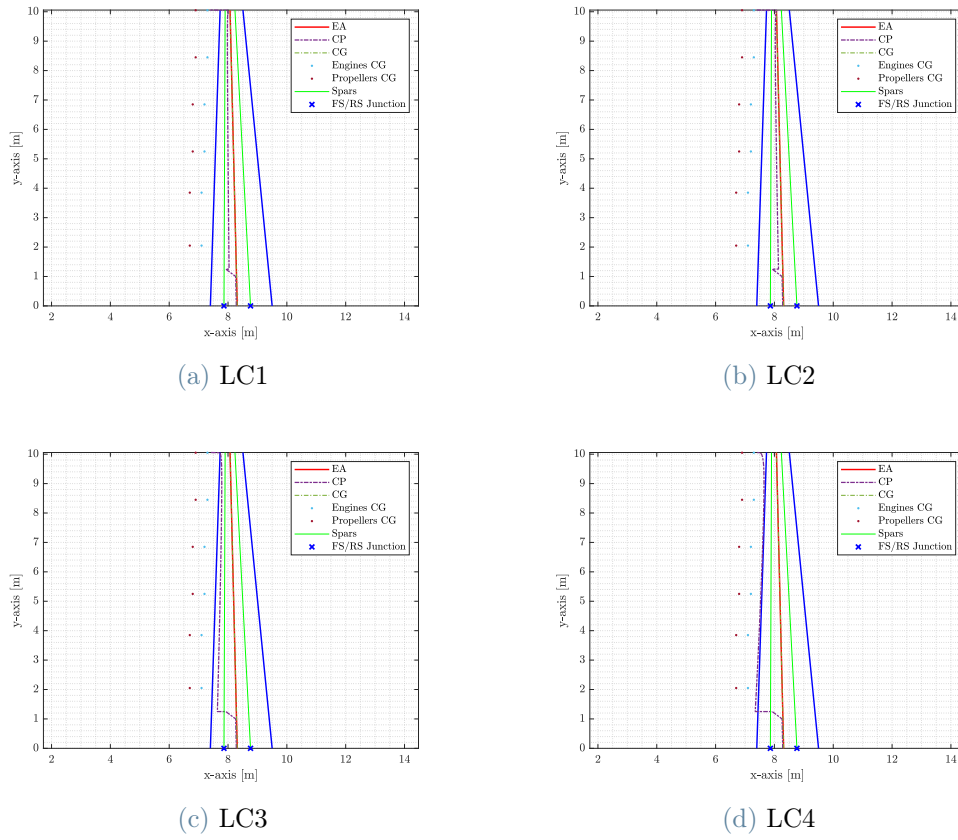
Figure 4.1: Wing planform scheme.

The internal forces analysis have been computed for all 32 load cases and the envelope of the internal forces is defined, from which the most critical load cases are identified in any node. In Figures 4.2 the envelope diagrams for torsion, bending and shear are shown, in Table 4.1 those numerical data are reported.

| $y$ | $T_z$ min | | $T_z$ max | | $M_x$ min | | $M_x$ max | | $M_y$ min | | $M_y$ max | |
|---|---|---|---|---|---|---|---|---|---|---|---|---|
| [m] | [kN] | LC | [kN] | LC | [kNm] | LC | [kNm] | LC | [kNm] | LC | [kNm] | LC |
| 0.00 | -39.24 | 3 | 103.59 | 2 | -165.77 | 3 | 437.83 | 2 | -22.58 | 4 | 16.13 | 1 |
| 1.00 | -33.90 | 3 | 89.52 | 2 | -129.21 | 3 | 341.30 | 2 | -22.41 | 4 | 15.69 | 1 |
| 2.05 | -28.52 | 3 | 75.32 | 2 | -96.45 | 3 | 254.81 | 2 | -18.41 | 4 | 12.31 | 1 |
| 2.90 | -24.47 | 3 | 64.64 | 2 | -73.89 | 3 | 195.22 | 2 | -15.00 | 4 | 10.11 | 1 |
| 3.75 | -20.48 | 3 | 54.11 | 2 | -54.79 | 3 | 144.78 | 2 | -11.85 | 4 | 7.75 | 1 |
| 5.00 | -15.12 | 3 | 39.94 | 2 | -32.52 | 3 | 85.96 | 2 | -8.07 | 4 | 5.14 | 1 |
| 5.80 | -11.99 | 3 | 31.69 | 2 | -21.67 | 3 | 57.29 | 2 | -6.11 | 4 | 3.87 | 1 |
| 6.80 | -8.25 | 3 | 21.83 | 2 | -11.57 | 3 | 30.61 | 2 | -3.91 | 4 | 2.15 | 1 |
| 7.80 | -5.06 | 3 | 13.31 | 2 | -4.90 | 3 | 12.98 | 2 | -2.28 | 4 | 1.13 | 1 |
| 8.55 | -3.02 | 3 | 8.00 | 2 | -1.92 | 3 | 5.10 | 2 | -1.35 | 4 | 0.64 | 1 |
| 9.30 | -1.20 | 3 | 3.18 | 2 | -0.36 | 3 | 0.96 | 2 | -0.51 | 4 | 0.06 | 1 |
| 10.00 | -0.31 | 25 | 0.13 | 28 | -0.02 | 25 | 0.01 | 28 | -0.41 | 26 | 0.14 | 27 |
| 10.05 | 0.00 | 1 | 0.00 | 1 | 0.00 | 1 | 0.00 | 1 | 0.00 | 1 | 0.00 | 1 |

Table 4.1: Numerical data for internal forces envelope for main wing.

(a) Torsion moment.



(b) Bending moment.



(c) Shear force.
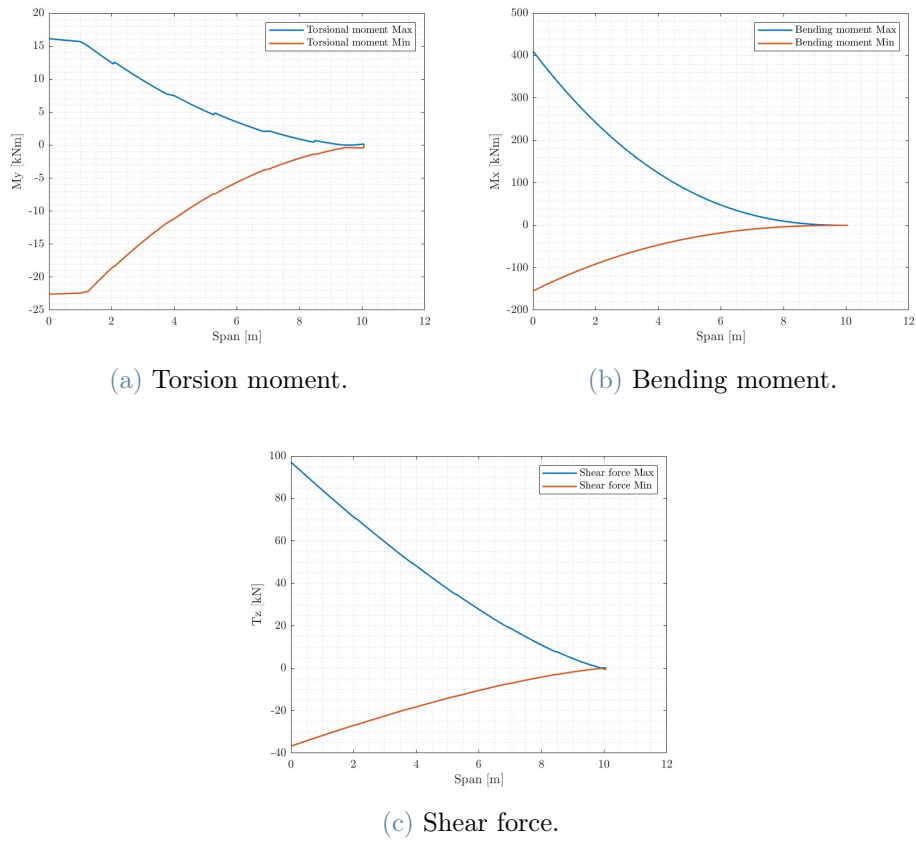
Figure 4.2: Wing internal forces envelope diagram.

The critical cases for the wing have been noticed to be LC1, LC2, LC3 and LC4. In all these flight condition the weight and balance configuration define the plane to be at maximum weight with the position of the center of mass as forward as expected. In particular LC1 and LC2 are representative of a pull up at load factor 3.01 at both designed maneuvering speed and maximum speed planned to reach in flight test. LC3 and LC4 are representative of a flight condition with the same characteristics but with a diving maneuvering at a load factor of -1.20. The internal forces diagrams for these load condition are shown in Figures 4.3

These will be the load condition that will be used in the detailed FEM analysis.
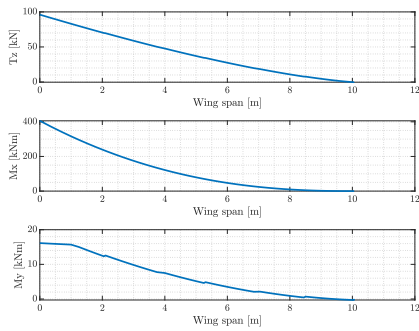
(a) LC1　　　　　　　　　　　　　　　　(b) LC2
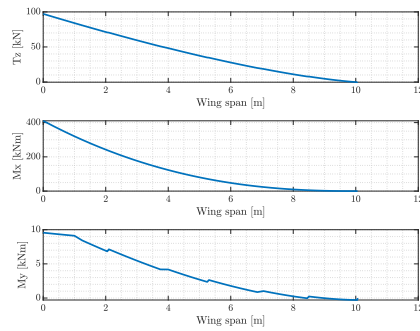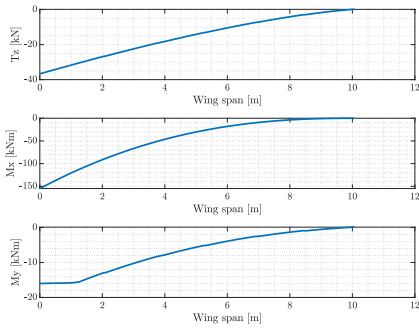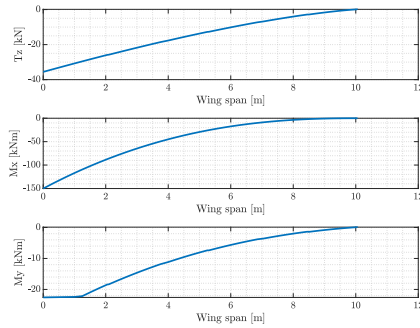
(c) LC3　　　　　　　　　　　　　　　　(d) LC4

Figure 4.3: Wing beam model internal forces for critical load cases.

## 4.2.   Wing structure

Unifier19 presents a relatively simple aerodynamic wing configuration: it is composed by a single, tapered unswept wing, the total wing span is $20.10m$ and the projected area is $28.9m^2$, the detail data for the wing dimensions are reported inn Table 4.2. The big innovation presented in Unifier19 is the presence of six wing engines (DEP) that provide extra lift when is needed by the flight condition, this aspect imposes directly a strong requirement on wing ribs position.

| AR | 7.0 |
|---|---|
| **Span** | $10.457\,m$ |
| **Area** | $14.45\,m^2$ |
| **Taper** | 0.36834 |
| **MAC** | $1.43676\,m$ |
| **Root chord** | $2.100\,m$ |
| **Tip chord** | $0.774\,m$ |
| **Dihedral** | $-3.0°$ |
| **Twist** | $-2.0°$ |

Table 4.2: Wing platform data relatively to one semi-wing.

The simple planform configuration allow the application of a standard wing box design, composed by two spars running parallel to both leading and trailing edge, several ribs parallel to the free stream velocity and stringers in pressure side and suction side that increase the buckling resistance of the skin. This simple concept however must satisfy the requirements that are imposed first of all by the DEP presence and then by other aspects which description follows:

- To withstand and transmit efficiently the thrust and gyroscopic loads produced by the DEP in any flight condition, it is necessary to fix a strong rib in correspondence of *each* engine.

- The root location of each spar must be perpendicular to the A/C symmetry plane in order to allow for an easy to manufacture wing-fuselage connection, for the other span-wise location the spars are located at a constant chord percentage.

- The tapered configuration of the wing imposes the necessity of having some stringers to be in run out, not being enough space to connect every stringer to the last rib.

- One strong rib must be located in the point where the main lugs connecting wing and fuselage are located.

- One strong rib must be located in correspondence of the connection between the wing skin and the external upper fairing.

According to these requirements the, a first airframe model is obtained by using the script as described in Section 2.2. The inputs used for the wing design scripts follows:

- Position of the fixed ribs location i.e. DEP $y$-coordinates.

- Position of strong rib for wing-fuselage connection.

- Position of rib connecting the wing with the fairing.

- Number of stringers in both pressure and suction side.

- Front and rear spars root and tip position, expressed in chord percentage.

- Front and rear spars flange dimension for both pressure and suction side.

- Front and rear spars flange dimension for root and tip location, assuming a linear variation.

- Reference ID for the load cases to be tested and choice for limit or ultimate load analysis.

In this first model the spars are located at 25% and 65% in chord respectively, the front spar location have been chosen to be in correspondence of the aerodynamic center, obtaining in this way due to the unswept wing characteristics, a perfectly straight spar which ease the manufacturing process. The rear spar has been located at 65% chord in order to keep enough room for the control surfaces and its actuators. Rear spar is composed by two straight sections, the first, perpendicular to the aircraft symmetry plane, and the second parallel to the wing trailing edge. The exact location of the spars is shown in Figure 4.4. The spar height occupy the whole wing box height and the flanges have been designed to be $5cm$.

As mentioned above, in the wing structrue eight ribs have a fixed position: six are located in correspondence of the engines, one is located in the lugs connecting wing and fuselage and the last one is positioned at the point where the leading edge is connected to the fairing. All these regions are location in which a stress concentration is expected, therefore the presence of a structural element is mandatory. The other ribs present a uniform spacing of $0.53m$ for a total of 20 ribs span wise. In the leading edge is possible to reduce the spacing in order to provide extra strength in case of an impact, but at this point the spacing have been considered equal to the spacing of the main ribs. The strength for impact condition can be increased by increasing the thickness of the shell in the leading edge reinforcement area.

To satisfy the bucking condition the presence of stringers both in pressure and suction side is necessary, the tapered wing plan form prevent the possibility to have the stringers running from the root to the tip, therefore is necessary to consider the



Figure 4.5: Wing stringers runout.
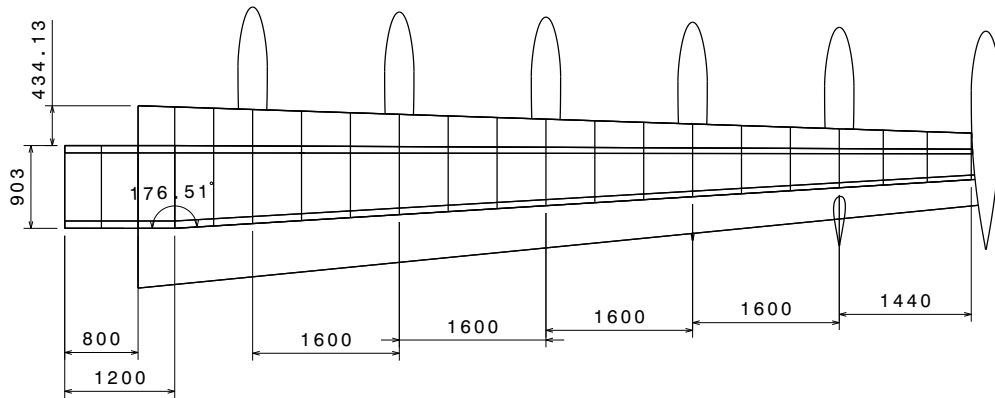
Figure 4.4: Main wing ribs and front, rear spars position. Top view, dimensions in [$mm$].

stringers runout. In detail the stringers in bot pres-
sure side and suction side are equally spaced an all
parallel to the leading edge, some stringer in this configuration would intersect the rear
spar so is necessary to stop those in the proximity of the spar in a given shell point as
shown in Figure 4.5. For this preliminary project the stringer spacing is constant of $9.5cm$
for both pressure and suction side allowing to the presence of seven stringer in both sides.
PS and SS stringer have different beam profiles: PS has a -shape and SS -shape, this
account for the different load condition that the wing shell is subject to, in particular
pressure side is in tension whereas suction side is in compression. Both profile types have
a flange-to-web ratio of 0.3 in order to account for fatigue condition.

In Figures 4.6 the wing box is shown, together with all the elements that can be modified,
in terms of material selection, thicknesses and proprieties, shown in different colors. The
material distribution used for the following analysis is shown in Figures 4.6b and 4.6c
with the color legend reported in Table 4.3.
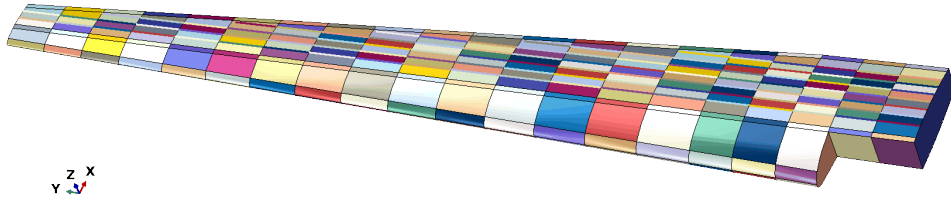
(a) Wing sectional elements.
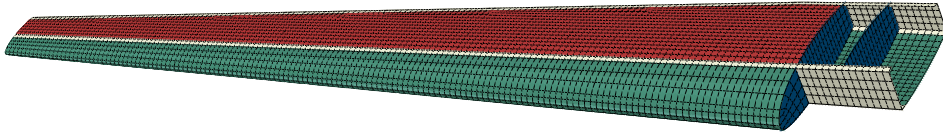


(b) Wing material shell assignment.
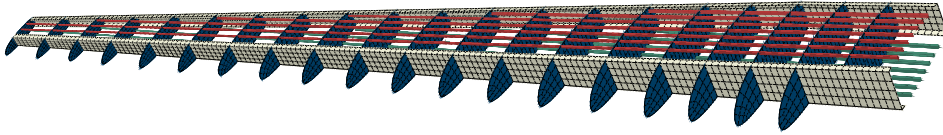


(c) Wing material stringers assignment

Figure 4.6: Wing material structure.

## 4.3.  Material selection

For the conceptual development of Unifier91 airframe only standard alloys have been
considered. In particular the material selection have been done considering the standard
material in common use in aeronautical applications and by considering the different
requirements in terms of failure modes that are characteristic for each wing section. The
choice have been done by considering the materials reported in Table 4.3.

| | $\rho \left[\frac{kg}{m^3}\right]$ | $E\ [GPa]$ | $\nu\ [-]$ | $\sigma_y\ [MPa]$ | **Legend** |
|---|---|---|---|---|---|
| **Al-2024-T351** | 2768.00 | 74.466 | 0.33 | 330.96 | |
| **Al-7010-T7651** | 2823.36 | 71.708 | 0.33 | 455.07 | |
| **Al-7075-T651** | 2795.68 | 72.397 | 0.33 | 475.76 | |
| **Al-7075-T7351** | 2795.68 | 72.053 | 0.33 | 393.02 | |

Table 4.3: Weight material proprieties.

Given the high toughness of the Al-2024, its application is suggested in wing pressure side which, in nominal condition, is in tension and in the leading edge that the high toughness increase the structure response in case of impact with debris, bird strike and even a propeller blade failure. regarding the damage tolerance of the leading edge, its section is made of the same material both in pressure side and suction side allowing the possibility of manufacture the leading edge in one single part, avoiding any kind of junction and increasing furthermore the impact resistance. The analysis presented in this thesis however do not account for any failure mode in impact conditions. Being the spars the two main structural elements in the wing, it is necessary to use a material that provide a good combination of high strength, high resistance to stress-corrosion cracking and good fatigue toughness, Al-7010 is a good material choice. The high strength of Al-7075 alloys convey its application in ribs and wing pressure side. The stringers in pressure side and suction side are made of the same material used for the wing skin in order to not increase furthermore the production costs.

In order to perform meaningful simulations and to stay in compliance with CS-23 regulations, it is necessary to model the material proprieties accounting for the plasticity behavior. The plasticity model used in the following steps is based on the *Ramberg-Osgood relation* that reads:

$$\varepsilon = \frac{\sigma}{E} + K \left( \frac{\sigma}{E} \right)^n \tag{4.3}$$

where $K$ and $n$ are constants that depend on the material. The actual model implemented in Abaqus CAE is obtained by a modification in Rangar-Osgood relation that reads the strain curve as:

$$E\varepsilon = \sigma + \alpha \left( \frac{|\sigma|}{\sigma_0} \right)^{n-1} \sigma \tag{4.4}$$

Is is important to notice that the term $n$ in equations 4.3 and 4.4 is different.

## 4.4. Load direcretization and boundary conditions

The load discretization is one of the steps that are necessary for running the simulations. The discretization process is composed by two steps:

1. Discretize a continuous lift distribution in concentrated forces to be applied to FEM

2. Apply the concentrated forces in a way that does not result in a concentrated stress distribution.

First step of the discretization algorithm is the definition of wing section along which the lift is discretized, the wing have been divided in nine section delimited by the fixed

ribs i.e. the engine ribs (fixed by the engine positions) and the ribs corresponding to the wing-fuselage attachment points and the ribs relative to the connection between the wing skin to the fairing, both of these position are defined by the user as input to the script. A MATLAB script reads the lift distribution for each load case and, by trapezoidal integration technique, the lift generated by each section is computed. Reducing the lift per unit of length to a series of concentrated forces is important to apply the forces in such a way that the bending moment is reproduced correctly. For this reason the span location of the lift for each section is computed considering the equilibrium of the section for bending moment. To represent the torsional moment, the lift is considered to be applied in the center of pressure location in correspondence of the span wise position of the force. In order to account for a non equal lift generation for pressure and suction side, is possible to share the force between PS and SS by defining a percentage. A output of this process a table in `.txt` file is generated for each load cases containing the data for the disretization process, as example one of these is reported in Table 4.4.

| **Load factor** | 3.01 | | |
|---|---|---|---|
| **Vertical force** $[N]$ | $x_{CP}$ $[mm]$ | $x_{CP}$ $[mm]$ | $L_{SS}$ $[-]$ |
| 10223.47 | 8274.17 | 347.87 | 100% |
| 7844.53 | 8259.64 | 973.55 | 50% |
| 11095.00 | 8032.11 | 1647.12 | 50% |
| 20925.34 | 8018.94 | 2838.08 | 50% |
| 18967.19 | 8004.90 | 4434.28 | 50% |
| 16611.73 | 7992.99 | 6028.36 | 50% |
| 13672.36 | 7983.55 | 7615.94 | 50% |
| 8791.39 | 7978.74 | 9111.86 | 50% |
| 575.65 | 7994.52 | 9971.37 | 50% |

Table 4.4: Wing loads discretization for LC1.

To import and apply the forces to the FEM model, a section in the general python script developed is present. This section reads the output produced by the diretization performed in MATLAB generating 18 reference points where the forces will be applied. Is is important to notice that being the wing in the $x - y$ plane, the $z$ position of the concentrated force is not important. In addition to the lift concentrated forces, the gravitational load given by the load factor is imported.

Al this point the loads are imported into the FEM but are not applied to the model.

To avoid any stress concentration due to the concentrated force, a structural coupling distribution have been considered. In particular for each wing section considered, the wing faces in pressure and suction side are identified and to those faces the relative concentrated force is applied. In this way the lift is distributed in the best way possible to the wing surface. In Figure 4.7b is the concentrated forces and the structural coupling are shown.
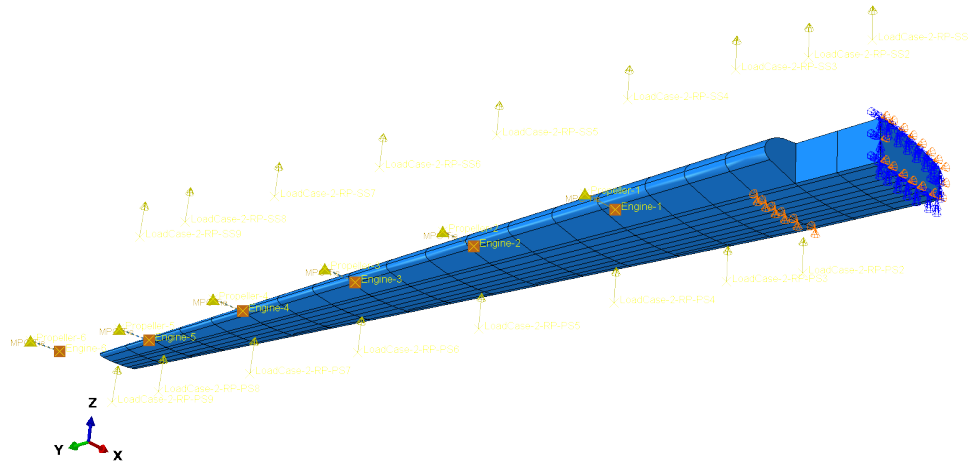


(a) Wing boundary conditions
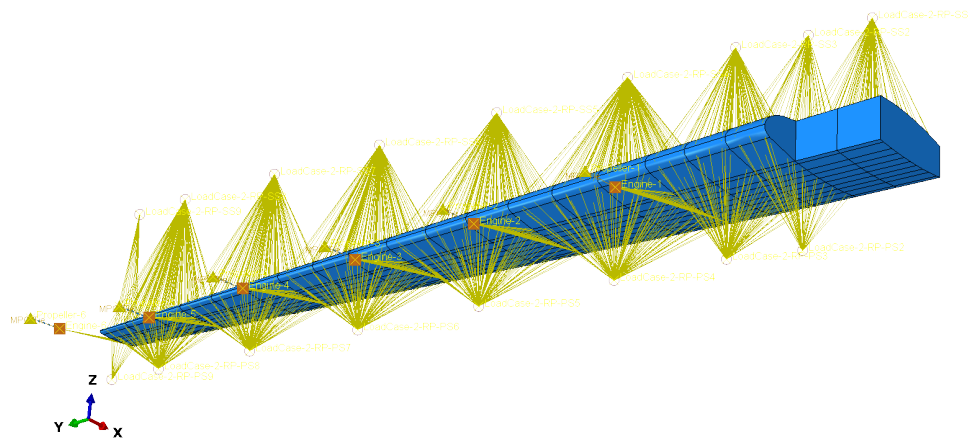


(b) Wing load discretization and application

Figure 4.7: Wing load discretization and boundary condition application

To consider the inertia loads generated by the engines a point mass is generated for each engine and each propeller considering the mass of both elements. The engine is connected to the wing sing a structural coupling, as done for the lift, assuming a rigid connection between the engine CG and the lower part of the relative engine rib. The propeller mass is connected rigidly to the engine CG assuming a rigid MPC to not introduce any

unconstrained degree off freedom to the model generated by the propeller mass.

The boundary conditions to apply to the model must represent in the best way as possible the wing-fuselage connection mechanism. The connection mechanism is shown in Figure 4.7a therefore the boundary conditions applied to the model are:

- Symmetry condition in $x - z$ plane.

- Displacement condition in correspondence of the wing fuselage connection.

Where $\vec{s} = \begin{bmatrix} \Delta x & \Delta y & \Delta z \end{bmatrix}$ represent the displacement vector and $\vec{\psi} = \begin{bmatrix} \vartheta & \varphi & \chi \end{bmatrix}$ the rotation vector. In Figure 4.7a the BCs point of applications are shown.

Important component for the FEM results is the definition and setup of a good meshing procedure, in order to have best possible mesh, considering the limited computational power available, a structured quadrilateral mesh have been used in every section where is possible. In particular the regions in which this mesh have been applied are shown in green in Figure 4.8a whereas in red are shown the location where an unstructured mesh is generated. In that regions is is not possible to use a structured quadrilateral mesh because those are the region where the stringers runout are located preventing the possibility of use a structured mesh. A global seeding of $5cm$ have been considered producing the mesh shown in Figure 4.8b.
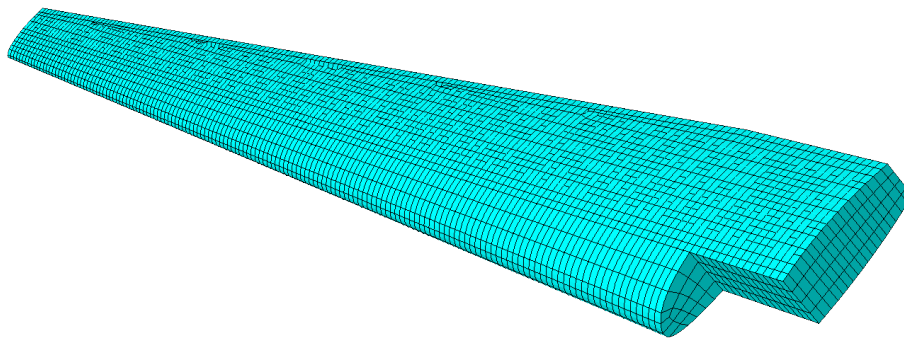
(a)
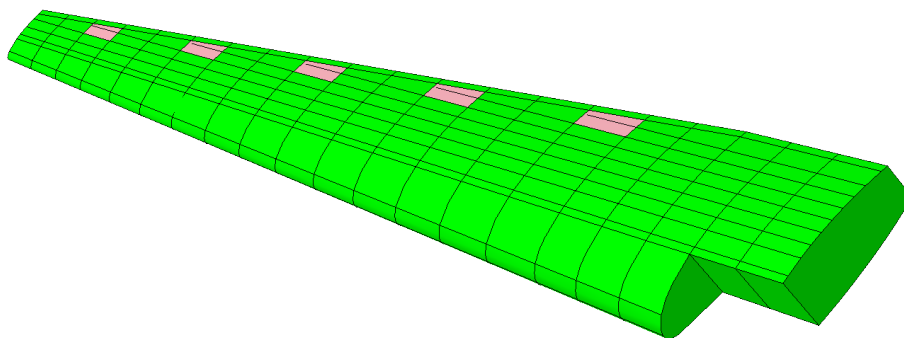


(b)

Figure 4.8: Wing mesh used for FEM analysis.

## 4.5. Analysis and results

Considering the load envelope and the the critical load cases highlighted in Section 4.1, the analysis have been done only for LC1, LC2, LC3 and LC4. The analysis performed consist in:

- Static analysis at ultimate load.

- Buckling analysis.

The wing sizing procedure performed in this research, is based on an euristic approach, in which, starting from a baseline considering constant elements thicknesses in the whole

wing, the analysis are executed and the results in terms of stresses and displacement are checked and the thicknesses are manually modified accordingly. Using this approach is is not expected to find the optimal solution to the wing, but rather the objective is to find a feasible solution that can and will be used in the next step of the development where a sophisticated optimizer will be used.

After several iterations the following wing structure is provided. The wing presents a total mass of $289kg$ where only the structure is considered, it is not comprehensive of control surfaces, actuators or additional weight relative bots and rivets that will be used for the system assembly. The overall thickness distribution is shown in Figures 4.9.
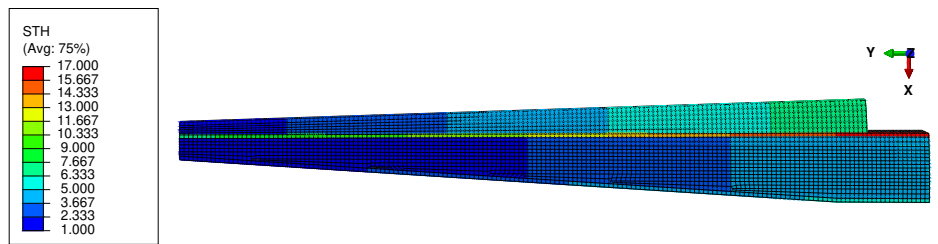
(a) Pressure side.
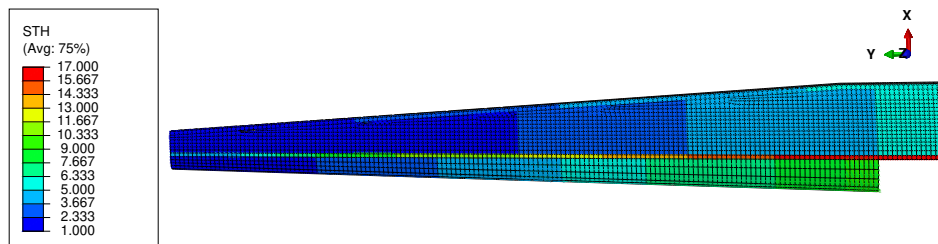


(b) Suction side.
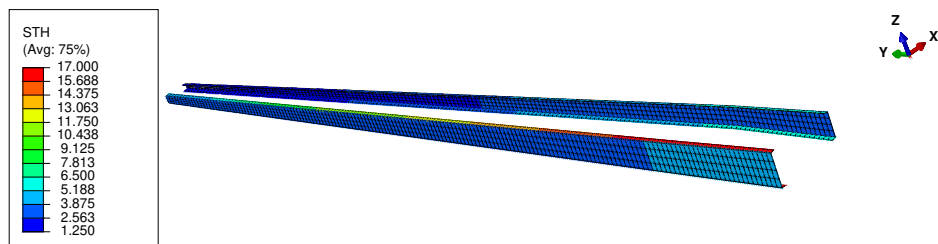


(c) Spars.
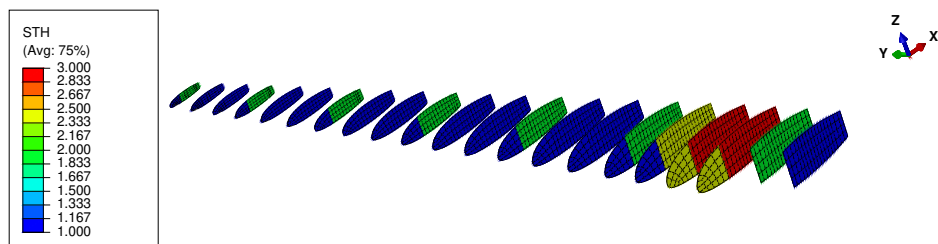


(d) Ribs.

Figure 4.9: Thickness wing distribution. Dimension is $[mm]$

After the simulation is possible to identify as the most critical load case LC1, which presents a maximum Von-Mises stress of $347.09 MPa$, corresponding to the $76.2\%$ of the allowable located in the front spar in correspondence of the wing-fairing connection. For load condition 3 is the second most critical one, where is considered a negative load factor, it is possible to notice that in this condition the wing point in the most critical condition reflect the same consideration just reported for LC1, with the difference that the point in which the maximum stress is present is located in the wing pressure side.

For LC1 the maximum stress is located in the front spar lower flange where the wing is connected with the fuselage fairing. The Von-Mises maximum stress is $347.091 MPa$ corresponding to the 76.2% of the allowable, leading to the possibility of accurately tune the spar thickness and dimension in the detailed structural design. It is important for the aeroelastic design to check the deformation of the wing in order to understand the variation in the aerodynamic profile for eventual increasing in the AOA. In this condition the maximum displacement of the wing tip is $\vec{s}_{max} = \{20.930;\ 1.393;\ 549.760\}\ mm$, and the variation in the angle of attack is negligible. This result is theoretically expected because that wing region is the mos critical in terms of bending and torsion, moreover the leading shell elements are no longer present thus a smaller resistant area is generated with the consequent stress increase. The stress distributions are shown in Figures 4.10 and 4.11 where are reported only the conditions at maximum positive an negative load factors.



(a)



(b)



(c) Zoom of figure 4.10b
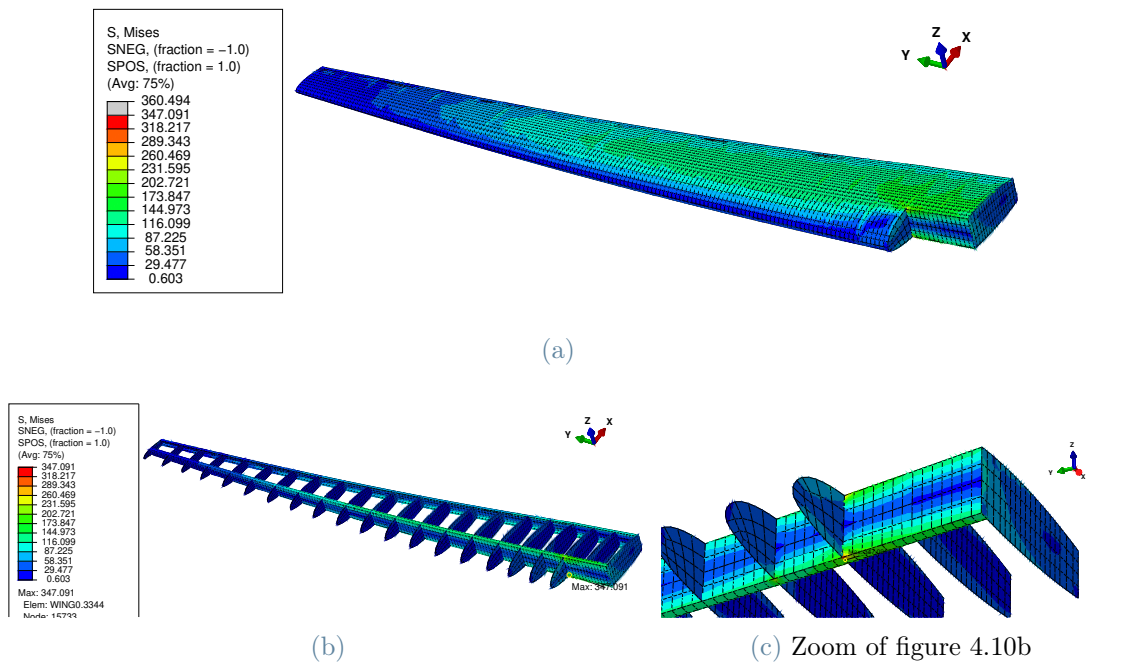
Figure 4.10: Static analysis for limit load case LC1. $[MPa]$



(a)



(b)
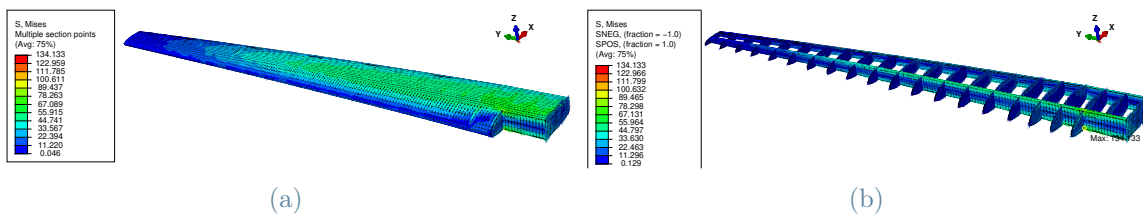
Figure 4.11: Static analysis for limit load case LC3. $[MPa]$

The second most critical condition is LC3, for load factor $n = -1.20$ the maximum V-stress is located in the same location as LC1, in this case the stress is $124.2 MPa$, far away from the yielding stress of the material. In this condition displacement vector reads $\vec{s}_{max} = \{-6.822; -6.893; -213.946\}\, mm$.

These conditions are the one that size the wing from a strength point of view under ultimate load cases, buckling condition instead are critical to avoid instability in the shell elements. These analysis have been performed considering limit load condition and are proven to be the sizing condition for the stringers and shell elements in the wingspan. The analysis have been considered computing the first 10 modes and eigenvalues producing the results reported in table 4.5. The eigenvalue results of the analysis are to be intended as a scaling factor of the load condition, representative of the condition in which the buckling occurs. In LC1 ($n = 3.01$) the buckling is located in pressure side but having negative eigenvalue the buckling condition does not occurs. In particular, in LC1, the pressure side is in tension, being the wing bent upwards, being the buckling a compression instability, the buckling instability is not possible where the section is in tension, therefore the minus sign in the eigenvalue, this is due to Abaqus buckling analysis which are defined by:

$$\left( K_0^{NM} + \lambda_i K_\Delta^{NM} \right) v_i^M = 0 \tag{4.5}$$

where $K_0^{NM}$ is the stiffness matrix corresponding to the base state, which includes the effects of the preloads, $P^N$ (if any); $K_\Delta^{NM}$ is the differential initial stress and load stiffness matrix due to the incremental loading pattern $Q^N$; $\lambda_i$ are the eignvalues; $v_i^M$ are the buckling mode shapes (eivenvectors). The magnitude of the loading is not important, it is scaled by the load multipliers $\lambda_i$ found in the eigenvalue problem.

The region affected by buckling conditions are shown in Figure 4.12 for only the first three modes.

(a) LC1: mode 1 eigenvalue −0.64224



(b) LC3: mode 1 eigenvalue 1.6524



(c) LC1: mode 2 eigenvalue −0.66299



(d) LC3: mode 2 eigenvalue 1.7001



(e) LC1: mode 3 eigenvalue −0.67358



(f) LC3: mode 3 eigenvalue 1.7129
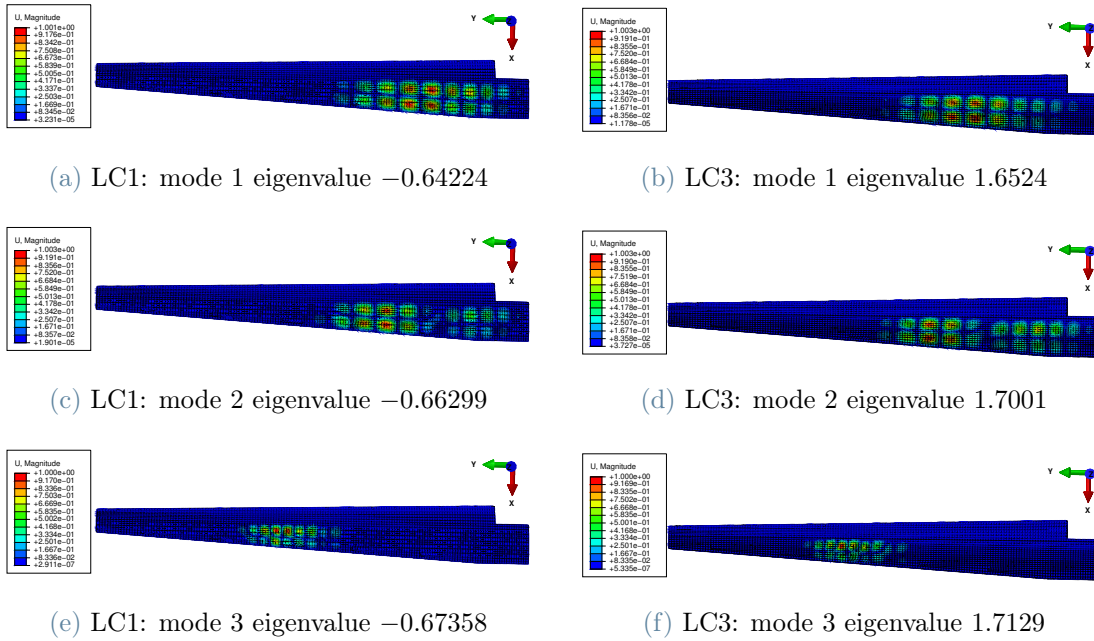
Figure 4.12: Buckle analysis results for load cases 1 and 3.

| | LC1 | | LC2 | | LC3 | | LC4 | |
|---|---|---|---|---|---|---|---|---|
| **Mode** | $\lambda$ | *Location* | $\lambda$ | *Location* | $\lambda$ | *Location* | $\lambda$ | *Location* |
| 1 | -0.64224 | PS | 1.6524 | PS | -0.6365 | PS | 1.6447 | PS |
| 2 | -0.66299 | PS | 1.7001 | PS | -0.6573 | PS | 1.6597 | PS |
| 3 | -0.67358 | PS | 1.7129 | PS | -0.6636 | PS | 1.7074 | PS |
| 4 | -0.69392 | PS | 1.7598 | PS | -0.6875 | PS | 1.7186 | PS |
| 5 | -0.69976 | PS | 1.7753 | PS | -0.6908 | PS | 1.7404 | PS |
| 6 | -0.71970 | PS | 1.8194 | PS | -0.7102 | PS | 1.7546 | PS |
| 7 | -0.72773 | PS | 1.8323 | PS | -0.7199 | PS | 1.7797 | PS |
| 8 | -0.74681 | PS | 1.9055 | PS | -0.7385 | PS | 1.8071 | PS |
| 9 | -0.76548 | PS | 1.9124 | PS | -0.7563 | PS | 1.8304 | PS |
| 10 | -0.76831 | PS | 1.9456 | PS | -0.7565 | PS | 1.8519 | PS |

Table 4.5: Wing buckling eigenvalues numerical data.

# 5 | Fuselage design

The fuselage airframe design, due to the innovative configuration on Unifier19, requires detailed analysis in terms of constraints, subsystem positions and dimension, in order to fully understand what is the stress distribution for a radical new airplane configuration. The constraints included in the airframe design take into consideration the aircraft role and features, in particular:

- Is necessary to include a cargo door to allow the possibility of use the plane in a full cargo configuration.

- In the fuselage compartment after the passengers' cabin the liquid hydrogen tank and the fuel cells are located.

- In the fuselage rear end is present the main engine with a pushing propeller.

Due to these high-level constraint a first model of the fuselage is generated using the script developed. The inputs required are:

- Floor position and shape given as a $N \times 2$ matrix, where the columns represent the $x$ and $z$ coordinate respectively, and $N$ are the points needed to define the floor.

- Floor support $x$ ad $y$ coorinates.

- Landing gear bay dimensions in terms of height, length and slant angle.

- Positions of the main frames.

- Maximum frame spacing.

- Number of stringers in the crown panel, in the fuselage side and in the bottom.

- Positions and dimension of each cutout as window and doors.

- Positions of the cockpit horizontal frames.

- Position of the pillars.

In particular the outcome expected is a PDR (Preliminary Design Review) with the purpose to accurately define the volumes and position of each system inside the fuselage

and define the proper interaction between the element in order to define the constraints and general shape that the structure has to fit in. In particular three aspect were taken into consideration:

1. *Airframe and other system interface:* the fuselage structure have the necessity to interface correctly with all the others elements in the plane, in this case like nose and main landing gear, $LH_2$ fuel tank, fuel cells and many others. The airframe is designed keeping all these elements in mind and considering a preliminary connection system. In particular, considering the small volume available for the landing gear bay.

2. *Safety and comfort:* In compliance with the CS-23 regulations, three emergency exits are present in Unifier-19 whose dimension are maximized in order to ease the evacuation procedure and creating a safer plane. Safety is granted even by maximizing the cockpit windows: the main windshield guarantee a big field of view for the pilot and the four side windows allow the pilot to visually inspect the DEP conditions.

   Comfort of the passengers is ensured by analyzing the cabin dimension to allow the passengers to stand in the cabin, the design of the entry door is critical, it must have height and width sufficient to guarantee an easy access for the passengers.

3. *Maintenance and cargo:* One of the main aspect of reducing the cost is to provide an easy to maintenance plane, therefore the necessity to accurately define the position and dimension of the access point in particular for the hydrogen tank and for the fuel cells.

   Cargo requirements impose the presence of a cargo door in the front section of the fuselage and another one in the back allowing the ground staff to load the luggage. The global volume for cargo is the equivalent of three LD3 containers.

## 5.1. Fuselage structure

The airframe for the fuselage structure is developed as follow considering as most important parameters the cutouts positions and structural element size and positions. In particular the fuselage is divided in three main compartments each one with different needs and constraint:

1. *Nose and cockpit:* is the forward part of the plane where the pilot and all avionics are fitted. From a structural point of view is necessary to study the cutouts and

the frame that hold in position the five big windshield and the nose landing gear. The bigger constraint is the windshields position which is developed and thought to ensure the maximum for the pilot, allowing the possibility to directly see the the DEP state on the wing.

2. *Passengers' cabin:* is the region where the seat passengers' are located, in this region is important to maximize the safety and the comfort for the people on board, in particular the presence of three emergency exits is mandatory from CS-23 regulations. Moreover the dimension of the cabin should ensure the possibility for the passengers' to stand up comfortably. Another constraint impose on this area is the presence of a big cargo compartment to allow the possibility of full cargo configuration.

3. *System compartment:* behind the passengers' cabin is located the system area, where all the big plane subsystems are located. This region is necessary to fit the liquid hydrogen tank and the fuel cells. In this region the airframe has to be defined according to the position of this subsystems, positions of frames and stringers as function as the location of those. In the last fuselage section is present a cargo compartment that is used to store the passengers' luggager during flight.

## 5.1.1. Cutouts and openings

The first step of the fuselage design is the definition of the location and size of the cutouts. The opnings are necessary for easy and good use of the plane, the cutouts are present both for technical aspects and both for passengers' comfort. In Unifier19 a total of 17 structural openings are presents listed below:

- 5 windshields in the cockpit.

- 2 cargo doors: one big in the forward fuselage section and one, smaller, in the aft compartment.

- 2 maintenance windows to allow technical operations on both fuel cells and tank.

- 6 passengers' windows.

- 2 (+1) emergency exits located in the right side of the fuselage. It is important to notice that the third emergency exits is the same door used for embark and disembark, which is fully contained in the main cargo door, therefore is not explicitly present in the model.

The openings dimensions are defined to be in compliance with CS-23 regulations and the dimensions are listed in Table 5.1. The passengers' window design is sketched in Figure 5.1.

The convention for the emergency exits used reads: EME-1 emergency exits coincident with the entrance; EME-2 and EME-3 forward and after emergency exits respectively.

| Cutout | Width [mm] | Height [mm] |
|---|---|---|
| **Entry door** | 750 | 1600 |
| **EME-2** | 650 | 1500 |
| **EME-3** | 650 | 1500 |
| **Fwd cargo** | 2000 | 1650 |
| **Aft cargo** | 600 | 700 |
| **Maintenance** | 700 | 1250 |

Table 5.1: Fuselage cutouts dimensions.

The cutouts positions and dimensions definition is very relevant for the preliminary design because those enforces the position of stringers and frame that are need to increase the structure strength in a location where the opening weaknesses it. In particular the cockpit dimension and size is developed with the objective of maximize the field of view for the pilot, who can directly see the wings and the DEP during flight. A total of 5 windshield are available for the pilot divided by four symmetrical pillars, being Unifier19 a single pilot commuter the principal wind shield does not account



Figure 5.1: Passengers' window design, [mm]

for a pillar placed in the symmetry plane because it would have vastly decreased the field of view for the pilot.

The doors and emergency exits locations have been imposed by the CS-23, regulation enforcing the position of one emergency exit symmetrical to the entry door and one located in the rear of the cabin in the right side of the plane. The emergency dimension are being maximized according to the frames position with the objective of ease the evacuation procedure and increase the safety for the passengers. The windows and dimension are designed with the objective of increase the comfort of the passengers' during flight: the wide dimensions and position ensure to each person on board a good view of the outside granting a nice flight.

On the other hand, cargo and maintenance openings are sized to be as small as possible granting a sufficient area to allow for technical operation. The objective is to have access

to the plane subsystem without impacting too much the aircraft structural efficiency. In particular the two symmetrical maintenance holed provide direct access to the fuel tank and liquid hydrogen tank, meanwhile the rear cargo door, commonly used to load and unload luggage, can be used as entrance for the maintenance crew allowing access to the system compartment area passing through a cosmetic wall that can be easy disassembled. All these feature have been designed with the objective of ease the use of Unifer19 in any circumstance.

All the coutouts are shown in different colours in Figures 5.2.
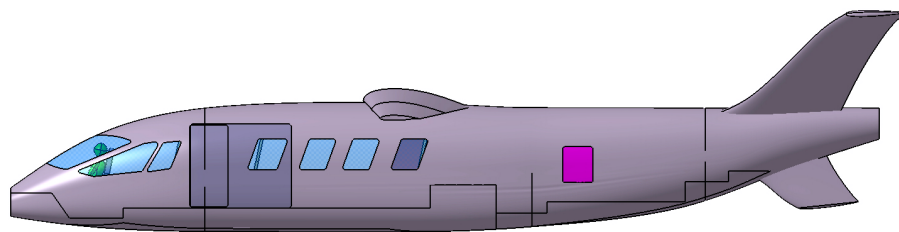


(a) Left side
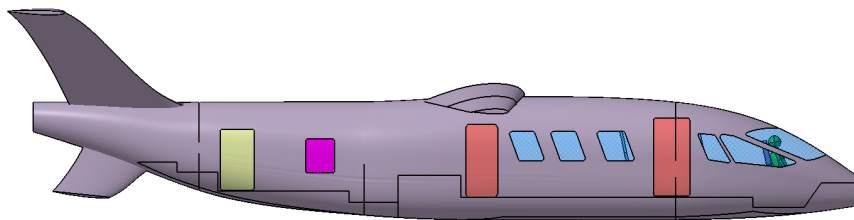


(b) Right side

Figure 5.2: Fuselage cutouts positions.

## 5.1.2. Floor

The definition of the floor is important because it separates the volume designated to the passengers and the volume for the subsystems. To increase the passengers comfort a good strategy is to maximize the cabin height by reducing the floor position, in this case this can lead to issues in the next project phases having preferred one priority to the other. For this reason the floor position have been chosen in such a way that allow the comfort passengers, with a cabin height of maximum $1.82m$ and, using a preliminary volume estimation of the subsystem, ensuring a tolerance for the under floor system compartment.
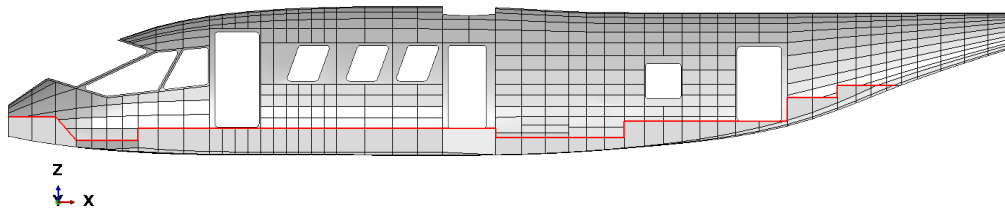
(a) Floor layout, left view.
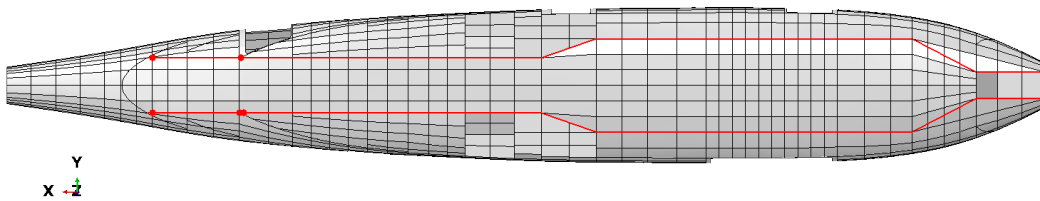


(b) Floor support, bottom view.

Figure 5.3: Fuselage floor layout

The floor layout is shown in Figure 5.3a, it is composed in different height levels: the cockpit is slightly lower than the passengers' cabin both because under the cabin there are not big subsystem and because in this way the pilot position is the best from an available field of view dimension. Behind the cabin, in the system compartment, the floor have to lower itself in order to allow the minimum volume required for the liquid hydrogen tank. After that the floor shifts upward to ensure and fixing in position the fuel cells and remains at the same height until is necessary to be moved upward in proximity of the fuselage boat tail. In particular the rear cargo compartment presents a three steps floor in order to maximize the volume available for the luggage and do not interfere with the boat tail. The floor is supported across the whole floor length, by two main support structures. These support structure, shown in Figure 5.3b, are the main element that withstand the floor vertical loads, and are used as attachment points to the subsystem located below the floor, as air conditioning, batteries and electrical system. In the forward end of the floor support, the nose landing gear is hinged, making the those support to be subjected to take off and landing gear loads. These supports does not provide enough horizontal strength, in particular between the supports itself. for this region it is mandatory to provide strength to the floor using horizontal beams perpendicular to the supports. These beams connect each section of the fuselage being riveted to the skin frames. To provide enough bending resistance these beams have a I-shape profile with a flange to web ratio of 0.3. To avoid buckling of the floor some stringers parallel to each others are implemented.

### 5.1.3.   Frames and stringers

Main airframe elements are the frames and the stringers for the fuselage skin. The initial spacing is defined accordingly with standard aeronautical solution, having a frames spacing almost instate of $0.5m$ ans stringers spacing of $0.2m$. The frames positions are defined according to the airframe constraints such as cutouts or structural discontinuities. In detail the frames that close the cutouts as cargo door, maintenance, etc. are defined in position according to the cutout position and dimensions. Other frames that are defined a priori are the frames located in correspondence of the front and rear spar. Those positions are tuned to be under the wing spars allowing for an easy connection mechanism, these two frames must be very strong because ave to withstand the lift force generated by the wing. The big cargo door in the front section of the fuselage vastly impact the structural integrity of the airframe not being present any shell elements that carry the load, to tackle this issue is necessary to decreased the spacing between the frames, in this region the spacing is half with respect to the otter plane sections to be $0.25m$. In the rear part of the fuselage the frames which position is defined by other subsystems are:

- The frames that hold in position the liquid hydrogen tank.

- The frame that close the landing gear bay cutout.

- The frames that connect the fuselage with the V-tail.

All the others are defined automatically by considering a spacing defined as input to the parametric script. The position of these frames is computed by searching the fuselage locations in which the spacing between two consecutive frames is grater that the maximum spacing defined as input. In this region the distance between the frames is computed and divided by the target, being the length in reference not divisible perfectly by the spacing chosen, the integer value of this ratio is considered to be the number of frames to be introduced between the starting two. The distance is that equally divided and the frames are located in these position. As an example if the spacing between two frames is $880mm$ and the maximum allowable frames spacing is $450mm$, the ratio $880/450 = 1.\bar{5}$ leads to the creation of one frame, located in a spacing of $s = \frac{880}{1+1} = 440mm$. All the frames and the stringers are a Z-shape profile.

The frames and stringers locations are shown in Figure 5.4.
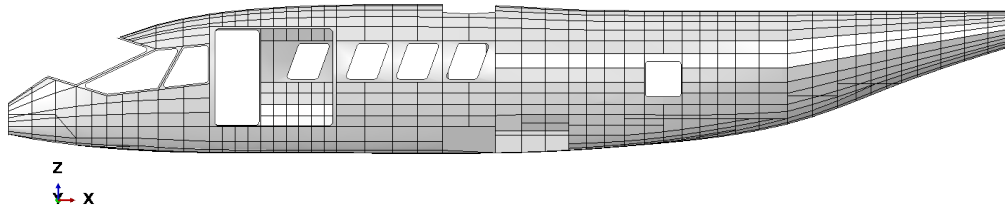
Figure 5.4: Fuselage frame and stringers locations.

## 5.2.   Preliminary load evaluation

The preliminary load evaluation have been performed considering the fuselage as a free-free beam in which the forces generated by the wing, the V-tail and the inertia are in equilibrium. This model is one dimensional and in order to not complicate further than necessary the model, a symmetrical load condition is considered, in this approach all the forces are applied directly on the fuselage elastic axis. Therefore is not possible to capture in this model any asymmetry due to the the uneven passengers distribution. The hypothesis in which this model is based are:

1. Straight elastic axis

2. Symmetrical condition with respect to the A/C symmetry plane.

3. Forces acting parallel to the elastic axis are neglected, therefore neither aerodynamic drag neither thrust is not considered.
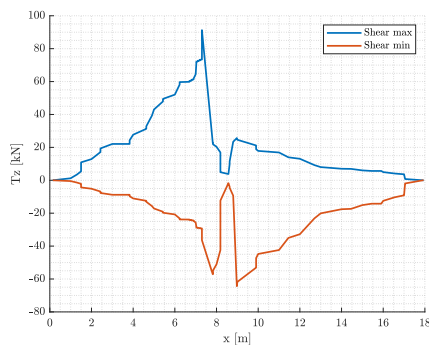


(a) Shear force envelope.
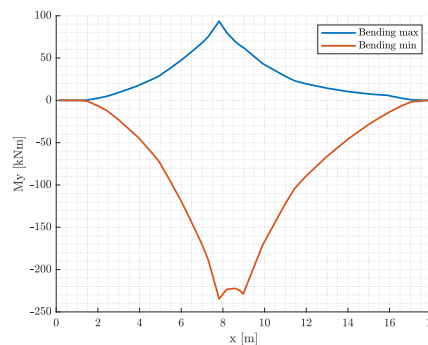


(b) Bending moment envelope.

Figure 5.5: Internal forces envelope for fuselage using beam model.

Having ensured the load equilibrium is possible to compute the internal forces without constraining the system. All the load cases provided by PVS are tested and the envelope of the internal forces is defined. The numerical results are reported in Table 5.3 and in Figure 5.5 the diagrams for bending and shear force are reported.

From which is possible to identify that the most critical conditions for the fuselage are given by different load cases. In particular maximum shear is given, depending on the fuselage position taken into consideration, bu LC1, LC3, LC17 and LC19 which correspond to high load factor maneuver at $V_A$, in both weight and balance configuration relative to maximum rear CG position (LC1 and LC3) and maximum forward position (LC19, LC19). For fuselage bending the sizing load cases are : LC1, LC2, LC3, LC17, LC18, LC19 and LC25.

Each fuselage section is sized by a different load case, leading to a difficult understanding on the condition that are critical for the fuselage, therefore is necessary to consider all these flight conditions in the FEM analysis in order to fully understand the stress characteristics in the fuselage airframe.

## 5.3. Loads discretization an boundary conditions

As done for the wing, the fuselage simulations are performed only for the most critical load cases, in this case however the loads to which the fuselage is subject are all inertia loads of the all subsystem and the reaction forces transmitted to the fuselage by the main wing and by the vertical tail. All of these data are computed by the load assumption provided by PVS. These load assumption are based on a beam model, where each load is applied in the A/C symmetry plane. With the FEM model developed the loads are introduced as point masses in the exact location where each element is located. Using this load definition is possible to represent in the best way as possible which is the load distribution across the fuselage, in this representation each subsystem is condensate in a point wise mass. The masses and positions used for the simulations are reported in Table 5.4. Regarding the passengers, the pilot and the relative seats, only one mass is considered for each person, comprehensive of the mass of the person itself and the mass of the seat.

| $y$ [m] | $T_z$ min [kN] | LC | $T_z$ max [kN] | LC | $M_y$ min [kNm] | LC | $M_y$ max [kNm] | LC |
|---|---|---|---|---|---|---|---|---|
| 0.141 | 0.00 | 1 | 0.00 | 1 | 0.00 | 1 | 0.00 | 1 |
| 1.000 | 1221.285843 | 17 | -486.891366 | 19 | 0.00 | 1 | 0.00 | 1 |
| 2.000 | 12871.032651 | 17 | -5131.308698 | 19 | 2596.216627 | 19 | -6512.176707 | 17 |
| 3.000 | 22084.830557 | 17 | -8804.583611 | 19 | 9203.057921 | 19 | -23084.336953 | 17 |
| 4.000 | 27697.503075 | 17 | -11042.193917 | 19 | 18157.645274 | 19 | -45545.426897 | 17 |
| 5.000 | 43016.780898 | 17 | -17149.547202 | 19 | 29900.216366 | 19 | -74999.709384 | 17 |
| 6.000 | 52065.873167 | 1 | -20757.158738 | 3 | 47552.717292 | 19 | -119278.065875 | 17 |
| 7.000 | 64443.780563 | 1 | -25691.872650 | 3 | 68014.920074 | 19 | -170604.091186 | 17 |
| 7.300 | 91290.366158 | 1 | -36394.830362 | 3 | 75306.363628 | 19 | -188893.462099 | 17 |
| 7.830 | 21888.916349 | 19 | -54904.698508 | 17 | 93155.220978 | 3 | -234284.409054 | 2 |
| 8.000 | 20357.476402 | 19 | -51063.336641 | 17 | 86775.427191 | 3 | -228822.832341 | 2 |
| 8.187 | 16910.793384 | 19 | -42417.906739 | 17 | 79955.166042 | 3 | -223310.523934 | 2 |
| 8.571 | 3801.711555 | 1 | -1727.684418 | 17 | 70020.394943 | 3 | -222247.184049 | 2 |
| 8.630 | 9890.856673 | 1 | -3943.198674 | 3 | 68685.873981 | 3 | -222512.178354 | 2 |
| 8.800 | 23396.027548 | 1 | -9327.319953 | 3 | 65307.869704 | 3 | -224580.090329 | 2 |
| 8.975 | 25662.532614 | 3 | -64370.185973 | 1 | 62666.235162 | 3 | -228805.094609 | 2 |
| 9.000 | 24624.543310 | 3 | -61766.562801 | 1 | 62126.431741 | 3 | -227192.728068 | 2 |
| 9.900 | 21164.757190 | 3 | -53088.265950 | 1 | 43627.698933 | 3 | -171490.793439 | 2 |
| 10.000 | 17853.329450 | 3 | -44782.101370 | 1 | 42148.915197 | 3 | -166748.072400 | 2 |
| 11.000 | 16894.164942 | 3 | -42376.197062 | 1 | 28365.981493 | 3 | -121841.495355 | 2 |
| 11.450 | 13963.937922 | 3 | -35026.210953 | 1 | 23057.545022 | 19 | -103875.693955 | 18 |
| 12.000 | 13066.329450 | 3 | -32774.709703 | 1 | 19509.717505 | 19 | -89292.648182 | 18 |
| 12.700 | 9219.518729 | 19 | -23125.626146 | 17 | 15905.331417 | 19 | -73017.576908 | 18 |
| 13.000 | 8011.885067 | 19 | -20096.478375 | 17 | 14360.594522 | 19 | -66042.546361 | 18 |
| 14.000 | 7010.364960 | 3 | -17584.332107 | 1 | 10419.105201 | 19 | -45821.592310 | 18 |
| 14.460 | 6922.632707 | 19 | -17364.270374 | 17 | 9107.076198 | 19 | -37776.769128 | 18 |
| 15.000 | 6013.117815 | 19 | -15082.903852 | 17 | 7566.868239 | 19 | -28332.846261 | 18 |
| 15.448 | 5671.862071 | 19 | -14226.920694 | 17 | 6696.528752 | 19 | -21519.940232 | 18 |
| 16.000 | 4978.898343 | 19 | -12488.736677 | 17 | 5425.831744 | 19 | -13609.794626 | 25 |
| 17.000 | 3640.800783 | 19 | -9132.341965 | 17 | 834.691650 | 19 | -2093.684889 | 25 |
| 17.900 | 0 | 5 | 0 | 22 | 0 | 30 | 0 | 5 |

Table 5.3: Numerical data for internal forces envelope for fuselage.

| Subsystem | Mass [$mkg$] | $x_{CG}$ [$mm$] | $y_{CG}$ [$mm$] | $z_{CG}$ [$mm$] |
|---|---|---|---|---|
| Air conditioning | 220 | 5950 | 0 | -1000 |
| Batteries | 593 | 7300 | 0 | -1000 |
| $LH_2$ tank | 195 | 9900 | 0 | 100 |
| Fuel cells | 250 | 11575 | 0 | 25 |
| Nose landing gear | 53 | 950 | 0 | -800 |
| Main landing gear | 200 | 900 | ±760 | -950 |
| Electric system | 201 | 8200 | 0 | -1000 |
| Main engine | 50 | 15650 | 0 | 850 |
| Main engine propeller | 45 | 17900 | 0 | 850 |
| Main engine electronics | 20 | 15000 | 0 | 850 |
| Luggage comp. 1 | 380 | 12700 | 0 | 145 |
| Luggage comp. 2 | 190 | 14460 | 0 | 325 |
| Seat and passengers | 86 | Table 5.5 | | |

Table 5.4: Fuselage subsystems mass and position.

The passengers are disposed in seven rows with three seats each, apart from the second one which is composed by only one seat. This is done both for have 19 seats and both to ease the evacuation procedure, because in correspondence of the second row the emergency exits are located. The center of gravity position for each passenger and the seat are reported in Table 5.5.

| Seat | $x_{CG}$ [mm] | $y_{CG}$ [mm] | $z_{CG}$ [mm] |
|------|------|------|------|
| **Row 1, L** | 3400 | -705 | 200 |
| **Row 1, C** | 3400 | 200 | 200 |
| **Row 1, R** | 3400 | 705 | 200 |
| **Row 2, C** | 4200 | 200 | 200 |
| **Row 3, L** | 5000 | -705 | 200 |
| **Row 3, C** | 5000 | 200 | 200 |
| **Row 3, R** | 5000 | 705 | 200 |
| **Row 4, L** | 5800 | -705 | 200 |
| **Row 4, C** | 5800 | 200 | 200 |
| **Row 4, R** | 5800 | 705 | 200 |
| **Row 5, L** | 6600 | -705 | 200 |
| **Row 5, C** | 6600 | 200 | 200 |
| **Row 5, R** | 6600 | 705 | 200 |
| **Row 6, L** | 7400 | -705 | 200 |
| **Row 6, C** | 7400 | 200 | 200 |
| **Row 6, R** | 7400 | 705 | 200 |
| **Row 7, L** | 8200 | -705 | 200 |
| **Row 7, C** | 8200 | 200 | 200 |
| **Row 7, R** | 8200 | 705 | 200 |

Table 5.5: Fuselage subsystems mass and position.

Using an approach analogue to the wing load application, the point masses are connected to the airframe using structural coupling that connect each point to the elements to which the relative subsystem is connected. To define these proprieties correctly is necessary to have a preliminary idea on how these element have to interface each other. Starting from the passengers' seats, to allow the possibility to store luggage and/or live vest under the seat, is not possible to connect the seat to the horizontal frames, therefore is necessary to connect the seat directly to the floor stringers. Liquid hydrogen tank and fuel cells must be strongly connected to the main frames and the floor in at least two points in order to ensure the fail safeness of the connections, furthermore the connection points are located only on the upper and lower part, to allow some space that will be used for inspection procedures. The luggages in the rear cargo compartment instead are just lend against the floor. In consequence of these solutions, the structural coupling between each subsystem

and the airframe are defined. The coupling used in the analysis are shown in Figures 5.6
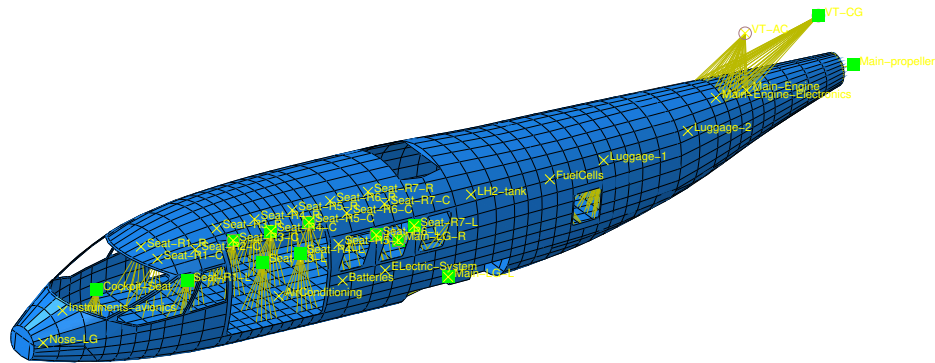


(a)
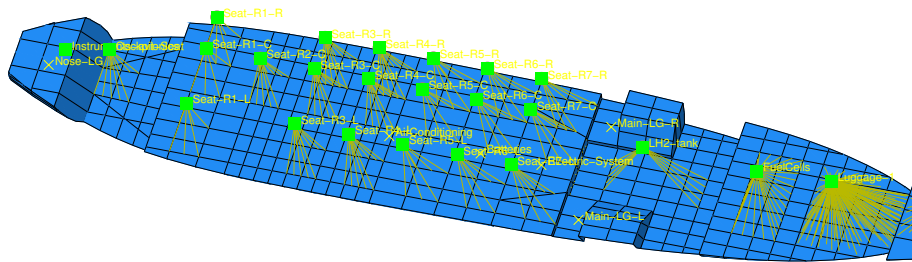


(b)

Figure 5.6: Kinematic coupling used in fuselage analysis.

The other loads to be applied are the aerodynamic loads given by the wing and the V-tail. It is not possible to apply directly the lift and the trim forces obtained by the load assumption by PVS because, in that computation, a fuselage mass have been hypothesized and it is not likely that it correspond to the airframe mass considered in the FEM model. for this reason, the lift and the trim force were applied, would not result a model in equilibrium with the consequent problems in terms of boundary condition definition. For this reason the methodology adopted consider the model boundary conditions in correspondence of the wing-fuselage connection and the trim force and position taken from the data provided by PVS. In this way the total lift force is computed by the reaction force in the model. In particular the boundary condition considered are:

- Null displacement in $y$ and $z$ direction in correspondence of the lug position.

- Null displacement in $x$ in the symmetry plane for the frames that connect to the
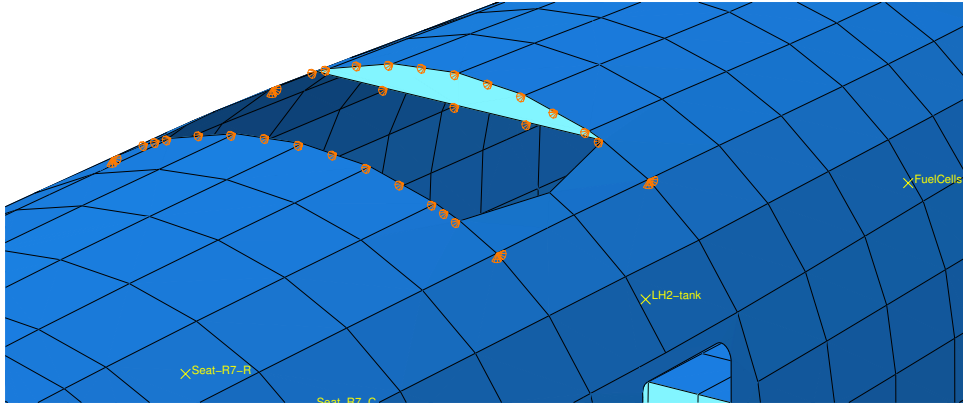
Figure 5.7: Fuselage FEM boundary conditions.

front and rear wing spar.

The exact point where the boundary conditions are applied is shown in Figure 5.7.

## 5.4.    Material selection

Following the same approach describe in the wing design, the fuselage material have been selected by considering the requirement of each element and only standard alloy is used. The material chosen for the structural design and their mechanical proprieties are reported in Table 5.6. Ramberg-Osgood plasticity model is used for the analysis in consistency with the plasticity used in the wing design.

|                | $\rho \left[\frac{kg}{m^3}\right]$ | $E \ [GPa]$ | $\nu \ [-]$ | $\sigma_y \ [MPa]$ |
|----------------|------------------------------------|-------------|-------------|---------------------|
| **Al-2024-T351** | 2768.00                           | 74.466      | 0.33        | 330.96              |
| **Al-7040**      | 2590.80                           | 71.708      | 0.33        | 434.02              |

Table 5.6: Fuselage material proprieties.

For the shell elements as external fuselage, floor and floor support Al-2024 has been chosen due to its light weight and resistance capabilities, whereas for the frames and stringers Al-7040 have been considered for its high strength and resistance.

## 5.5.    Analysis and results

Crucial aspect for the fuselage FEM analysis is the mesh definition and controls. Given the complexity of the model, both 1D and 2D elements are considered: the external shell, the

(a)



(b)
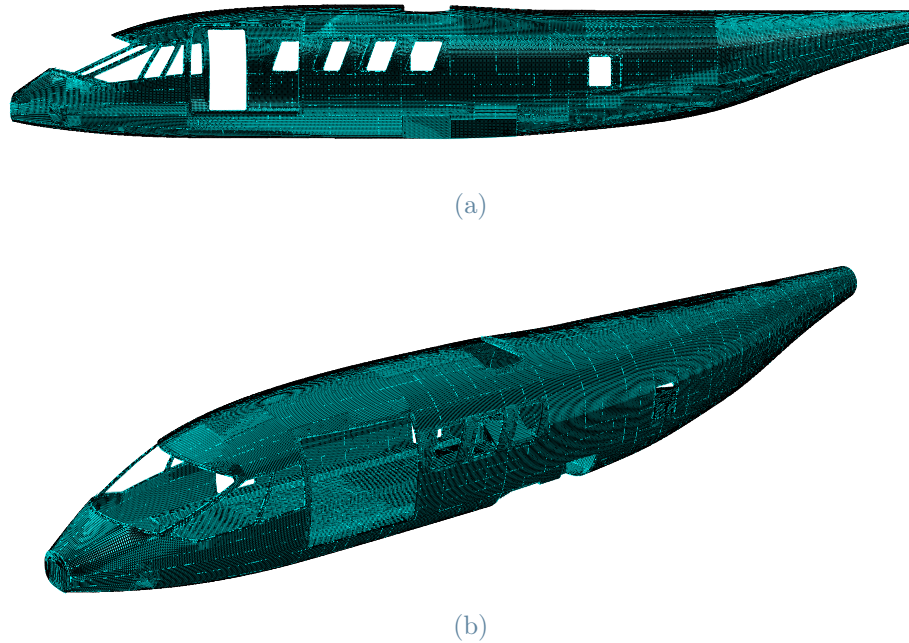
Figure 5.8: Wing fuselage mesh.

floor and the floor support are modelled as bidimentional elements, whereas both frame, stringers and floor beams are considered to be one dimensional elements. In order to have valuable results the mesh controls are detailed tuned to create a structured quadrilateral mesh where possible. This is well achieved in the floor and in the fuselage side and roof, but where big curvature or section variation are present is have been necessary to use a structured quad-dominated mesh, allowing the possibility to have few triangular elements that can reduce the high element aspect ratio. An overall seeding of $25mm$ is considered and the mesh used in the Analysis is reported in Figure 5.8.

Following an euristic sizing in which, using the script developed, the thicknesses and beam profiles have been changed accordingly to the simulation results, the fuselage structure sizing have been achieved. The total fuselage mass is $1289Kg$, slightly higher with respect to the statistical regression made in the previous months. The thicknesses distributions are reported in Figures 5.9

(a) Left view.



(b) Top view.



(c) Bottom view.



(d) Floor supports.



(e) Floor.
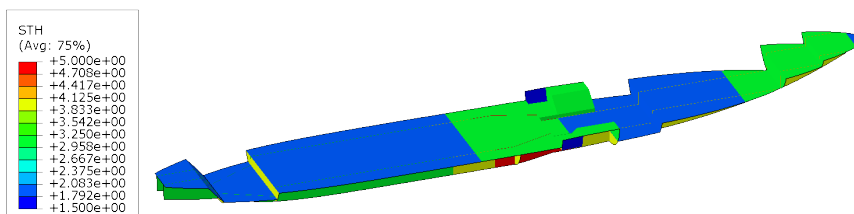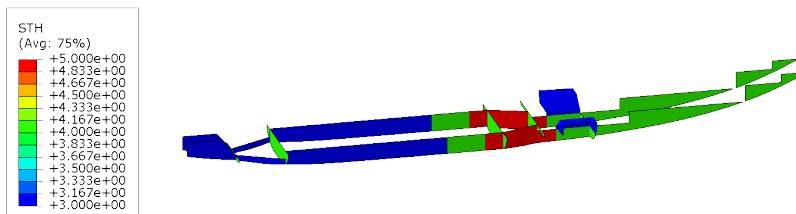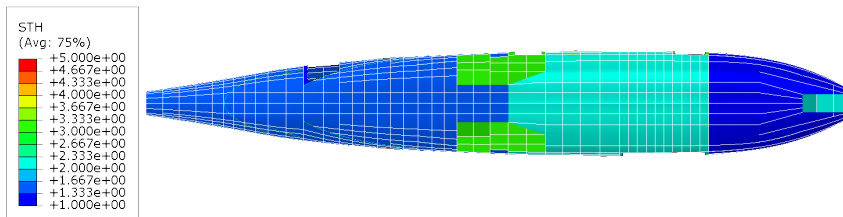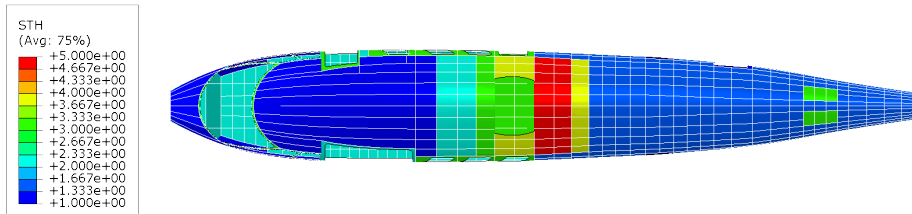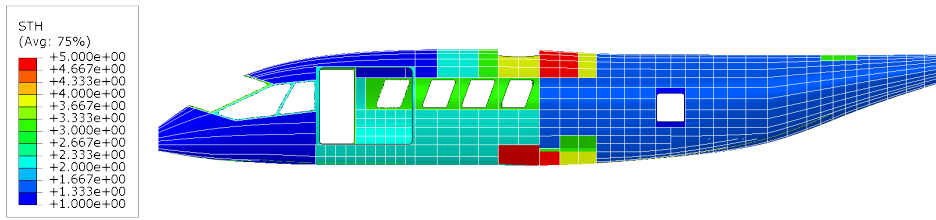
Figure 5.9: Fuselage elements thickness distribution. Units in [$mm$].

Analyzing the result is possible to notice that all the fuselage elements, with the exception of the frames connecting the fuselage and the wing, are sized considering buckling

condition. In particular the static analysis, done for all the load cases highlighted in the preliminary load condition, the most critical case is find to be LC18 for which the results are reported in Figures 5.10, in this configuration the maximum stress is $281.1 MPa$ located in the frame connecting the wing with the front spar. In this region is present a stress concentration which is due to the connection with the wing. The stresses in the other fuselage pars are much lower with respect to the yielding stress of the material, satisfying the strength requirements. For LC25 the maximum stress is located in the frame connected to the V-tail generating a maximum stress of $257.1 MPa$. The stress distributions for this case are reported in Figures 5.11.
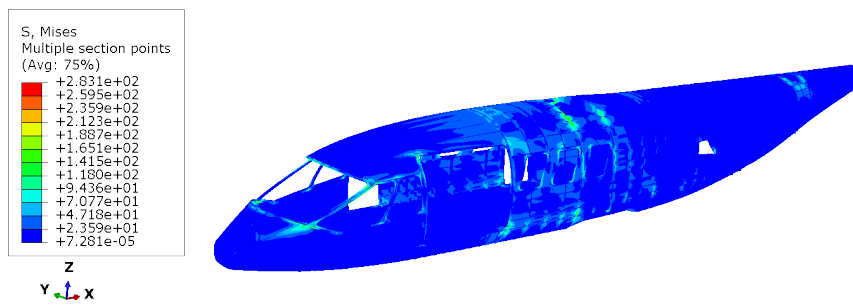


(a) Shell elements.
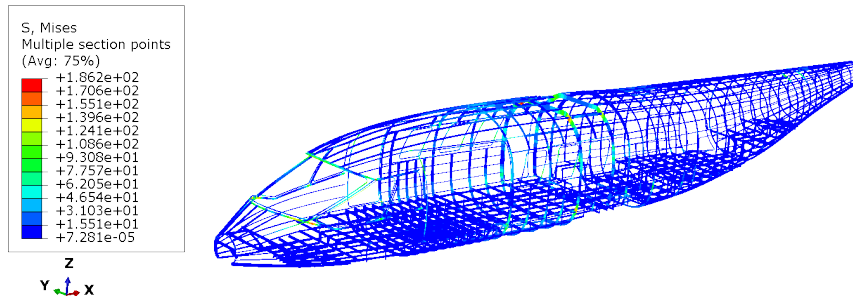


(b) Frames and stringers.
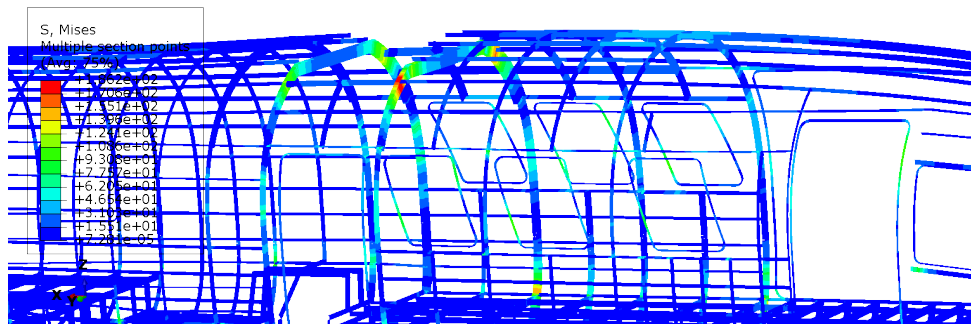


(c)

Figure 5.10: Fuselage stress concentration, LC18. $[MPa]$

(a) Shell elements.


(b) Frames and stringers.


(c)
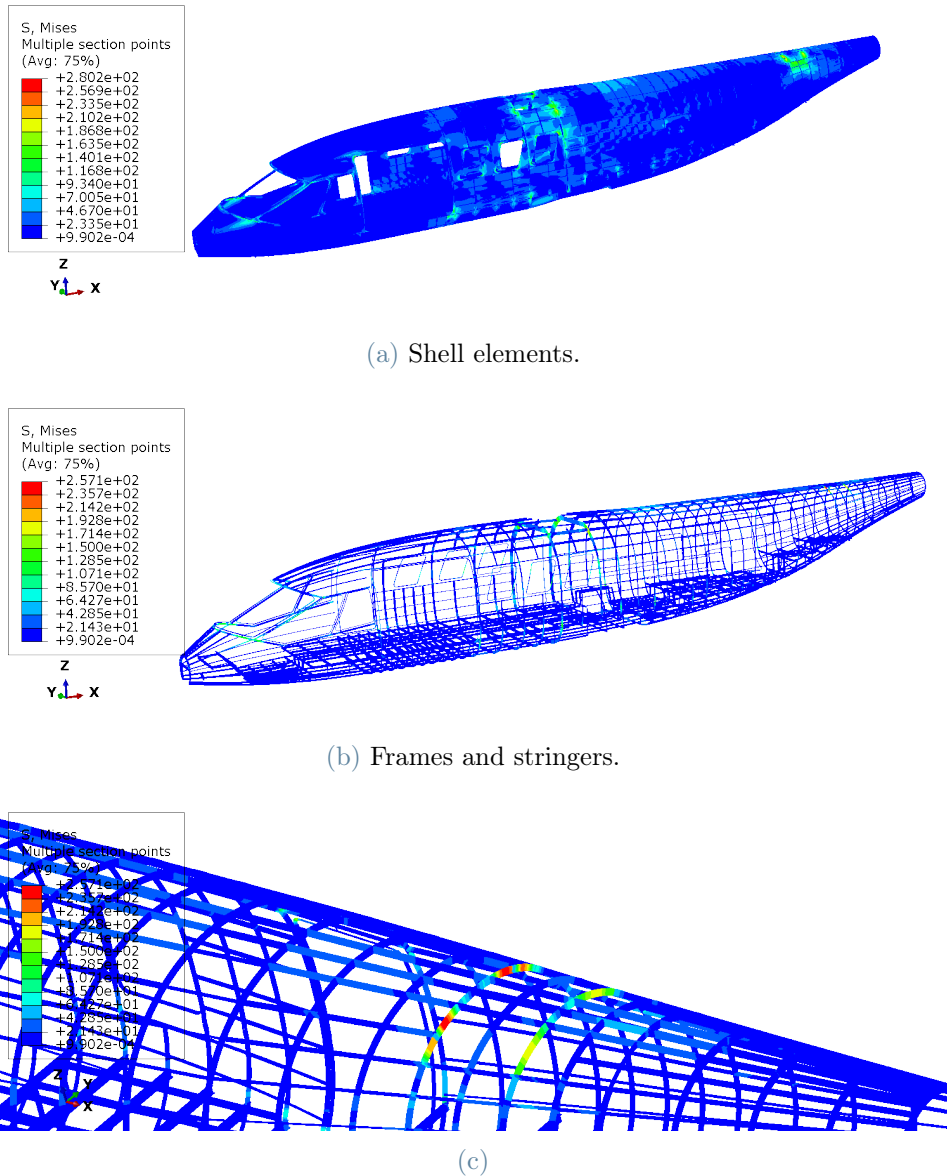
Figure 5.11: Fuselage stress concentration, LC25. [$MPa$]

The buckling simulations have been performed for all the load cases highlighted in the preliminary load design, obtaining the results reported in Table 5.7. From which is possible to prove the structural stability for the whole flight envelope. Because the relevant eigenvalues are all greater than 1.5 therefore the instability occurs after the ultimate load. It is important to notice that the eigenvalue smaller than 1.5 are non relevant because the instabilities are non-physical. This is due to the necessity, for the simulations, to model using a fake non-resistant material to model the region where the V-tail is connected to the fuselage. In those region a shell element is not present, therefore the instabilities of those are captured numerically but are not real instabilities (Figure 5.12).
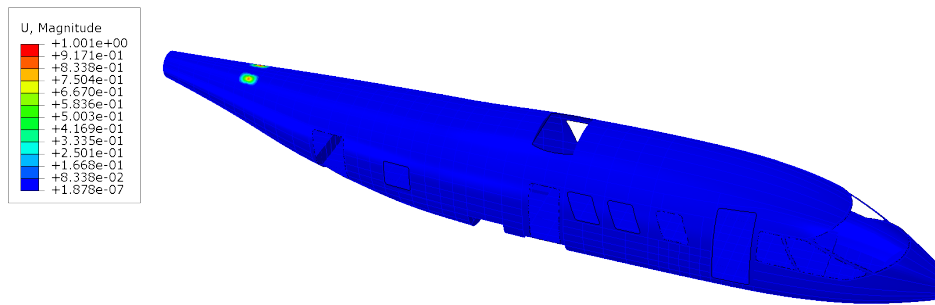
Figure 5.12: Non physiscal buckling region. , $[mm]$

In Appendix D the result for each simulation is provided.

| Mode | LC1 | LC2 | LC3 | LC17 | LC18 | LC19 | LC25 |
|---|---|---|---|---|---|---|---|
| 1 | -0.898 | -0.756 | 1.504 | -0.620 | 0.440 | 1.503 | 0.170 |
| 2 | -0.913 | -0.768 | 1.522 | -0.630 | 0.443 | 1.553 | 0.171 |
| 3 | -0.979 | -0.807 | 1.559 | -0.676 | 0.634 | 1.567 | 0.244 |
| 4 | -1.001 | -0.827 | 1.590 | -0.691 | -0.700 | 1.600 | 0.245 |
| 5 | -1.004 | -0.844 | 1.660 | -0.694 | 0.633 | 1.666 | 0.332 |

Table 5.7: Fuselage buckling eigenvalues numerical data.

# 6 | Assembly elements design design

The connection between the fuselage and the aerodynamic surfaces is one of the most important elements to be taken into consideration for the preliminary design because neglect small but important sub elements may provoke a big effect on the next project development if any issue is encountered on those. Moreover the definition of high lever system directly impact the overall airframe design. For these reasons analyze a concept of the wing fuselage connections is mandatory.

The wing connection mechanism is based on a relatively simple pin-bolt connection: each wing (or tail) spar is directly connected to one strong fuselage frame and held in position using a pin, shown in Figure 6.1. The connection in order to be in compliance with the regulations is necessary to be proven fail-safe, its design is performed in two steps which follow.
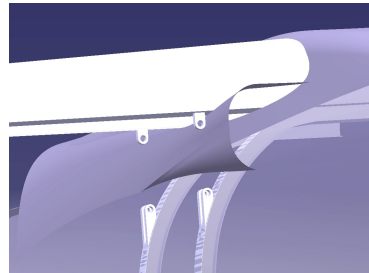


Figure 6.1: Wing fuselage connection lug concept.

## 6.1. Analytical

Many references are reported in technical books, article and studies regarding the analytical lug model and sizing, one accurate sizing procedure is available in [8], which is used to have a preliminary lug size. Considering Figure 6.2 a given lug can be modelled using three dimensions: $D$, $t$ and $a$. The analytical sizing procedure have been followed to define the preliminary dimensions of the lugs considering the maximum force expected to be transmitted. To size the junction is necessary to size both male and female side of the lug. In particular the inner one is need to withstand all the force $P$ multiplied by the factor of safety, bu the female one (the external) being composed by two parts, need to withstand only to $P/2$ multiplied bu the safety factor. Sizing both individually

the connection is defined.



(a) Lug axial load          (b) Lug failure modes
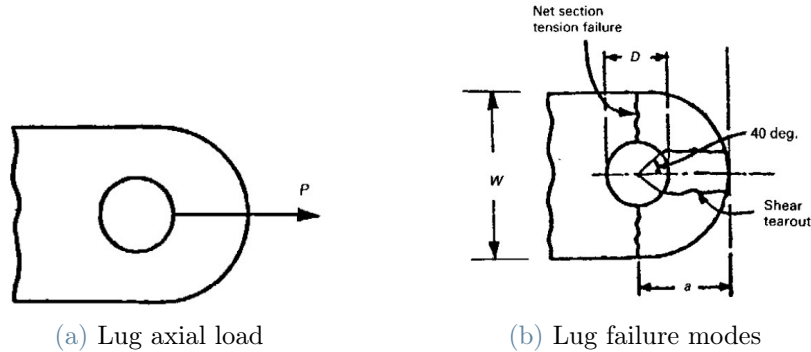
Figure 6.2: Lug analytical model.

## 6.2.   Junction fail safeness

The connection just sized is tested using FEM model to check in detail the stress concentration, due to the symmetry of the problem, only a fourth of the lug is considered to save computational time and resources, Figure 6.3.

In this condition symmetry boundary conditions are considered in the relative faces and an ensacter constrain is defined at the basis of female lug.  The force applied is $104000N$ relative to LC1 is applied to a reference point which, considering kinematic coupling is connected to the whole basis of the internal lug. Using a quadrilateral structured mesh obtaining the stress distribution shown in Figures 6.4. Being the maximum stress is located



Figure 6.3:   Wing-fuselage connection lug mesh.

in the internal lug (Figure 6.4c) of $275MPa$, well below the yielding stress of the titanium, is possible to prove the safeness of the connection. As for the wing and the fuselage the sizing developed in this section can and will be furthermore optimized in the next project phases.

The connection just developed is not a fail safe mechanism: is a crack if generated in one element it can propagate and never stop with consequent catastrophic failure. The model therefore has to be modified to be in compliance with CS-23 regulations. The changing consists in doubling any element present in the junction: two concentric pin are present

(a)



(b)



(c)
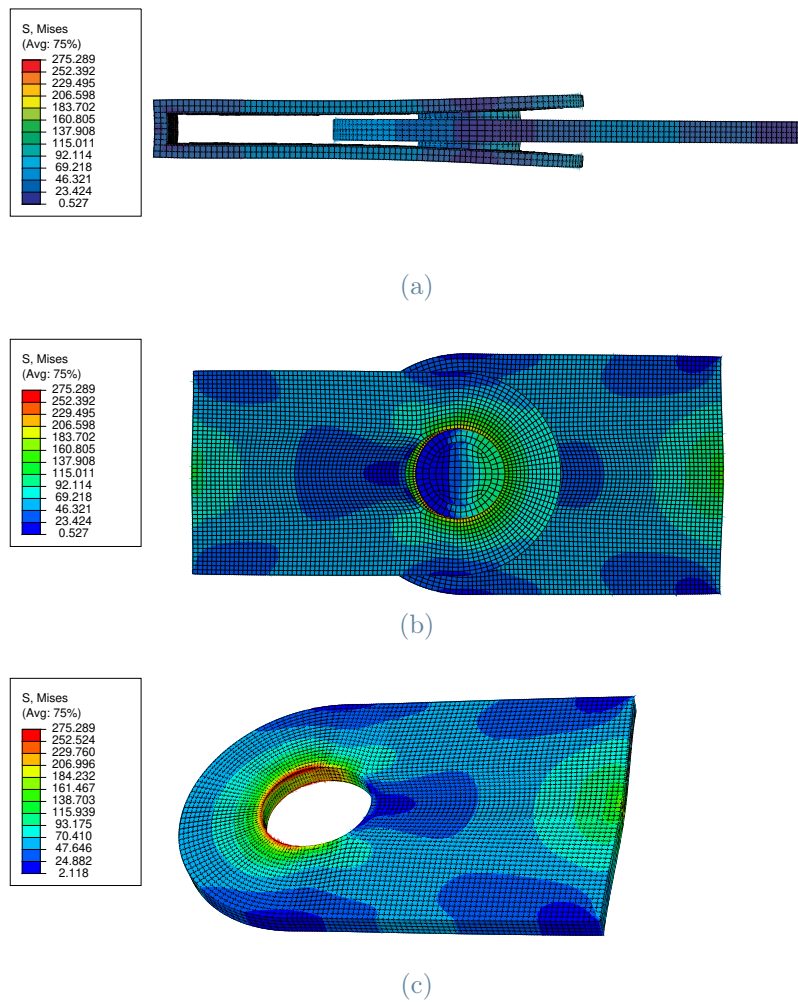
Figure 6.4: Stress distribution in wing-fuselage connection lugs. Stresses in $[MPa]$

and two lugs are defined in each connection end, considering that each element must be able so withstand the limit load.
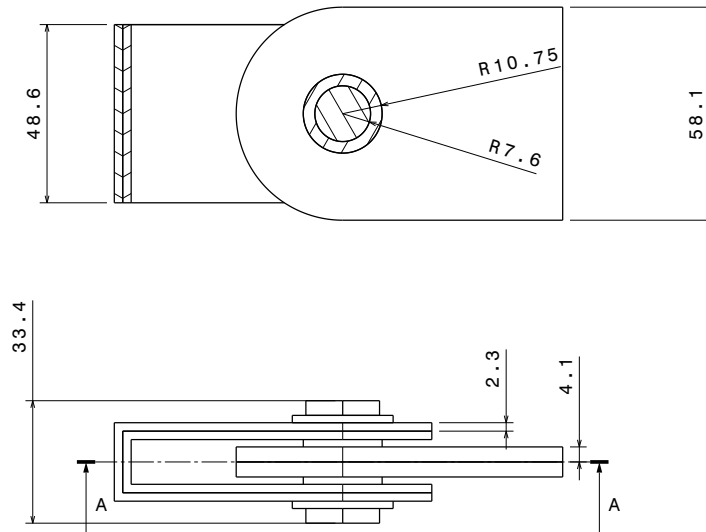


Figure 6.5: Lug fail-safe concept, dimensions in $[mm]$

In this configuration shown in Figure 6.5 if is a crack is generated in one element, there is a backup element that prevent a catastrophic failure. The dimensions considered in this design are the same dimension obtained by the analytical sizing, these may not be optimal but are a good starting point for begin a future optimization procedure. The junction obtained in this way has to be proven fail safe, this require a more detailed methodology as FEM analysis. To ease the model generation, the geometry generated in CATIA is imported and assembled in Abaqus, the material proprieties are applied and the mesh and analysis are executed. The material chosen for this element is titanium, because is necessary to have a very Strong material due to the importance and critical condition of these elements.

# 7 | Conclusion and next steps

This research wanted to study and develop two main aspects in Unifier19 development, one is to intended as a more theoretical and on methodology development of study the feasibility of a new aircraft concept, and the other more practical which consist in the actual sizing of the full aircraft airframe. Regarding the first aspect a fully working parametric model generation is developed, in which, given the external loft, the designer can generate quickly and efficiently countless new configuration in terms of wing spacing, material selection, cutout frames and many other parameters. This tool can and will be very useful for future research allowing the possibility to develop accurately sensitivity analysis on any given parameter both in wing and fuselage design in order to find which are the most relevant parameters for a concept like Unifier19. It is important to notice that this methodology and the tool developed can, in principle, being applied to any innovative A/C design because there are not any constraints that impact the design, the only constraints in terms of frame and rib position are provided by the designer in input, considering his experience and the actual system design.

Considering the development of Unifier19 airframe the initial objective was to define a structure architecture that satisfy all the requirements and, considering the FEM analysis, is possible to conclude that this objective is fully achieved. Nevertheless the structure developed have many possibility of improvement that can be achieved with the development and use of an optimizer tool that can find the optimal thickness distribution both in wing and fuselage. The airframe described and developed in this research consider only in-flight conditions, in order to finish the airframe design is a detail project, is necessary to consider all the other constrains and critical load conditions. In particular is necessary to develop a methodology for damage tolerance analysis in case of debris impacts or failure of some structural elements, and detailed analysis on the wing box in maneuvering conditions should be developed, considering the chord pressure distribution for the elevators deflection. Other critical aspect that is not analyzed in this work is the feasibility of the airframe from a manufacturing point of view: a detailed study on the manufacturing process is very important in this stage of the project because is can provide constraint on the minimum and maximum element dimensions or can highlight

problems on the element connection points. In parallel to this future task the development of an optimizer is crucial in order to find the minimum weight solution, considering the possibility of chaining the material selection used in this work. In particular the use of composite material will be taken into consideration, allowing the possibility of have a lighter airframe design. The use of composite should consider the different failure modes with respect to standard alloys and the non-trivial increase in production cost that may balance out the performance increase obtained with composite materials.

## 7.1. Final weight considerations

Unifier19 airframe developed presents a fuselage and wing mass respectively of $1243kg$ and $289kg$ for a total of $1821Kg$. Considering the statistical regression made in the project early phases and the masses obtained in this steps are higher of $95Kg$ being the fuselage and wing masses hypothesized to be $1005Kg$ and $721Kg$ respectively. This result however is considered a good result because, both for the wing and the fuselage the stress distribution is quite far from the optimal one, in particular considering the static load condition. This will lead to the possibility for the next project phases to develop a optimizer for the material distribution and the use of the developed automatic GFEM scripts to test different configuration in terms of frame spacing that vastly impact the structural efficiency. Moreover the introduction of composite materials will produce a lighter structure with non-trivial weight saving.

# Bibliography

[1] M. Richetta A Varone A. Gloria, R. Montanari. Alloys for aeronautic applications: State of the art and perspectives. *Metals*, 9(6):662, June 2019.

[2] European Aviation Safety Agency. Certification specifications and accetable means of compliance for normal, utility, aerobatic, and commuter category aeroplane, 2015.

[3] European Aviation Safety Agency. Easy access rules for light sport aeroplanes $(\text{cs}_l sa)(amendment - 1), 2018.$

[4] European Aviation Safety Agency. Electric propulsion units for cs-23 normal-category aeroplanes up to level 1, amc 20-115d, 2020.

[5] European Aviation Safety Agency. General accetable means of compliance for airworthiness of products, parts and applinces (amc-20), amendament 22, 2021.

[6] ASTM International. Standard specification for structures, 2021.

[7] T. H. G. Megson. *Aircraft Structurs for engineering students*. Elsevier, 2007.

[8] M. C. Y. Niu. *Airframe Structural Design*. Conmilit Press LTD., 1988.

[9] M. C. Y. Niu. *Composite Airframe Structures*. Conmilit Press LTD., 1992.

[10] M. C. Y. Niu. *Airframe Stress Analysis And Sizing*. Conmilit Press LTD., 2001.

[11] T. Warner Ph. Lequeu, Ph. Lassince. Aluminum alloy development for the airbus a380 - part 2. *Advanced materials processes*, (2):41–43, 7 2007.

[12] Gong Song and Guan Long Song. Theoretical investigation for building aircraft finite element modeling and its validation. In *AIAA Modeling and Simulation Technologies Conference*. American Institute of Aeronautics and Astronautics, August 2012.

[13] Yue Wu. Application of aluminum alloy in aircraft. *Journal of Physics: Conference Series*, 2228(1):012024, March 2022.

[14] Ming Zhang, Rongmin Jiang, and Hong Nie. Design and test of dual actuator nose wheel

steering system for large civil aircraft. *International Journal of Aerospace Engineering*, 2016:1–14, 2016.

# A | Load Assumption

First step of the structural sizing is the definition of the aircraft flight envelope and the definition of the load condition that are expected in service. This study, performed by Pipistrel Vertical Solution using confidential algorithm, produced as result 32 load cases reported in Table A.2, where the weight and balance configurations (W&B) are reported in Table A.1

| | $m$ $[kg]$ | $x_{CG}$ $[m]$ | $y_{CG}$ $[m]$ | $z_{CG}$ $[m]$ | $I_{xx}$ $[kg\,m^2]$ | $I_{yy}$ $[kg\,m^2]$ | $I_{zz}$ $[kg\,m^2]$ |
|---|---|---|---|---|---|---|---|
| max F | 7437.6 | 8.085 | 0.0 | 0.208 | 23527 | 89829 | 102125 |
| max R | 7437.6 | 8.444 | 0.0 | 0.208 | 23527 | 89528 | 101823 |
| min F | 5129.6 | 8.085 | 0.0 | 0.094 | 22643 | 76066 | 88486 |
| min R | 5129.6 | 8.444 | 0.0 | 0.094 | 22643 | 76618 | 89038 |

Table A.1: Weight and balance configuration.

| Case | W&B | Airspeed | $V_{EAS}$ [$^m/_s$] | Status | $n$ [$-$] | $L$ [N] | $L_{VT}$ [N] | $C_L$ |
|---|---|---|---|---|---|---|---|---|
| LC1 | max F | $V_A$ | 82.3104 | man+ | 3.01 | 217448.80 | 2095.81 | 1.813 |
| LC2 | max F | $V_D$ | 115.2346 | man+ | 3.01 | 219669.09 | $-124.47$ | 0.934 |
| LC3 | max F | $V_A$ | 82.3104 | man- | $-1.20$ | $-83455.70$ | $-4070.39$ | $-0.695$ |
| LC4 | max F | $V_D$ | 115.2346 | man- | $-1.20$ | $-81235.41$ | $-6290.68$ | $-0.345$ |
| LC5 | max F | $V_C$ | 82.3104 | gust+ | 2.47 | 178776.84 | 1303.34 | 1.490 |
| LC6 | max F | $V_D$ | 115.2346 | gust+ | 2.03 | 149500.05 | $-1562.39$ | 0.636 |
| LC7 | max F | $V_C$ | 82.3104 | gust- | $-0.47$ | $-31203.72$ | $-2999.63$ | $-0.260$ |
| LC8 | max F | $V_D$ | 115.2346 | gust- | $-0.03$ | 2513.65 | $-4574.48$ | 0.010 |
| LC9 | max R | $V_A$ | 82.3104 | man+ | 3.01 | 207586.25 | 11958.36 | 1.730 |
| LC10 | max R | $V_D$ | 115.2346 | man+ | 3.01 | 209806.54 | 9738.07 | 0.892 |
| LC11 | max R | $V_A$ | 82.3104 | man- | $-1.20$ | $-79523.78$ | $-8002.31$ | $-0.663$ |
| LC12 | max R | $V_D$ | 115.2346 | man- | $-1.20$ | $-77303.49$ | $-10222.60$ | $-0.328$ |
| LC13 | max R | $V_C$ | 82.3104 | gust+ | 2.47 | 170687.14 | 9393.04 | 1.423 |
| LC14 | max R | $V_D$ | 115.2346 | gust+ | 2.03 | 142854.28 | 5083.37 | 0.607 |
| LC15 | max R | $V_C$ | 82.3104 | gust- | $-0.47$ | $-29667.21$ | $-4536.14$ | $-0.247$ |
| LC16 | max R | $V_D$ | 115.2346 | gust- | $-0.03$ | 2606.22 | $-4667.05$ | 0.011 |
| LC17 | min F | $V_A$ | 82.3104 | man+ | 4.36 | 217448.80 | 2095.81 | 1.813 |
| LC18 | min F | $V_D$ | 115.2346 | man+ | 4.36 | 219669.09 | $-124.47$ | 0.934 |
| LC19 | min F | $V_A$ | 82.3104 | man- | $-1.74$ | $-83455.69$ | $-4070.39$ | $-0.695$ |
| LC20 | min F | $V_D$ | 115.2346 | man- | $-1.74$ | $-81235.40$ | $-6290.68$ | $-0.345$ |
| LC21 | min F | $V_C$ | 82.3104 | gust+ | $-3.08$ | 154154.58 | 798.77 | 1.285 |
| LC22 | min F | $V_D$ | 115.2346 | gust+ | 2.46 | 125610.69 | $-2051.94$ | 0.534 |
| LC23 | min F | $V_C$ | 82.3104 | gust- | $-1.08$ | $-50939.95$ | $-3404.07$ | $-0.424$ |
| LC24 | min F | $V_D$ | 115.2346 | gust- | $-0.46$ | $-17955.48$ | $-4993.94$ | $-0.076$ |
| LC25 | min R | $V_A$ | 82.3104 | man+ | 4.36 | 207586.25 | 11958.36 | 1.730 |
| LC26 | min R | $V_D$ | 115.2346 | man+ | 4.36 | 209806.54 | 9738.07 | 0.892 |
| LC27 | min R | $V_A$ | 82.3104 | man- | $-1.74$ | $-79523.78$ | $-8002.31$ | $-0.663$ |
| LC28 | min R | $V_D$ | 115.2346 | man- | $-1.74$ | $-77303.49$ | $-10222.60$ | $-0.328$ |
| LC29 | min R | $V_C$ | 82.3104 | gust+ | 3.08 | 147193.65 | 7759.71 | 1.227 |
| LC30 | min R | $V_D$ | 115.2346 | gust+ | 2.45 | 120060.09 | 3498.65 | 0.510 |
| LC31 | min R | $V_C$ | 82.3104 | gust- | $-1.08$ | $-48498.67$ | $-5845.35$ | $-0.404$ |
| LC32 | min R | $V_D$ | 115.2346 | gust- | $-0.45$ | $-16924.53$ | $-6024.89$ | $-0.072$ |

Table A.2: Load cases.

# B | Landing gears technical drawings
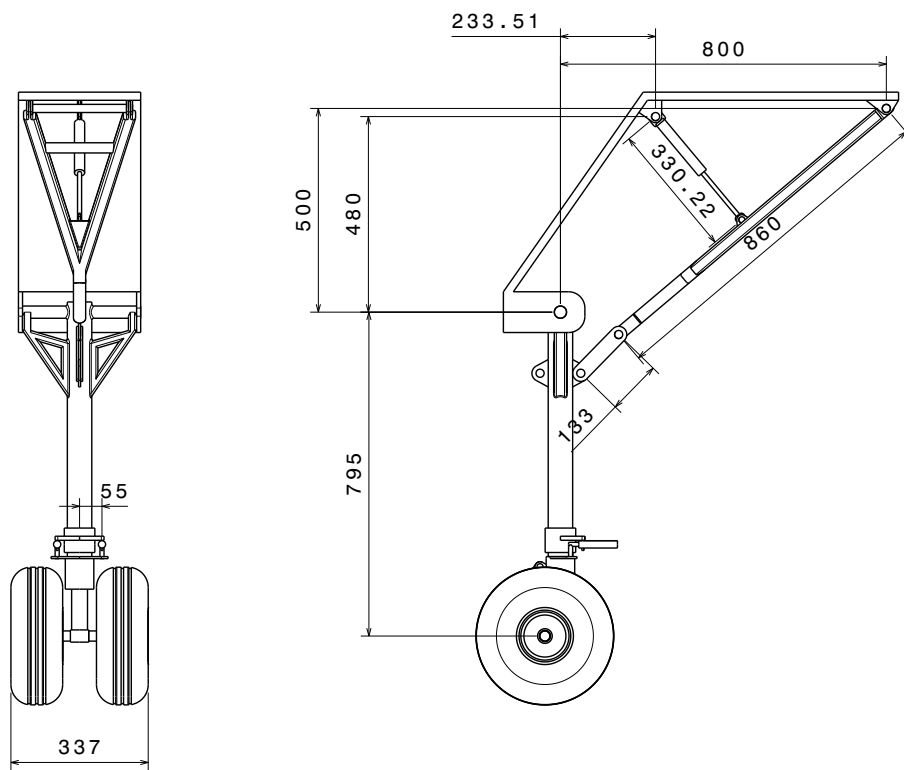


Figure B.1: Nose landing gear extended position, dimension in [$mm$]
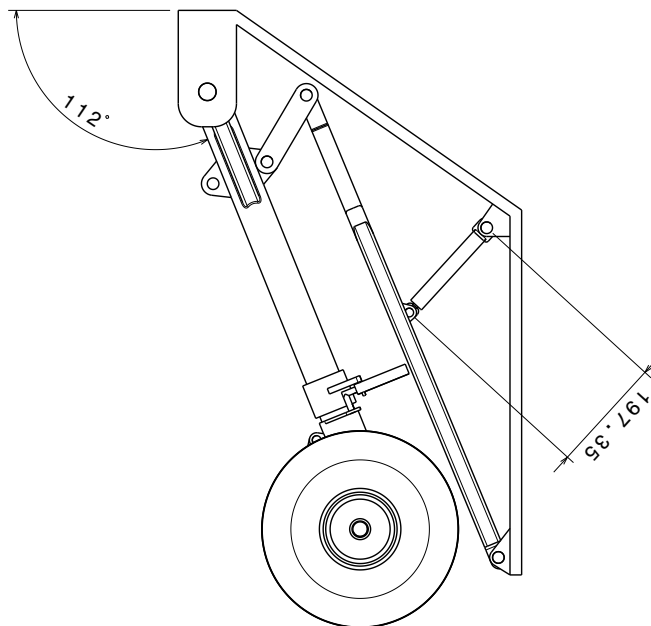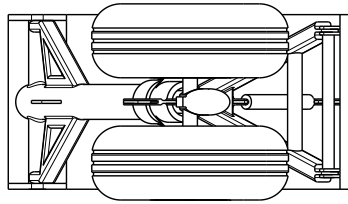
Figure B.2: Nose landing gear retracted position, dimension in [$mm$]
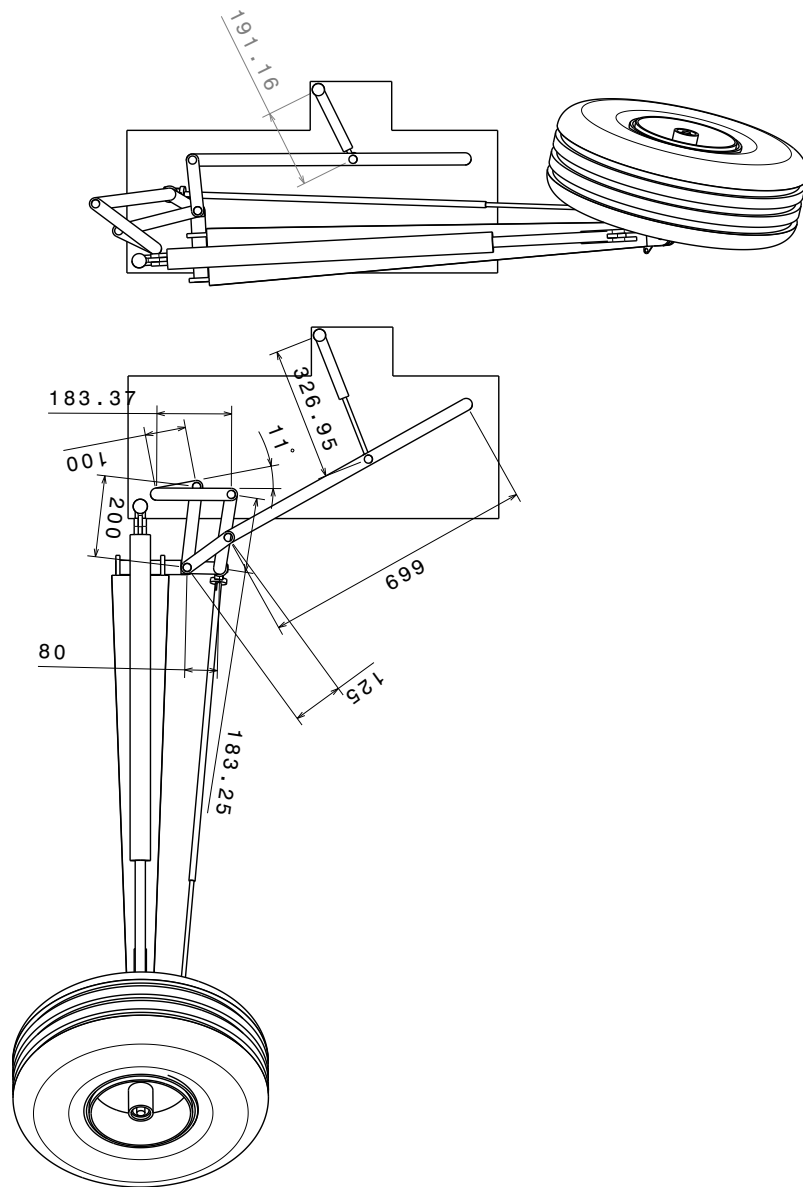
Figure B.3: Main landing gear kinematic system dimensions, dimension in [$mm$]
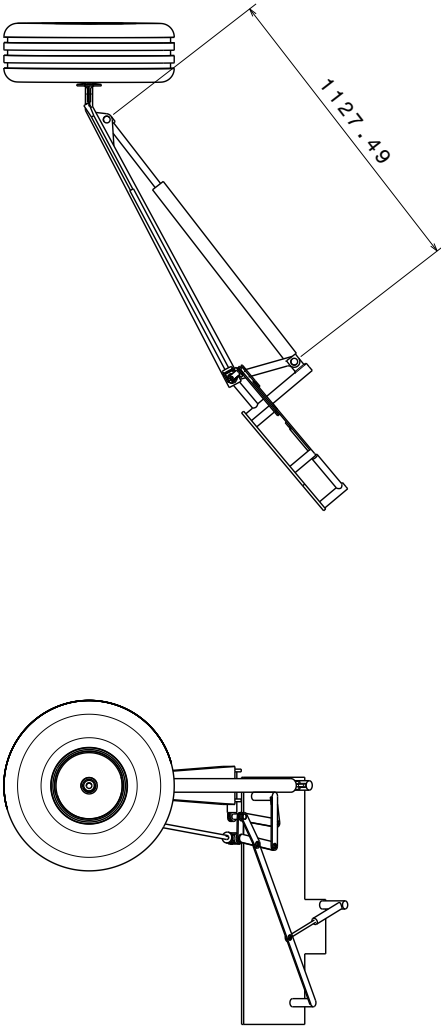
Figure B.4: Main landing gear assembly, dimension in [*mm*]

# C | Main wing simulations

In the following pages are reported the numerical results for the wing static simulations at ultimate load condition.
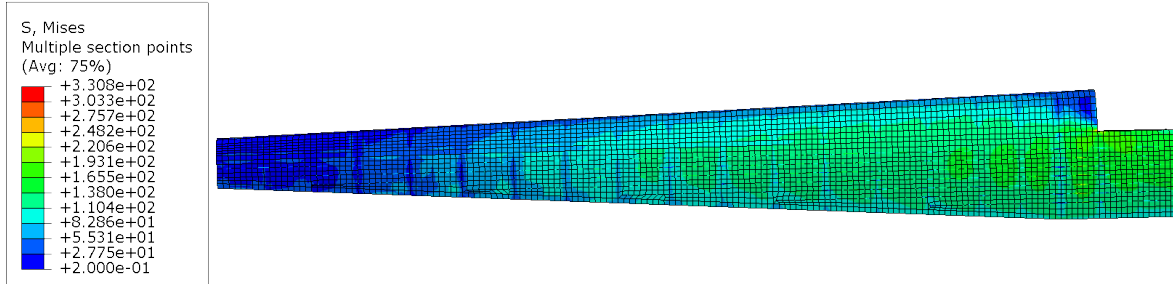
(a) Pressure side.
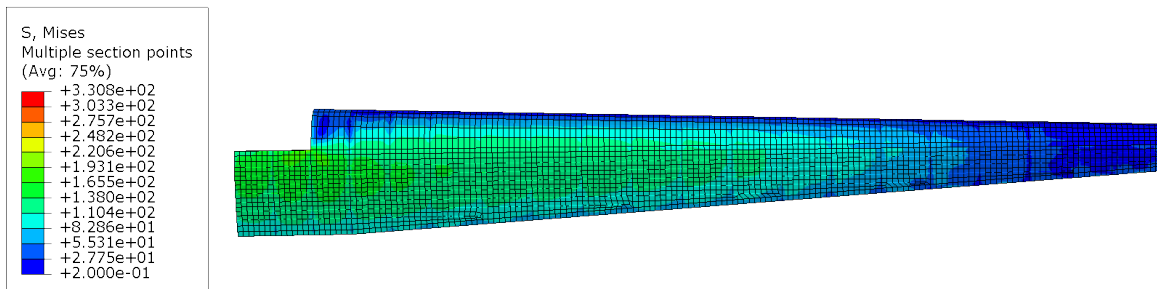


(b) Suction side.
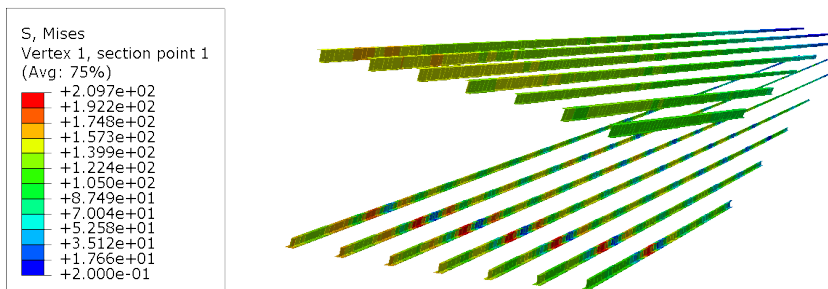


(c) Stringers.

Figure C.1: Wing static simulation for LC1, $[MPa]$
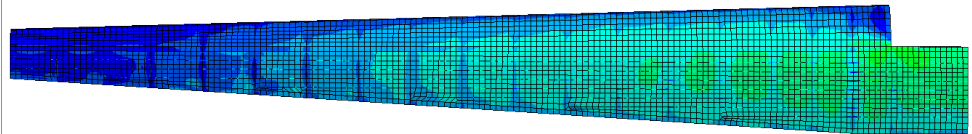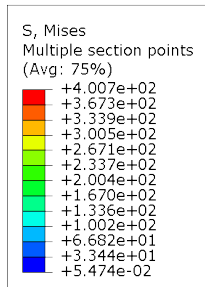
(a) Pressure side.
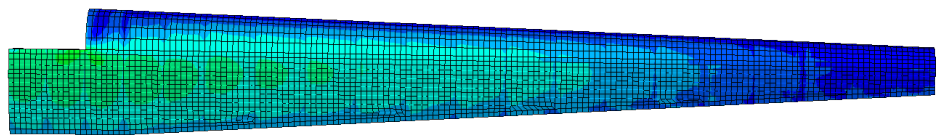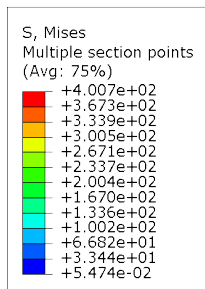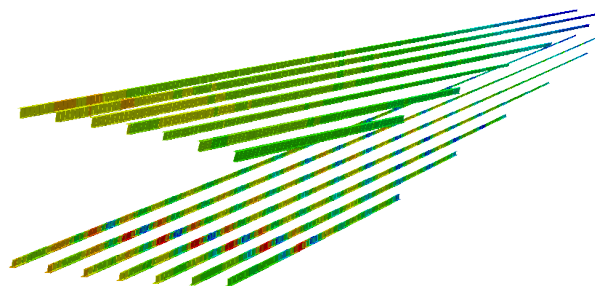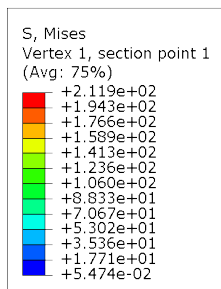


(b) Suction side.



(c) Stringers.

Figure C.2: Wing static simulation for LC2, $[MPa]$
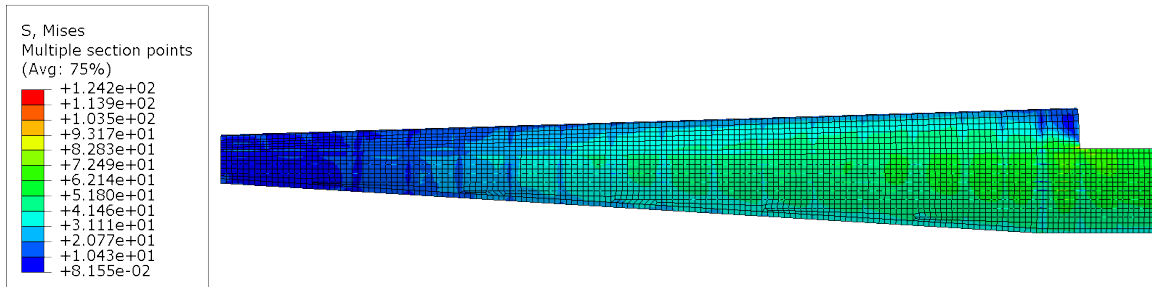
(a) Pressure side.
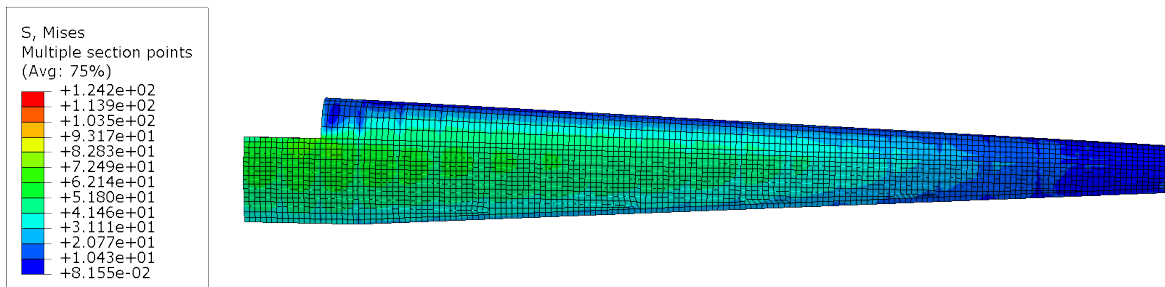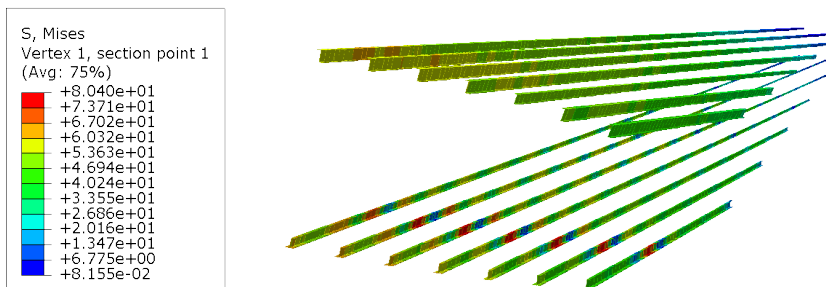


(b) Suction side.



(c) Stringers.

Figure C.3: Wing static simulation for LC3, $[MPa]$
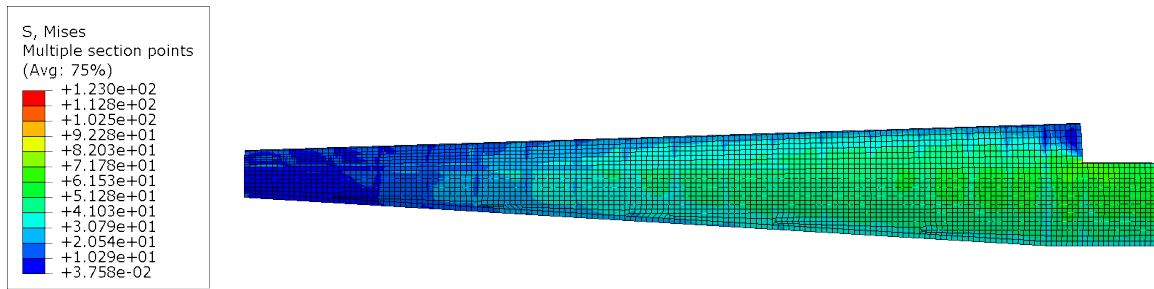
(a) Pressure side.
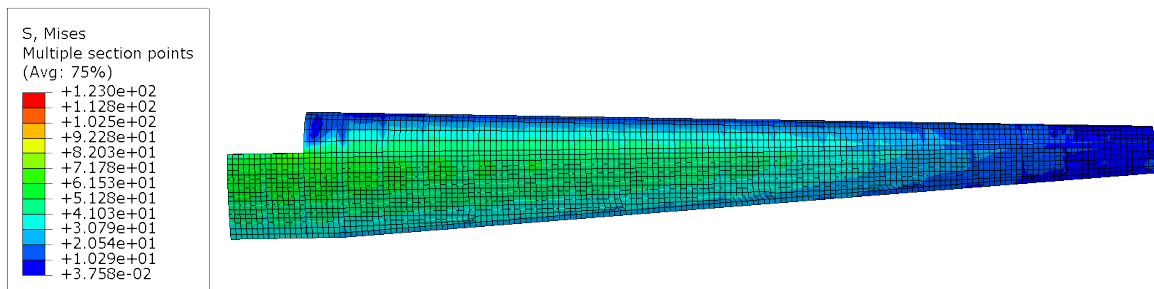


(b) Suction side.
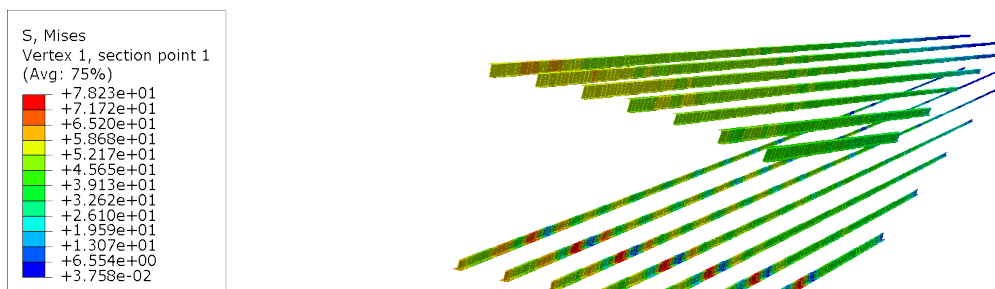


(c) Stringers.

Figure C.4: Wing static simulation for LC4, $[MPa]$

# D | Fuselage simulations

In the following pages are reported the numerical results for the fuselage static simulations at ultimate load condition.
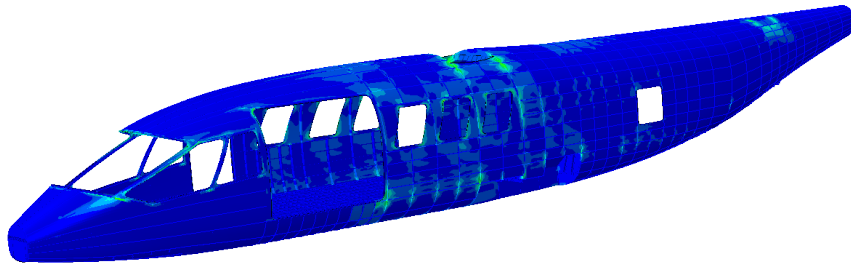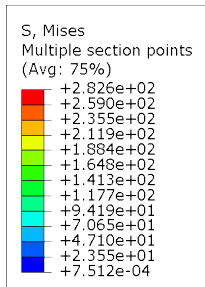
(a) Left side.
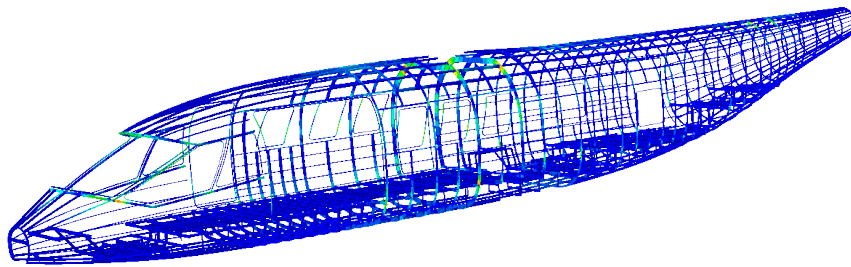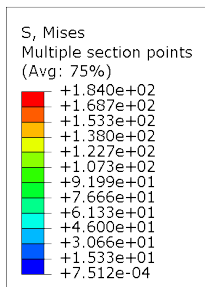


(b) Floor and floor support.
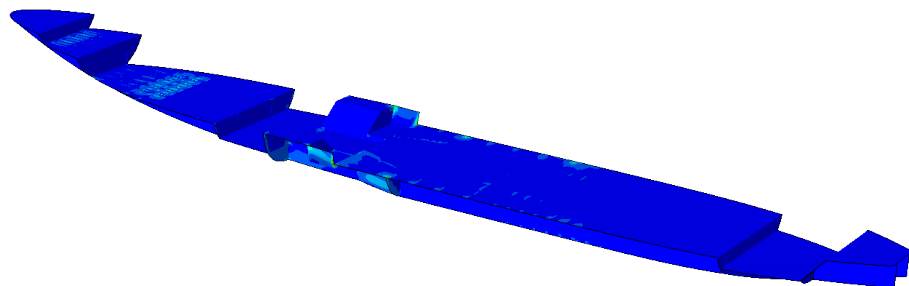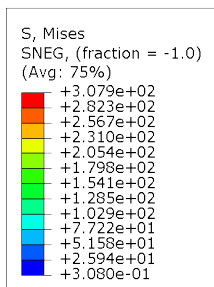


(c) Frames and stringers.

Figure D.1: Fuselage static simulation for LC1, $[MPa]$
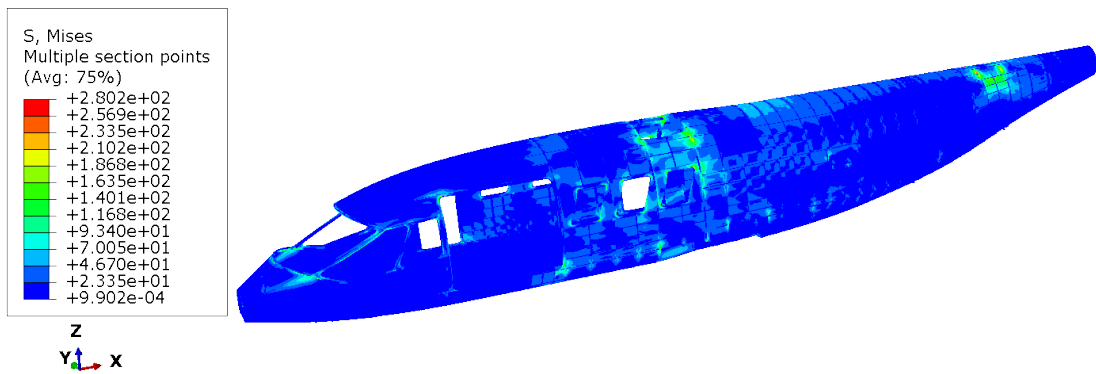
(a) Left side.
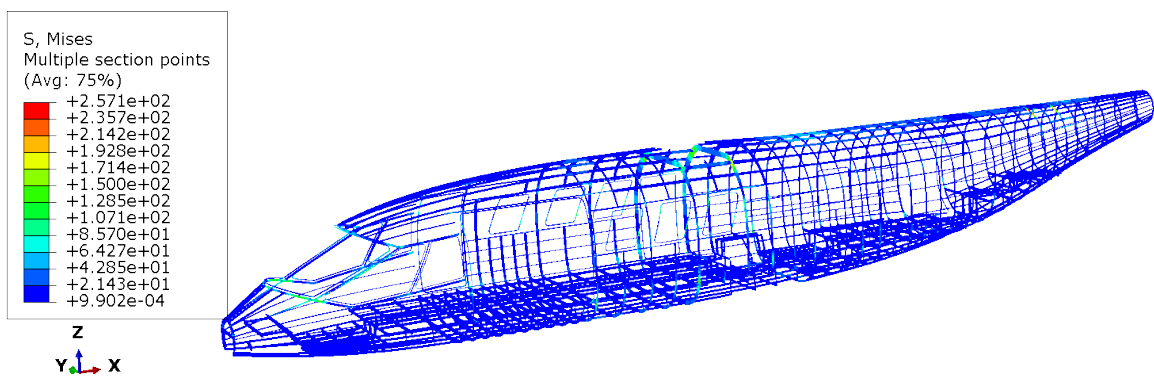


(b) Floor and floor support.
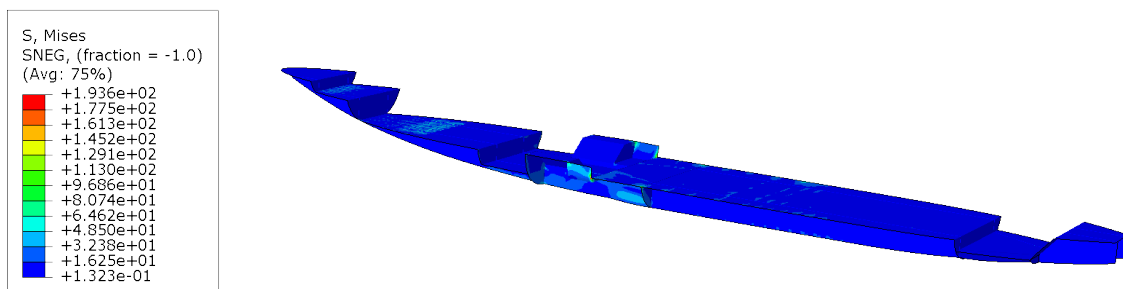


(c) Frames and stringers.

Figure D.2: Fuselage static simulation for LC2, $[MPa]$
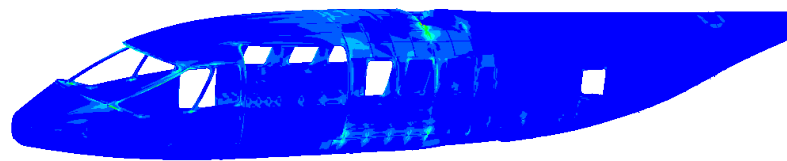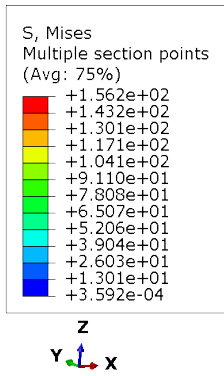
(a) Left side.
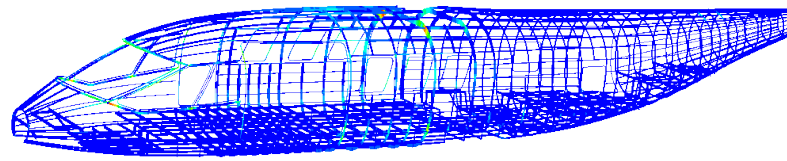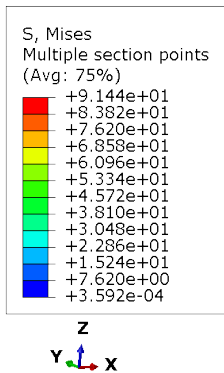


(b) Floor and floor support.
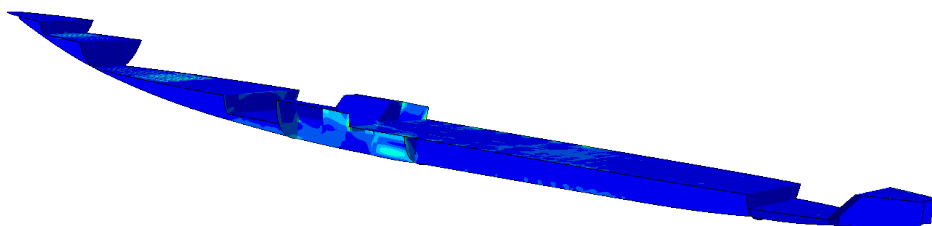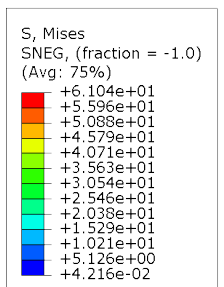


(c) Frames and stringers.

Figure D.3: Fuselage static simulation for LC3, $[MPa]$
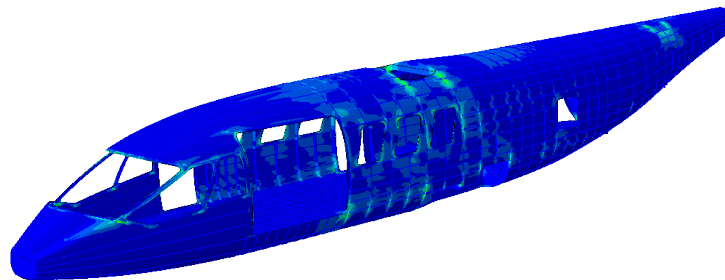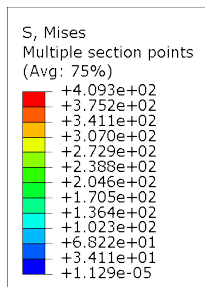
(a) Left side.
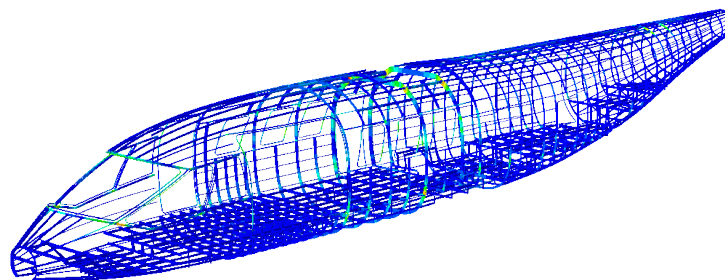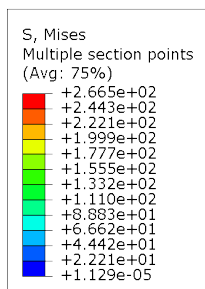


(b) Floor and floor support.
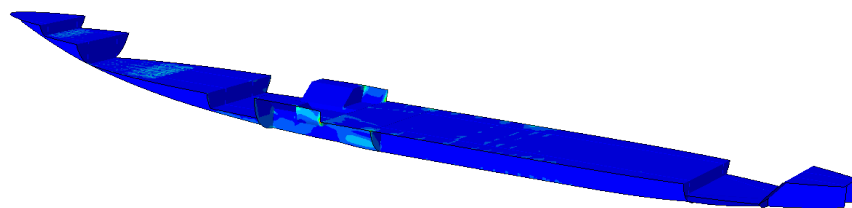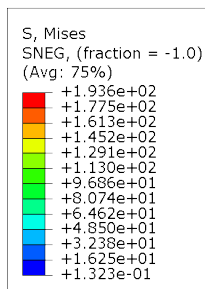


(c) Frames and stringers.

Figure D.4: Fuselage static simulation for LC17, $[MPa]$
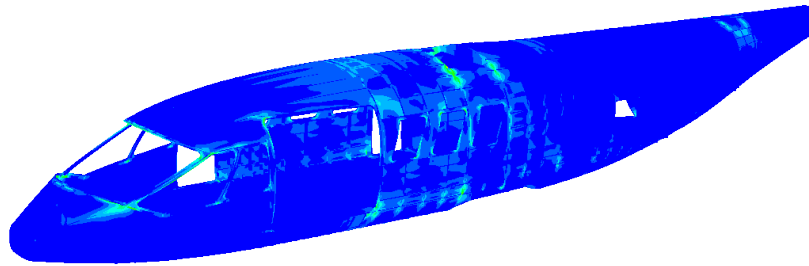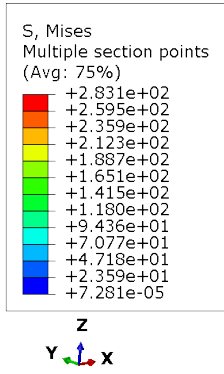
(a) Left side.
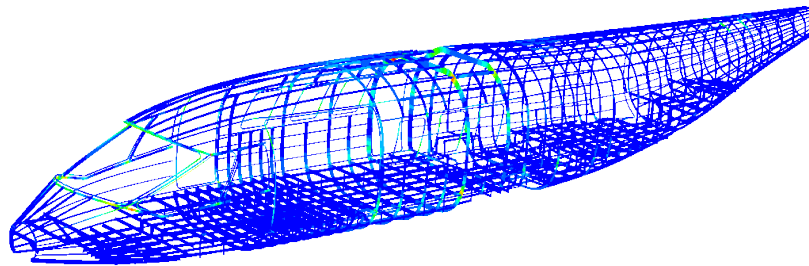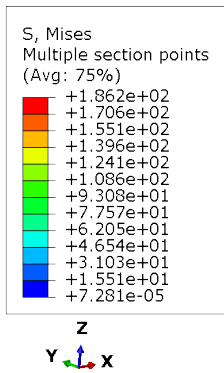


(b) Floor and floor support.
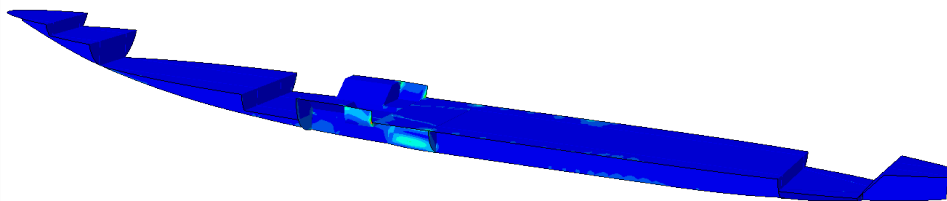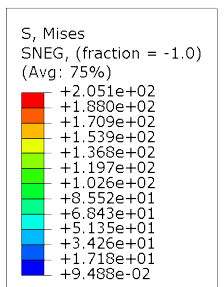


(c) Frames and stringers.

Figure D.5: Fuselage static simulation for LC18, $[MPa]$
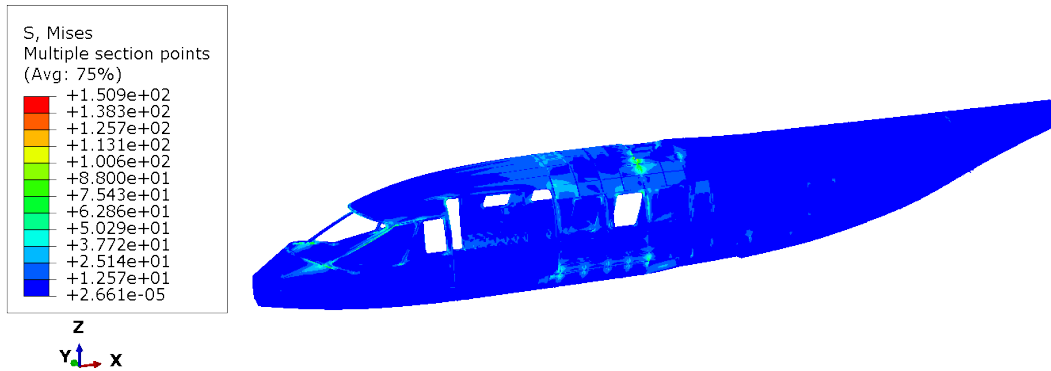
(a) Left side.
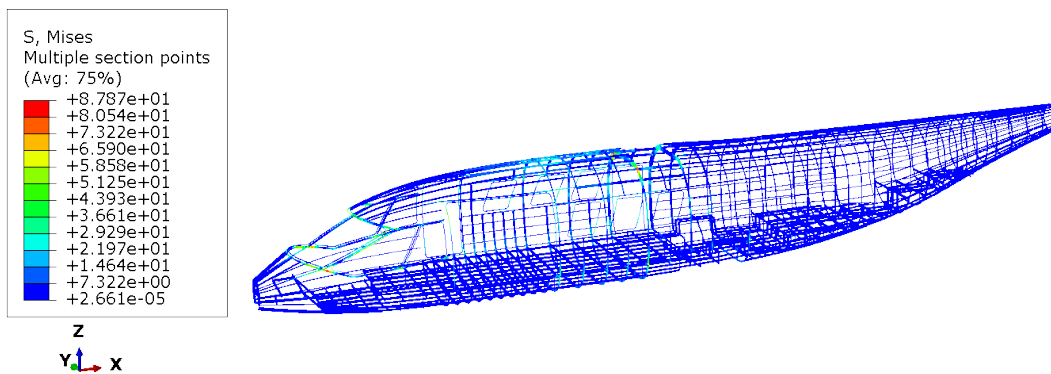


(b) Floor and floor support.
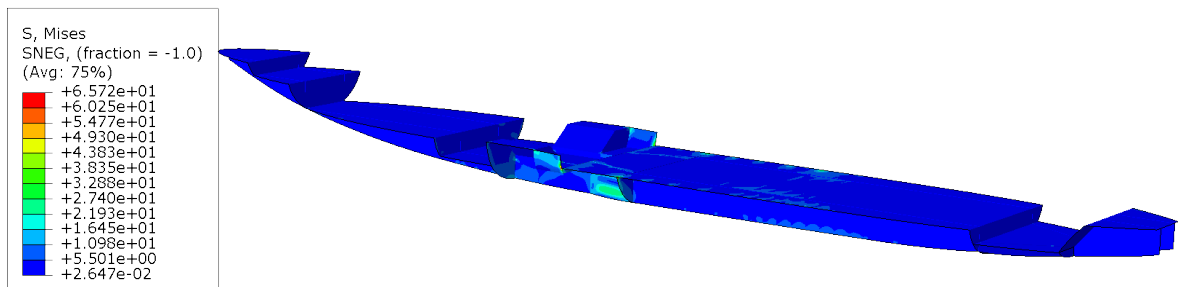


(c) Frames and stringers.

Figure D.6: Fuselage static simulation for LC19, $[MPa]$
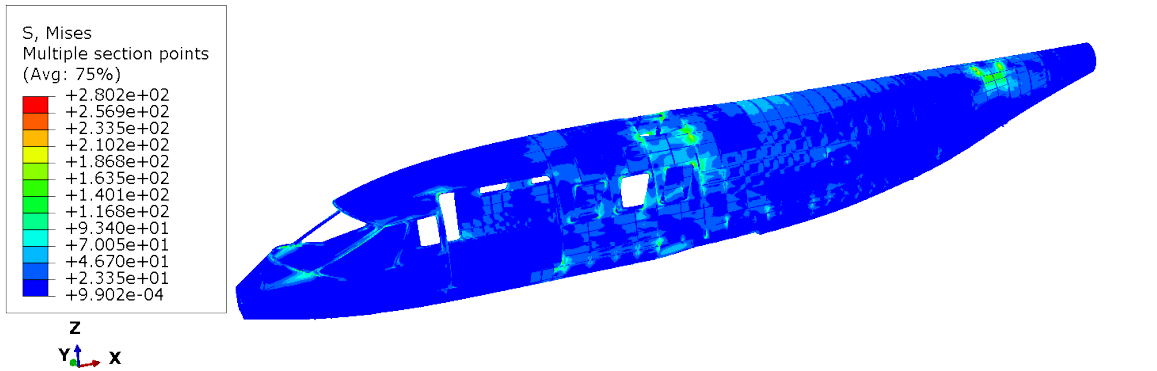
(a) Left side.
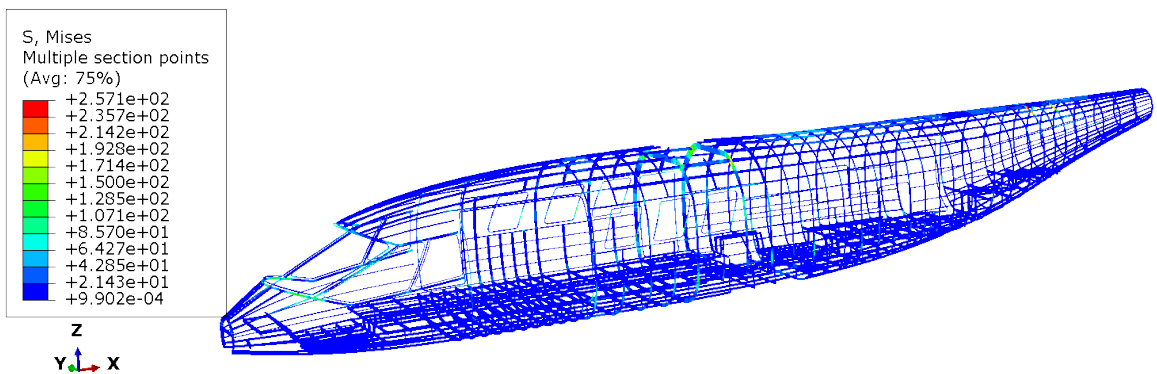


(b) Floor and floor support.
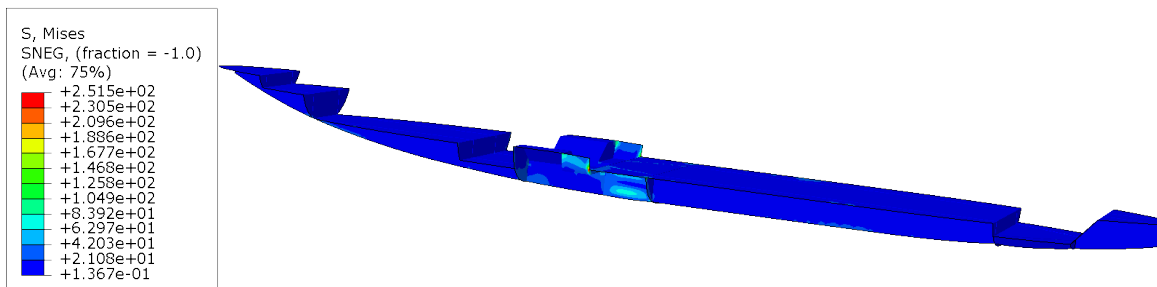


(c) Frames and stringers.

Figure D.7: Fuselage static simulation for LC25, $[MPa]$

# E| Cutaways
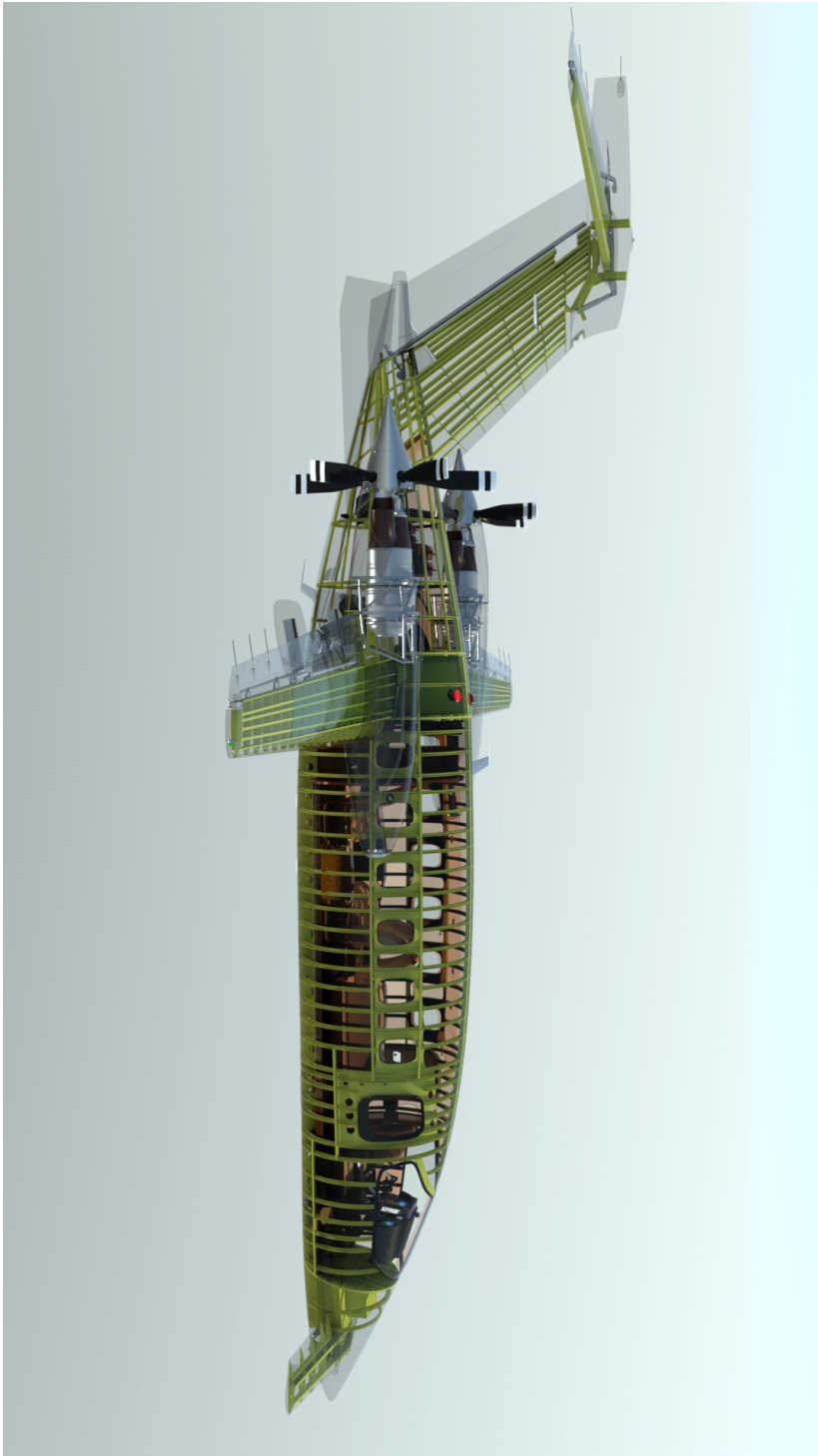


Figure E.1: Piaggio P180 Avanti cutaway

programme, based on the previously-described timetable for certification. First flight was to be made in August 1984.

On 4 November 1981, a new co-operative agreement was signed by the two companies, confirming the 50/50 division of costs and work-sharing, and providing for the setting up under French law of a Groupement d'Intérêt Economique (GIE) to manage the programme. This GIE, with the name Avions de Transport Régional and headquartered in Toulouse, was established on 5 February 1982. Investment of FFr1,500m, at 1981 values, was approved to launch the baseline version of the ATR 42.

After further consideration of the available engines, which had included the General Electric CT7-9 as well as the PW117, the ATR management had meanwhile confirmed, on 8 June 1981, the choice of the Canadian engine, in its newly-available PW120.

### Avions de Transport Régional ATR 42-200 Specification

**Power Plant:** Two Pratt & Whitney Canada PW120 turboprops each rated at 1,800 shp (1,342 kW) for take-off, and emergency reserve power of 2,000 shp (1,492 kW), up to ISA + 13 deg C at sea level. Hamilton Standard four-bladed composite construction constant-speed fully-feathering and reversing propellers of 13 ft 0 in (3.96 m) diameter. Fuel capacity, 1,254 Imp gal (5,700 l) in two integral tanks between wing spars.

**Performance:** Max operating speed, 250 kts (463 km/h) CAS or Mach=0.55; Max cruising speed, 266 kts (497 km/h) at 17,000 ft (5,180 m); initial rate of climb, 2,100 ft/min (10.67 m/sec); take-off field length required, 3,575 ft (1,090 m); landing field length, 3,150 ft (960 m); max range with max payload, 645 naut mls (1,195 km); max range with max fuel, 2,750 naut mls (5,096 km); single-engine ceiling, 25,000 ft.

**Weights:** Operating weight empty, 21,986 lb (9,973 kg); fuel weight, 9,920 lb (4,500 kg); max payload, 9,980 lb (4,527 kg); max take-off weight, 34,725 lb (15,750 kg); max zero fuel weight, 31,965 lb (14,500 kg); max landing weight, 34,171 lb (15,500 kg).

**Dimensions:** Span, 80 ft 7½ in (24.57 m); overall length, 74 ft 4½ in (22.67 m); overall height, 24 ft 10 in (7.59 m); wing area, 586.6 sq ft (54.5 m²); aspect ratio, 11.08:1; undercarriage track, 13 ft 5½ in (4.10 m); wheelbase, 28 ft 9¾ in (8.78 m).

**Accommodation:** Flight crew of two. Standard layout for 42 passengers four-abreast at 32-in (81-cm) pitch or up to 50 at 30-in (76-cm) pitch. Baggage compartments above floor, fore and aft, max volume, 324 cu ft (9.1 m³).

### ATR 42 Cutaway Drawing Key

1 Radome
2 Weather radar scanner
3 Scanner tracking mechanism
4 ILS glideslope aerial
5 Front pressure bulkhead
6 Pitot heads
7 Twin nosewheels, forward retracting
8 Nosewheel leg doors
9 Taxiing lamps
10 Nose undercarriage wheel bay
11 Static ports
12 Rudder pedals
13 Instrument panel shroud
14 Windscreen wipers
15 Windscreen panels
16 Overhead systems switch panels
17 Instrument panel (electronic flight instrument system)
18 Co-pilot's seat
19 Emergency equipment stowage
20 Centre control pedestal
21 Control column handwheel
22 Side console panel
23 Cockpit floor level
24 Underfloor control linkages
25 Pilot's seat
26 Angle of attack transmitter
27 Oxygen bottle
28 Pilot's folding seat
29 Avionics equipment racks
30 Central observer's folding seat
31 Electrical equipment racks
32 Cockpit doorway
33 Cockpit roof escape hatch
34 VHF aerial
35 Control cable runs
36 Baggage restraint net
37 Baggage cabin doorway
38 Forward baggage/cargo compartment
39 Baggage loading floor
40 External power socket
41 External power socket, open
42 Door latch
43 Wing inspection light
44 Main cabin door (movable to suit internal layout)
45 Four-abreast passenger seating, 46-seat layout (48- and 50-seat alternative configurations)
46 Emergency escape window hatch, port and starboard
47 Recirculating air fans
48 Floor beam construction
49 Underfloor conditioned air distribution ducting
50 Fuselage skin panel doubler/construction
51 Fuselage frame and stringer construction
52 Cabin wall trim panelling
53 ADF loop aerials
54 Fuselage skin panelling
55 Cabin wall soundproofing panels
56 Cabin roof lighting panels
57 Overhead stowage bins
58 Passenger service units
59 Cabin air distribution duct
60 Conditioned air delivery duct risers
61 Engine bleed air duct to conditioning plant
62 Wing/fuselage attachment main frames
63 Spar attachment joints
64 Wing centre section rib construction
65 Centre section dry bay
66 Control cable runs to engines
67 Wing leading-edge fillet framing
68 Honeycomb leading-edge fillet panels
69 Fuel guards
70 Starboard wing integral fuel tank, total fuel capacity 1,254 Imp gal (5,700 l)
71 Detachable leading-edge
72 Engine bleed air ducting
73 Ventral exhaust nozzle
74 Starboard engine nacelle
75 Pratt & Whitney Canada PW120 turboprop
76 Engine accessory equipment gearbox
77 Digital engine controller
78 Particle separation intake air duct
79 Ventral oil cooler
80 Propeller reduction gearbox
81 Hamilton Standard four-bladed variable pitch, reversible propeller
83 Propeller hub pitch-change mechanism
84 Detachable engine cowling panels
85 Spinner
86 Propeller blade root attachment joint
87 Outboard integral fuel tank
88 Fuel system piping
89 Pressure refuelling connection
90 Ground fuelling point
91 Fuel system hydraulic valves
92 Outer wing panel multi-bolt access panel
93 Outer wing panel leading-edge de-icing boot
94 Starboard navigation (red) and strobe (white) lights
95 Aileron horn balance
96 Static discharges
97 Aileron tab
98 Port aileron
99 Carbon-fibre aileron skin panelling
100 Starboard spoiler, open
101 Outboard double-slotted flap, open position
102 Flown position
103 Ventral flap hinge fairings
104 Flap slot closure panels
105 Inboard double-slotted flap segment, down position
106 Wing root trailing-edge fillet
107 Fillet honeycomb
108 Flap honeycomb
109 Aileron control linkage
110 Engine fire extinguisher bottles, port and starboard
111 Overhead stowage bins
112 Rear cabin seating
113 Starboard wardrobe
114 Galley unit
115 Passenger cabin rear bulkhead
116 Starboard side service/emergency exit door
117 Rear baggage compartment door
118 Port aileron
119 Interphone
120 Cabin attendant's folding seat
121 Toilet compartment door
122 Starboard rear baggage/cargo compartment
123 Rear pressure bulkhead
124 Glass-fibre fin root fillet
125 Kevlar/Nomex honeycomb extended chord fin root section
126 Fin spar attachment joints
127 Three-spar tailfin construction
128 VOR aerial
129 Elevator control rods
130 Fin leading-edge
131 Tailplane attachment joints
132 Tailplane leading-edge
133 Starboard tailplane
134 Starboard elevator
135 Rudder horn balance
136 Anti-collision light
137 Static dischargers
138 Rudder
139 Leading-edge nose ribs
140 Elevator horn balance
141 Port elevator
142 Elevator tab
143 Elevator horn balance
144 Leading-edge construction
145 Port tailplane construction
146 Rudder tab
147 Tailcone transparency
148 Tail navigation and strobe lights (white)
149 Composite tailcone
150 Rudder hinge control
151 Tailcone vent
152 Autopilot controller
153 Tailcone rear bulkhead
154 Fin spar attachment main frames
155 Ventral access hatch
156 Crashproof cockpit voice and data recorders
157 Toilet compartment
158 Water tank
159 Wash basin
160 Toilet
161 Cabin pressurisation valves
162 Counterbalance spring
163 Rear passenger entry door/airstairs
164 Entry lobby
165 Rear fuselage frame and stringer construction
166 Port inboard double-slotted flap
167 Port inboard double-slotted flap
168 Honeycomb flap shroud
169 Flap vanes
170 Flap honeycomb core construction
171 Outboard double-slotted flap
172 Spoiler hydraulic jack
173 Port aileron
174 Aileron spring tab
175 Port aileron rib construction
176 Aileron trim tab
177 Outer wing panel skin construction
178 Port navigation (red) and strobe (white) lights
179 Outer wing panel rib construction
180 Leading-edge de-icing boot
181 Fuel filler cap
182 Fuel tank end rib
183 Fuel tank and rib
184 Outer wing panel bolted joint
185 Port wing rib construction
186 Port wing integral fuel tank
187 Port wing nacelle
188 Rear spar
189 Front spar
190 Port engine exhaust nozzle
191 Ventral engine nacelle
192 Fireproof bulkhead
193 Sponson mounted hydraulic reservoirs and filters, port and starboard
194 Sponson fairing
195 Engine mounting frame
196 Main engine mounting frame
197 Twin mainwheels, inward retracting
198 Forward suspension axle beam
199 Mainwheel doors
200 Shock absorber strut
201 Main undercarriage pivot
202 Forward engine mounting/gearbox support struts
203 Hydraulic retraction jack
204 Port fuselage frame and stringer construction
205 Static dischargers
206 Oil cooler air intake
207 Air conditioning system ram air intake
208 Engine air intake
209 Fuselage sponson fairing

Figure E.2: ATR42 Colibrì cutaway

Figure E.3: Dornier Do228 cutaway

# List of Figures

# List of Tables